NASA Conference Publication 2332

Assessment of Techniques for Measuring Tropospheric H_xO_y

Proceedings of a workshop held in
Palo Alto, California
August 16-20, 1982

NASA

NASA Conference Publication 2332

Assessment of Techniques for Measuring Tropospheric H_xO_y

Edited by
James M. Hoell
Langley Research Center

Proceedings of a workshop sponsored by the
NASA Office of Space Science and Applications,
Washington, D.C., and NASA Langley Research Center,
Hampton, Virginia, and held in
Palo Alto, California
August 16–20, 1982

NASA
National Aeronautics
and Space Administration

Scientific and Technical
Information Branch

1984

PREFACE

The National Aeronautics and Space Administration through its Tropospheric Chemistry Program has sought and utilized the advice of the scientific community in the formulation of its research efforts. The NASA Working Group on Tropospheric Program Planning, led by Dr. John Seinfeld, established a foundation to guide program development (NASA RP-1062, 1981). One of four areas recommended for expanded activities was instrument development aimed at improving our capability to measure the important trace gases and aerosols which are the key species in the major atmospheric biogeochemical cycles. To assist in guiding our utilization and development of instrumentation and to focus more clearly on specific needs, the Instrument Workshop for H_xO_y Tropospheric Species was conducted in Palo Alto, California, August 16-20, 1982. The workshop participants were asked to provide assessments of existing sensors and of new technologies deemed to have potential for measuring H_xO_y species at levels characteristic of the nonurban troposphere.

The availability of adequate instrumentation is a prerequisite for the implementation of a program to address the pertinent scientific issues of trace constituents within the global troposphere and the factors that control their concentrations. The efforts of this workshop provide meaningful guidance for future instrument developments. The assistance of all who contributed to this workshop is sincerely appreciated. Special thanks are extended to James M. Hoell, Jr, Workshop Chairman; Malcolm J. Campbell, Coordinator, and Warren D. Hypes and Richard J. Bendura, NASA Rapporteurs. The support of the Bionetics Corporation, and particularly the assistance of Howard J. Curfman, Jr., and Helen Ann Thompson, is also gratefully acknowledged.

Robert J. McNeal, Manager
Tropospheric Chemistry Program
Office of Space Science and Applications

CONTENTS

LIST OF TABLES

LIST OF FIGURES

ATTENDEES

James G. Anderson
Harvard University

Richard J. Bendura
NASA Langley Research Center

John Bradshaw
Georgia Institute of Technology

Malcolm J. Campbell
Washington State University

David R. Crosley
SRI International

Howard J. Curfman, Jr.
The Bionetics Corporation

Douglas D. Davis
Georgia Institute of Technology

L. I. Davis
Ford Motor Company

Carl Farmer
Washington State University

Thomas M. Hard
Portland State University

Robert C. Harriss
NASA Langley Research Center

William S. Heaps
NASA Goddard Space Flight Center

E. David Hinkley
Jet Propulsion Laboratory

James M. Hoell, Jr.
NASA Langley Research Center

Warren D. Hypes
NASA Langley Research Center

I. Stuart McDermid
Jet Propulsion Laboratory

Robert J. McNeal
NASA Headquarters

John P. Mugler, Jr.
NASA Langley Research Center

Matthias Rateike
Kernforschungsanlage, Julich

Michael O. Rodgers
Georgia Institute of Technology

Hanwant B. Singh
SRI International

Richard M. Stimpfle
Harvard University

Charles C. Wang
Wayne State University/
Ford Motor Company

EXECUTIVE SUMMARY

The National Aeronautics and Space Administration through its Tropospheric Chemistry Program has sought and utilized the advice of the scientific community in the formulation of its research efforts. The NASA Working Group on Tropospheric Program Planning established a foundation to guide program development (Seinfeld et al., 1981). One of the four areas recommended for expanded activities was instrument development, which is aimed at improving our capability to measure the trace gases and aerosols which are the key species in the major atmospheric biogeochemical cycles. To focus more clearly on specific needs, the Instrumentation Workshop for H_xO_y Tropospheric Species was conducted in Palo Alto, California, August 16-20, 1982. The objectives of this workshop were:

1. To provide an assessment of the capability of the existing sensors of H_xO_y species at levels characteristic of the nonurban troposphere

2. To identify those techniques adaptable to real-time measurement (sampled or continuous) onboard an aircraft platform

3. To address the concern for intercalibration and intercomparison of techniques for measuring specific species

4. To recommend promising technologies for research and development for measuring important species for which a capability does not now exist or is presently of inadequate sensitivity

Workshop attendees included approximately 16 invited participants from government, universities, and industry. Each participant was selected based on a demonstrated expertise in either the development or application of H_xO_y monitoring techniques for global tropospheric research.

As input into the workshop, NASA prepared an overview of its current Global Tropospheric Program, highlighting ongoing activities as well as long-range plans. Included in these discussions was a brief summary of H_xO_y species chemistry in the troposphere and required measurement capabilities for various H_xO_y species. These measurement capabilities (horizontal and vertical spatial resolution and required concentration levels), combined with the experiences of the workshop participants, became the basis for discussion of the various techniques. This workshop report is a summary of those discussions and written material prepared by the participants to describe the techniques discussed.

The species discussed in this workshop document include OH, H_2O_2, HO_2 and CH_3OOH. The techniques encompassed direct measurement concepts utilizing various approaches to the laser-induced

fluorescence technique, absorption spectroscopy, wet chemical techniques and several indirect approaches which depend upon measurements of reactant products or rate of removal of global tracers. The major emphasis at the workshop, however, centered on an assessment of techniques for the measurement of OH. That this was so recognizes the fact that OH is the single most important constituent in the troposphere and that major differences currently exist in the understanding of its global distribution. Moreover, efforts to develop techniques suitable for measuring tropospheric OH span more than a decade and have included university, private industry, and government laboratories. The few OH measurements that have been reported by any approach are, at best, questionable. Further, it was recognized that of the various approaches to measure OH, the ones that have received the most attention and indeed generated the most controversy are those that employ the LIF concept. Accordingly, a large fraction of the workshop's discussion was in fact devoted to an assessment of existing and proposed LIF sensors for measuring OH. The workshop focused on assessment of the more prominent LIF concept, namely, a single photon excitation process. Techniques utilizing multiple photon excitation steps were not evaluated and hence will not be discussed in this document. The assessment activity included (1) developing a generalized or "central" LIF equation from which the working expression (e.g., relating OH concentration to observed signal) for any LIF approach could be derived, (2) developing a common formulization for the interference due to laser-generated OH, and (3) using the results from (1) and (2) to compare the expected or achieved performance of various LIF approaches.

The formulation of a "central" LIF equation was, in fact, initiated at an ad hoc meeting of OH investigators convened at the 2nd Symposium on the Composition of the Nonurban Troposphere, held in Williamsburg, VA, May 1982. The rationale for such an effort stems from the fact that all LIF approaches for OH measurements are based upon a common physical phenomenon which can be mathematically formulated to explicitly relate the OH concentration to an observed signal for a given laser flux. Such a formalization can be cast in terms of standard spectroscopic quantities and can be general enough to encompass the various approaches for implementation of the LIF technique. The working expression for each LIF instrument would, in effect, be a specialized case of the central equation. The advantage of such an approach is that comparisons of current and future LIF systems can be implemented from a common basis.

The OH measurement techniques discussed in the document are at various stages of development, ranging from concepts (on paper only) to operational in-the-field instruments. For techniques existing as a concept or as laboratory instruments, discussion focused on anticipated measurement capabilities and future research and/or hardware development required to obtain anticipated capabilities. For operational techniques, discussion focused on current

capabilities, known instrument interferences and shortcomings, and research required to improve instrument cabilities. A brief description of each technique discussed at the workshop is included in the document.

Conclusions, observations, and the consensus of opinion arising from the workshop are briefly noted in the following summary material.

1. Alternate techniques for OH measurement should continue to be explored and supported if found to offer significant advantages. These techniques include:

   a) LIF measurement with sample expansion to low pressures

   b) LIF measurement using higher repetition rates

   c) LIF measurement using narrower band detectors

   d) LIF measurement using 308-nm excitation in the 0-0 band

   e) LIF measurements using short laser pulse widths

   f) Measurement techniques analogous to the radiochemical method but using other, possibly nonradioactive, reagent species

2. A better understanding, at least at the empirical level, is needed of the dynamics of the OH radical, in order to assess the improvements to be expected in reducing interference in the LIF method from ozone photolysis.

3. NASA should encourage the assembly of carefully reviewed compilations of data, such as quenching constants for OH^* and HO^*_2, of interest to experimentalists.

4. There should be coordinated studies of the relationship of the nonresonant fluorescent background to LIF measurements and the results of such studies should be disseminated. Features of interest include meteorology, on which some data may already be available, spectrum, and two-point autocorrelation function.

5. Development of OH calibration techniques should be expedited, including exploration of common calibration systems such as that proposed by the Ford group and improvements in the open-air long-path absorption technique.

6. Intercomparison of OH instruments at an early time should be encouraged. NASA should endeavor to see that the best

calibration feasible is utilized in each field expedition, and both the relative calibration factors and calibration stabilities of all instruments should be determined and treated as part of the record of the field expedition.

7. Through this report and other means, NASA should request the community to consider possible techniques for aircraft measurement of HO_2, H_2O_2, and CH_3OOH.

INTRODUCTION

In its continuing efforts to direct its applications programs toward relevant national needs, NASA is conducting the Tropospheric Chemistry Program. The long-range objective of this program is to apply NASA's space technology to assess and predict human impact on the troposphere, particularly on the regional to global scale. The increasing importance of pollution on these scales and the synoptic view afforded from satellites suggest that space observations can play a unique and critical role in satisfying the objective. A NASA-sponsored working group of scientists prepared an overview of the scientific problems that need to be addressed in order to understand the large-scale troposphere (Seinfeld et al., 1981). The group recommended that NASA undertake expanded efforts to develop space applications for tropospheric air quality monitoring in the areas of instrument development, modeling, laboratory studies, and field measurement activities.

To help NASA in formulating a detailed implementation plan, assistance has been sought from workers in this field to identify the high-priority research required in each of the four components. Such studies included specific regional scientific concerns (Levine and Schryer, 1978); the results from and the needs of tropospheric modeling (National Aeronautics and Space Administration, 1981); multiphase processes, including heterogeneous catalysis (Schryer, 1982); passive remote sensing (Keafer, 1982); and instrumentation for N_xO_y tropospheric species (National Aeronautics and Space Administration, 1983).

This volume reports the results of the Instrumentation Workshop for H_xO_y Tropospheric Species. The workshop was sponsored by the NASA Office of Space Science and Applications and conducted under the direction of the Global Tropospheric Experiment Project Office of NASA Langley Research Center.

OBJECTIVES AND ORGANIZATION

The objectives of this workshop were:

(1) To provide an assessment of the capability of existing sensors of H_xO_y species at levels characteristic of the nonurban troposphere

(2) To identify those techniques adaptable to real-time measurement (sampled or continuous) onboard an aircraft platform

(3) To address the concern for intercalibration and intercomparison of techniques for measuring specific species

(4) To recommend promising technologies for research and development for measuring important species for which a capability does not now exist or is presently of inadequate sensitivity

All workshop participants were actively involved in the development of instruments or the utilization of promising techniques for the measurement of gaseous H_xO_y species. The planning for the workshop and the overall leadership was the responsibility of the workshop chairman. A coordinator was selected from the participants to conduct the workshop, make writing assignments, and assist the chairman in this final documentation. Two NASA rapporteurs also provided assistance in coordinating the documentation assignments. Those contributing to the discussions and documentation are as follows:

James M. Hoell, Jr., Workshop Chairman
Warren D. Hypes, NASA Rapporteur
Richard J. Bendura, NASA Rapporteur
Malcolm J. Campbell, Coordinator

PARTICIPANTS

James G. Anderson
John Bradshaw
David R. Crosley
Douglas D. Davis
L. I. Davis
Carl Farmer
Thomas M. Hard
William S. Heaps
I. Stuart McDermid
Matthias Rateike
Michael O. Rodgers
Hanwant B. Singh
Richard M. Stimpfle
Charles C. Wang

MEASUREMENT REQUIREMENTS FOR H_xO_y TROPOSPHERIC SPECIES

Highly reactive free-radical molecules are recognized as critical to maintaining atmospheric homeostasis. Because free radicals have an unpaired electron in their outer shell they can act as strong oxidizers of reduced gases emitted to the atmosphere from the biosphere. The H_xO_y species, and in particular the OH radical, have been identified as pivotal in tropospheric photochemistry (Levy, 1971). A large literature documents hypothesized photochemical reaction pathways for H_xO_y species in the troposphere (e.g., Wofsy et al., 1972; Crutzen, 1973; Seinfeld et al., 1981; National Aeronautics and Space Administration, 1981), and the detailed scientific rationale for the importance of these species to understanding atmospheric chemical processes need not

be repeated here. The critical fact to this workshop is that few, if any, widely accepted measurements exist for H_xO_y species in non-urban air. Mathematical models have been used to calculate concentrations of species such as OH. Such calculations suggest an average value of $7 \pm 3 \times 10^5$ cm^{-3} in the remote troposphere, with highest levels in the tropics. Direct measurement of gas phase OH, HO_2, and H_2O_2 is a top priority for further progress in understanding the chemistry of the troposphere.

In contrast to OH and HO_2, the most interesting aspects of the chemistry of H_2O_2 may occur in the liquid phase, especially in cloud droplets. Chameides and Davis (1982) have proposed a mechanism by which H_2O_y radicals generate H_2O_2 in solution, with the H_2O_2 subsequently becoming involved in heterogeneous oxidation of species like SO_2. It is important to pursue the development of direct measurement techniques for H_2O_2 in both gas and liquid phases.

A summary of requirements identified in existing literature for instrument sensitivity, spatial resolution, and estimated residence times for OH, HO_2, and H_2O_2 are given in table 1.

TABLE 1. REQUIREMENTS FOR H_xO_y MEASUREMENTS

Species	Residence Time	Spatial Resolution, km		Detection Requirement
		Vertical	Horizontal	
OH	<1 sec - 1 day	0.5	200	5×10^5 cm^{-3}
HO_2	<1 sec - 1 day	0.5	200	1×10^7 m^{-3}
H_2O_2	<1 day - 1 week	0.5	200	200 pptv

SPECIES AND TECHNIQUES CONSIDERED

Table 2 lists the techniques considered by the workshop participants along with the respective species. Most of the workshop discussion centered on techniques for detection of OH. This reflects the uncertain state of OH measurements and the long history associated with efforts to develop techniques to measure tropospheric OH coupled with the scarcity of techniques for measuring the other H_xO_y species. Among the OH techniques listed in table 2, the laser-induced fluorescence (LIF) method received the most consideration. The workshop discussion addressed only LIF approaches utilizing a single photon excitation step.

The major emphasis was placed on a detailed assessment of the status of LIF systems that have undergone some level of either field or laboratory testing. The approach taken for the assessment focused on the development of a generalized central equation to relate OH concentration to observed signal, laser flux and standard spectroscopic quantities. The working expression used by each LIF system to relate the OH concentration to observed signal was obtained from the central equation as a specialized case. A major concern for implementation of the LIF technique for OH measurements is the potential interference effects produced by laser-generated OH. The various approaches for implementing the LIF concept are, in fact, fostered in large measure by a need to minimize the seriousness of this interference. Accordingly, it was felt by all participants that an assessment of the OH LIF systems required an evaluation of the magnitude of the laser-generated OH as well as a common formulation of this phenomenon for several of the current and proposed techniques. The actual status assessment culminated in a comparison of the signal-to-noise ratio expected from several LIF systems "operating" in two different model atmospheres.

In the following sections, a brief description of the various approaches to measure OH is given. The next section will summarize the workshop evaluation of the LIF concepts discussed.

TABLE 2. TECHNIQUES CONSIDERED

Detection Principle	Technique	Species
Laser-induced fluorescence	(1) Single Photon	OH
	a) Atmospheric pressure in situ	
	b) Low pressure in situ	
	c) Lidar	
	(2) Photofragmentation	H_2O_2, CH_3OOH
Radiochemical	(1) ^{14}CO/OH reaction	OH
Global Tracers	(1) Emission vs. Removal via OH reaction	OH
Absorption Spectroscopy	(1) Long-path UV	OH
Wet Chemical	(1) Condensation sampling	H_2O_2

MEASUREMENT OF OH

Laser-Induced Fluorescence

Laser-induced fluorescence (LIF) is a measurement technique that, under laboratory conditions, has demonstrated measurement sensitivities suitable for detection of single atoms and molecules. This demonstrated sensitivity, coupled with the fact that LIF reresents one of the few techniques for direct detection of OH, has been the impetus for developing this technique for ambient OH measurements.

It should be recognized at the outset that there has been and currently exists a wide diversity in the research and development efforts directed toward developing field-compatible LIF systems. Because of this diversity, it is easy to lose sight of the fact that all the LIF approaches are based upon a single fundamental phenomenon. Simply stated, this phenomenon involves resonant excitation of a molecule either with a single photon at λ_1 or with two sequential photons at λ_1 and then λ_2, followed by detection of the resulting fluorescence. In general, the single-photon excitation scheme discussed at the workshop has typically been initiated using excitation wavelengths of either 282 nm or 308 nm. The 282-nm excitation scheme, illustrated in figure 1, is the only one which to date has been employed for atmospheric measurements. As shown in figure 1, the OH radical is initially excited into the v' = 1 manifold of the $A^2\Sigma$ electronic state by

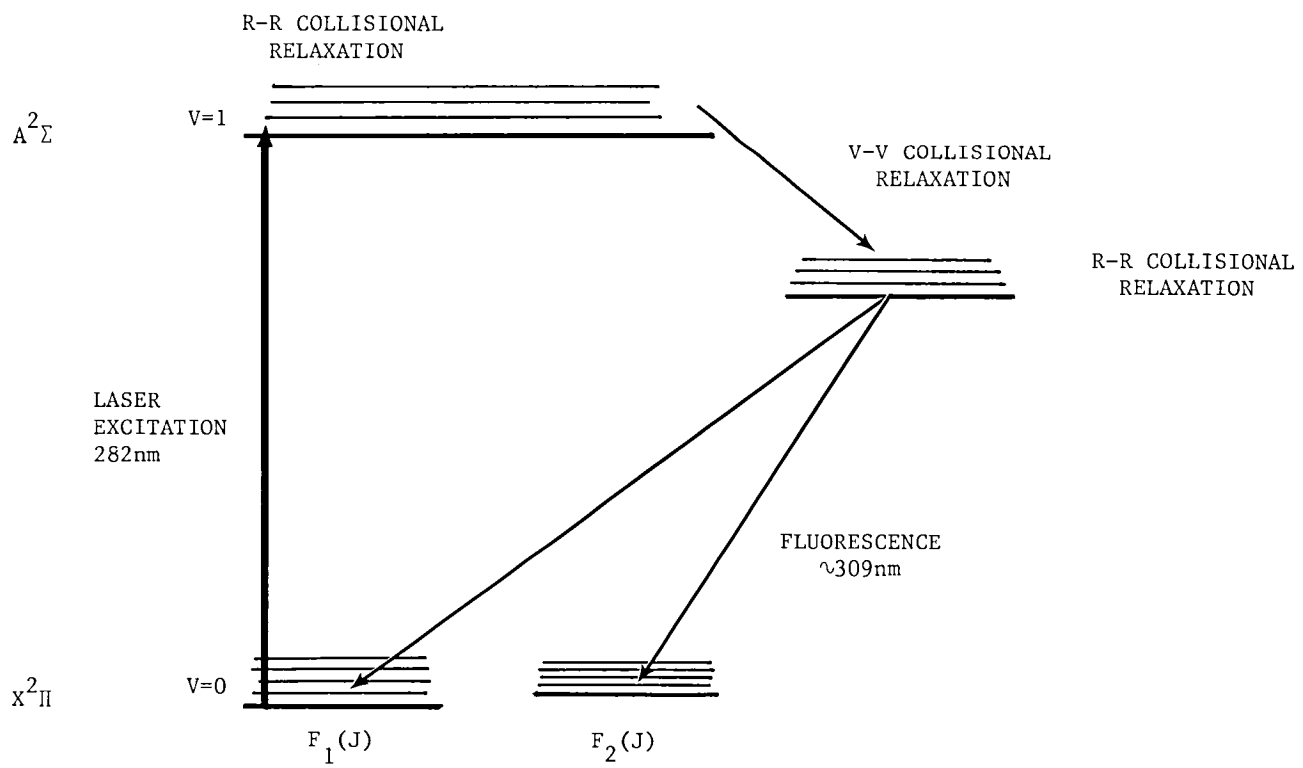

Figure 1. Laser-induced fluorescence, 282-nm excitation.

pulsed laser excitation in the region of 281.9 to 282.5 nm. This corresponds to either $Q_1(1)$, $Q_1(2)$, $P_1(1)$ or $P_1(2)$ transitions and will be referred to here as 282-nm excitation. Rotational and vibrational relaxation of this excited state causes a significant part of the OH fluoresence to occur from the $(A^2\Sigma, v' = 0) \rightarrow (X^2\Pi, v' = 0)$ transition around $\lambda = 309.5$ nm. However, due to collisions with N_2, O_2, and H_2O, significant electronic quenching occurs resulting in attenuated fluorescence from rotational states in the $v' = 1$ and $v' = 0$ manifold of the $A^2\Sigma$ state. The relatively large red shift in the fluorescence signal (e.g., 309 nm) relative to the pump wavelength (e.g., 282 nm) is one of the advantages of this particular excitation scheme. In particular, the OH fluorescence can be detected with minimal interference from the pumping frequency. The disadvantage relative to the 308-nm excitation scheme discussed below is the increase in photolytic interference (e.g., laser-generated OH, discussed below). For the scheme shown in figure 1, the fluorescence emission centered at 309 nm is typically measured using a narrow bandpass filter backed by a high-efficiency photomultiplier tube and photon-counting electronics.

The LIF scheme just outlined is deceptively simple, particularly when considered for field measurements of a trace atmospheric constituent such as OH. Successful implementation of this technique requires development of state-of-the-art laser excitation and detection systems that optimize the return signal while minimizing the contribution from a number of noise sources. It is important to note that the various LIF approaches currently being considered for OH measurements differ primarily in the rationale and procedures used to minimize the noise contribution. The major noise sources that must be overcome are: (1) nonresonant fluorescence (NRF) from other atmospheric constituents; (2) Rayleigh, Raman and Mie scattering; (3) photolytic interference, resulting from photolysis of other molecules to produce OH; and (4) external background radiation such as solar background. The Rayleigh, Raman and Mie scattering, as well as contributions from external background radiation, represent well-understood and characterized phenomena which, while not insignificant, can be minimized with straightforward design precautions and use of narrowband filters.

Nonresonant fluorescence is generally attributed to broadband fluorescence from aerosols. This noise source has not been fully characterized and several instrumental approaches involving combinations of spectral, temporal and baric filtering are under consideration for minimizing its effect. To date photolytic interference has been the major source of uncertainty in the measurement of tropospheric levels of OH via the LIF approach. This interference originates from the production of OH via photolysis of O_3 by laser radiation producing $O(^1D)$ followed by its subsequent reaction with ambient H_2O. Like the LIF phenomenon itself, photolytic interference is a fundamental process inherent in the LIF measurement approach and represents a major noise source for which a number of instrument approaches have been employed to minimize its consequences.

An excitation and detection scheme which has been suggested as a method for minimizing the photolytic interference is illustrated in figure 2. Conceptually this is similiar to the 282-nm excitation scheme. Here, however, the excitation is with λ = 308 nm. The OH fluorescence originates from the same manifold, resulting in a shift of only a few tenths of a nanometer. Thus, the prime disadvantage of this excitation scheme is the need for a high resolution filter to discriminate between signal and the background originated from the excitation pulse. An important advantage is that O_3 absorption at 308 nm is significantly less than at 282 nm, resulting in less photodissociation of O_3 and therefore lower OH generated from the excitation laser. A more detailed discussion of this excitation/detection scheme will be given below.

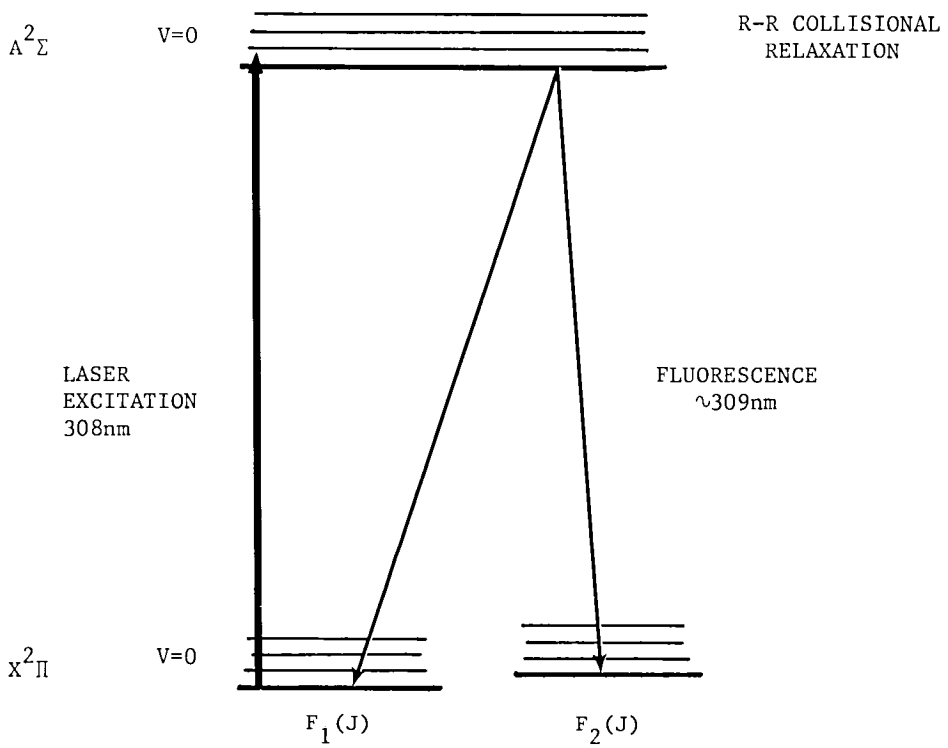

Figure 2. Laser-induced fluorescence, 308-nm excitation.

There are a number of LIF approaches in various stages of development. In general, the distinguishing feature between those approaches is the method employed to minimize contributions from the noise sources noted above while maximizing the SNR. Table 3 identifies the major LIF techniques currently under consideration, along with the more obvious distinguishing features. The status column provides a general assessment of the field readiness of the approach while the comment column indicates the major advantage or objective of the given approach. The source column identifies one or more of the laboratories that support a given technique. Each

TABLE 3. SALIENT CHARACTERISTICS OF LASER-INDUCED FLUORESCENCE (LIF) TECHNIQUES FOR MEASUREMENT OF TROPOSPHERIC OH

TECHNIQUE	λ_{on} (nm)	λ_{det} (nm)	STATUS	COMMENTS	SOURCE
(1) Lidar	282	309	Field Tested	Large sample volume to minimize laser-generated OH and absorption saturation	Ford, Goddard
(2) In Situ					
(a) Atmospheric Pressure	282	309	Field Tested	Short pulse to minimize laser-generated OH; near-simultaneous λ_{on} & λ_{off} to freeze non-resonant fluorescence	Ga. Tech
	282	309	Proposed	Low pulse energy, high repetition rate	Harvard
	308	309	Proposed	Excimer laser with high-resolution filtering	JPL
(b) Low Pressure (Baric filtering)	308	309	Under development	Minimize laser-generated & background noise	Portland State/Institut für Chemie

of these approaches was discussed at the workshop. A brief description of each technique will follow the discussion of the dominant noise sources.

Interferences. Of the four major sources of noise or interference noted in the previous section, two are considered well understood. These are Rayleigh, Raman, and Mie scattering and external radiation, particularly the solar background. These phenomena are well characterized and, while not insignificant, can be minimized through various design considerations and filtering techniques. This leaves the nonresonant fluorescence and photolytic interference as the two remaining major sources of noise. To appreciate the impact of these two noise sources, one must realize that the raw measured signal in an LIF system is, in general, the sum of the desired atmospheric OH fluorescence plus contributions due to fluorescence associated with the photolytically generated OH and the NRF. The NRF is generally a slowly varying function of both the excitation and fluorescence spectrum. Accordingly, correction for the NRF contribution can be implemented through simultaneous measurements in a spectral channel close to the OH fluorescence channel or by temporally separated measurements in the single OH fluorescence channel with the NRF excited by wavelength λ_{on}

and then λ_{off}. To account for the contributions from photolytically generated OH, the sampling geometry and operating parameters are designed to minimize the amount of OH created. In addition, the signal contribution due to the laser-generated OH can be estimated and mathematical corrections implemented.

Nonresonant Fluorescence. The nonresonant fluorescence phenomenon concerns a large and often variable nonresonant, broadband fluorescence background signal. In some environments, it has been observed that the uncertainty in this background signal does not follow simple Poisson statistics (Wang and Davis, 1982; Rodgers et al., 1982). These observed fluctuations appear to be related to inhomogeneities in the levels of aerosol species. The net effect of this nonstatistical noise source is that the SNR in a given system does not increase with the square root of the integration time. Hence, a significant deterioration occurs between the calculated or expected detection limit and that actually obtained during field measurements. In principle, the above problem could be solved if the switching time for tuning the laser "on" and "off" the OH resonance frequency is made short compared to the rate at which changes occur in the environment. It is known for example that at time intervals as short as 1 ms, atmospheric motion is unimportant. What is not yet known is whether the "on"/"off" cycling time for an LIF system needs to be this fast.

It is clear, from the measurements which have been made, that NRF can dominate the noise in all but the lidar-type instruments with unterminated beams. The noise in unterminated lidar systems is generally dominated by solar scattering. It is less clear, but nevertheless true, that the flux of air through the sample volume interrogated by the instrument (a parameter partly determined, for example, by the speed of the aircraft on which the instrument is mounted) has a major influence on the impact of NRF. At this point our knowledge of the causes and properties of the NRF is very limited. A crucial characteristic of NRF is the autocorrelation function describing the NRF signal, both in time and space. Optimum instrument design to minimize NRF requires that signal and background measurements be spaced temporally (or spectrally) close enough so that the NRF signal on the two occasions is essentially unchanged. Unpublished data from the Ford group suggest that the autocorrelation function (at ground level, in moderate winds) is close to unity for times less than 1 second. These limited data are encouraging. The universality of this figure and the validity of relating correlations in space to correlations in time in this context remain to be established.

It is reasonable to assume that the NRF signal is proportional to the spectral bandwidth of the detector. Typical values, measured in units of equivalent hydroxyl radical fluorescences per unit volume, range from 10^7 to 10^8 cm^{-3} for a 2.7 nm bandwidth. These values seem to apply to both the boundary layer and the mid-troposphere over land, with the lower figure more common for the mid-troposphere over oceans. Much lower values occur oc-

casionally, but apparently not for a sufficiently large proportion of the time to permit representative hydroxyl data to be collected.

In summary the impact of the NRF is twofold. Not only does it decrease the signal-to-noise ratio by raising the background count, but it also causes an additional degradation unless the signal and background measurements are close enough in time for the background to remain constant.

Photolytic Interference. As noted above, photolytic interference has, in general, represented a major source of uncertainty in measurements of OH with LIF techniques. This interference originates from laser-induced production of the OH radical which is then detected and interpreted as ambient OH. As discussed by Wang et al. (1976), Hanabusa et al. (1977), Davis et al. (1981a, b), Ortgies et al. (1980), and Wang and Davis (1982), at wavelengths in the region of 282 nm, the laser photolysis of atmospheric O_3 results in the production of metastable atomic oxygen $O(^1D)$. And, even though only a small fraction of this $O(^1D)$ goes on to react with atmospheric H_2O to produce OH radicals, the artificial OH so produced can prove to be quite troublesome. In fact, depending on the laser energy density and the laser pulse width, the signal produced from laser-generated OH can overwhelm the signal from natural atmospheric OH. Potential solutions to the LIF artificial OH problem include the use of expanded laser beams (Wang et al., 1981), the use of very short laser pulses (Davis et al., 1981a, b; Rodgers et al., 1982), the use of sampling manifolds that operate at reduced pressure (Hard et al., 1979, 1980), the use of high-repetition-rate low-peak-power laser excitation (Stimpfle and Anderson, 1982), or the use of 308-nm excitation. The physical process for photolytic production of OH is understood, and perhaps more importantly, the severity of the interference can be estimated and in some cases measured for a given experimental configuration. The purpose of this section is to describe the physical process which gives rise to laser-induced OH interference and to present the "working expressions" for the in situ configuration employed by Georgia Tech and Harvard Univ. and the lidar configuration employed by Wayne State Univ./Ford Motor Co.

As noted earlier the single-photon excitation schemes can employ either 282 nm or 308 nm wavelength. Excitation of atmospheric OH at 282 nm introduces a potentially more serious complication than might be experienced at 308 nm. This stems from the larger O_3 absorption cross section at 282 nm than at 308 nm. The photolysis of O_3 at 282 nm produces atomic oxygen in the ^1D excited state which reacts with ambient H_2O to yield OH:

$$O_3 + h\nu(282\ nm) \rightarrow O(^1D) + O_2(^1\Delta) \quad (1)$$

$$O(^1D) + M \rightarrow O(^3P) + M \quad (2)$$

$$O(^1D) + H_2O \rightarrow 2OH^* \quad (3)$$

$$OH^* + M \rightarrow OH + M \qquad (4)$$

where OH* signifies vibrationally and/or rotationally excited OH generated as a result of process (3). Interference then results when the excited OH generated in this manner is relaxed through collisions into the particular rotational level from which excitation to the $^2\Sigma^+$ state of OH takes place. The key time constants for the relevant molecular processes as a function of altitude are summarized in figure 3. Note that the $O(^1D)$ lifetime throughout the troposphere is less than 10 nsec. The extremely rapid R-R relaxation rate of OH further implies that the OH formed from reaction (3) in the v=0 level (approximately 70%) appears rotationally thermalized to the laser pulse, although the nascent rotational distribution is "hot". Hydroxyl formed by reaction (3) in the v=1 and 2 levels is not seen by the laser because the v-v transfer rate is insufficiently fast (see figure 3) in the $X^2\Pi$ state. Thus, within the troposphere a significant fraction of the $O(^1D)$ can form OH during the laser pulse. The atmospheric pressure and laser pulse width play critically important roles, since they define the time constants of the system.

Prior to writing down the LIF-lidar expression used by the Ford group and the LIF in situ expressions used by the Georgia Tech and Harvard groups for estimating the laser-induced OH, two different quantities with which the results are cast are defined:

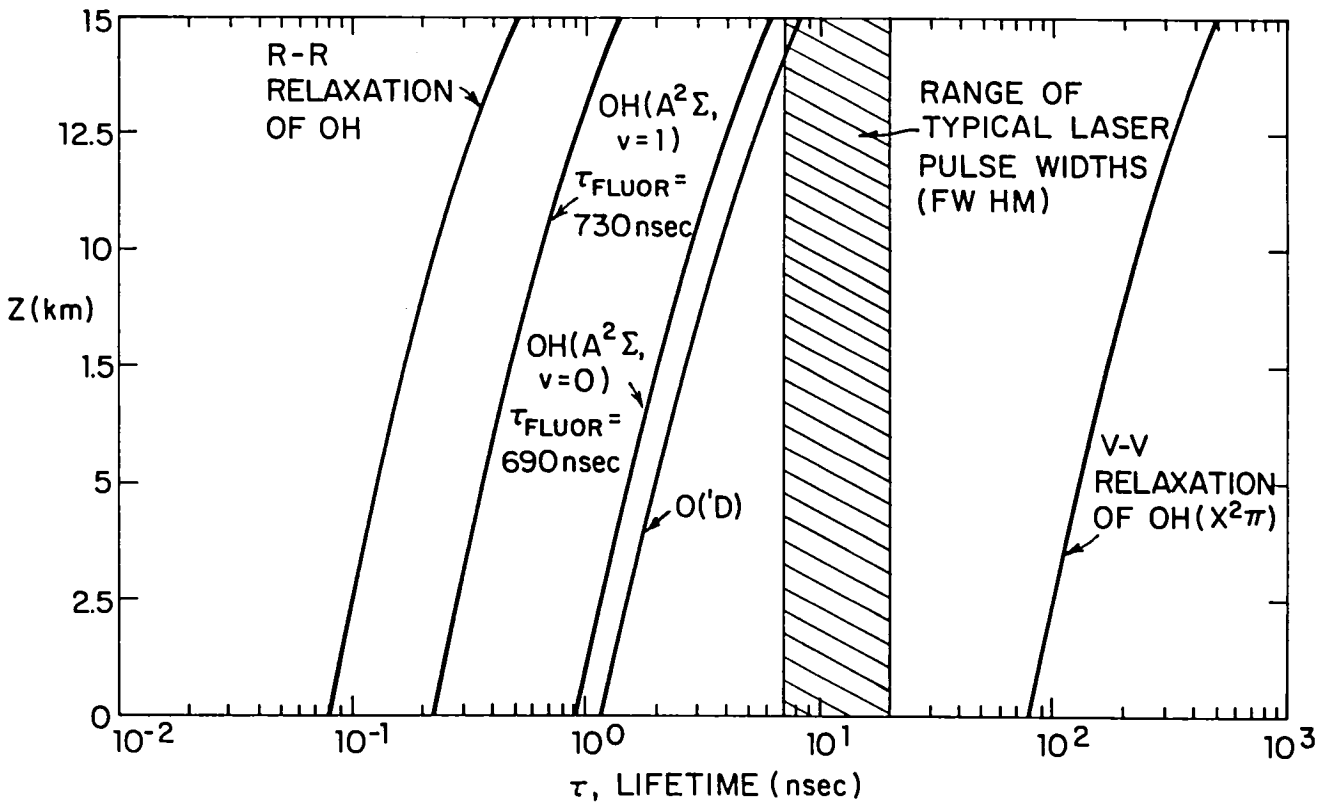

Figure 3. Key time constants in the ozone photolysis process.

$[OH]^{laser}$ = the average laser-induced OH density which one would derive by converting an observed laser-induced OH count rate to an effective "steady state" density via knowledge of the absolute OH calibration of the instrument; in general, $[OH]^{laser}$ is never in steady state during the course of a laser pulse

$[OH]^{laser}_{total}$ = the total amount of laser-induced OH formed per pulse, allowing for all $O(^1D)$ formed to decay; in general $[OH]^{laser}$ does not exceed 1/2 $[OH]^{laser}_{total}$

The format used here for comparison of the three expression is to first give the actual expression as cited in the literature along with definitions of the specific parameters used in each case. The similarities and differences are then noted.

The expression used by the Ford group to estimate this interference for their lidar system is given by

$$[OH]^{laser} = A'_c\, F(\chi)\, [OH]^{laser}_{total} = A_c\, [OH]^{laser}_{total} \qquad (5)$$

$$[OH]^{laser}_{total} = \sigma_O\, \phi\, E\, [O_3]\, \frac{k[H_2O]}{k[H_2O] + k_n[N_2] + k_O[O_2]} \qquad (6)$$

where:

σ_O = absorption cross section of ozone, cm^2/molec.

ϕ = quantum yield of $O(^1D)$, unitless

E = integrated energy flux per pulse, J/cm^2

k = rate constant for generation of OH from the reaction of metastable oxygen atoms with water, cm^3/molec/s

$[H_2O]$, $[O_3]$, $[N_2]$, $[O_2]$ = concentration of water vapor, ozone, nitrogen, and oxygen, respectively, molec/cm^3

k_n, k_O = rate constants for collisional de-excitation of $O(^1D)$ due to nitrogen and oxygen respectively

A'_c = the ratio of the laser OH density residing in the quantum state pumped by the laser to that expected if thermal equilibrium is attained; in principle, A_c may take on values, $0 \leq A_c \leq 1$

$$F(\chi) = 1 - \frac{2}{\chi}\left(1 - \frac{1 - \exp(-\chi)}{\chi}\right)$$

= the deviation of $[OH]^{laser}$ from the "steady state solution" due to the pulse width being of finite width: primarily, it provides the means to predict the amount of $O(^1D)$ which forms OH during the pulse, $0 \leq F(\chi) \leq 1$

$\chi = At$

t = laser pulse length

$A = k[H_2O] + k_n[N_2] + k_o[O_2]$

$A_c = A_c' F(\chi)$

The corresponding expressions used by the Georgia Tech group to estimate the OH interference for their in situ sampling configurations are given by:

$$[OH]^{laser} = [OH]^{laser}_{total} \frac{F_{interf}}{F_{nat}} \left[\frac{1}{2} - \frac{1}{\pi\chi} 1 + \left(\frac{\exp(-\pi\chi) - 1}{\pi\chi}\right)\right] \quad (7)$$

$$[OH]^{laser}_{total} = \left(\frac{4E\ \sigma\ \phi\ \lambda}{\pi d^2 hc}\right)[O_3] \frac{2k_3[H_2O]}{k_3[H_2O] + k_2[N_2] + k'_2[O_2]} \quad (8)$$

where E = laser energy per pulse, J

σ = absorption cross section of ozone, cm^2/molec

ϕ = quantum yield of $O(^1D)$, unitless

d = laser beam diameter, cm

h = Planck's constant, Js

c = speed of light, cm/s

λ = excitation wavelength (e.g., 282 nm), nm

k_3 = rate constant for generation of OH from the reaction of metastable oxygen atoms with water, cm^3/molec/s

k_2, k'_2 = rate constants for collisional de-excitation of $O(^1D)$ due to nitrogen and oxygen respectively, cm^3/molec/s

$\chi = \frac{K\tau}{\pi}$

τ = laser pulse width, s

$K = k_3[H_2O] + k_2[N_2] + k'_2[O_2]$

F_{interf} = the fraction of the OH^{laser} that resides in the quantum state pumped by the laser

F_{nat} = the fraction of ambient OH (in thermal equilibrium) that resides in the quantum state pumped by the laser

The corresponding expression used by the Harvard group to estimate the OH interference is derived from a computer simulation of the problem by numerically solving the differential equations that describe the interference:

$$[OH]^{laser} = 3.8 \times 10^{-2} \frac{[O^3]\ [H_2O]}{[M]} \frac{E}{N_P A} f(x) \qquad (9)$$

where $[M]$ = molec cm^{-3}

E = average power, mW

N_P = pulse repetition frequency, Hz

A = beam area, cm^2

$f(x)$ = a polynomial in x which gives the fraction of $[OH]^{laser}_{total}$ that is actually detected by the laser pulse; the separate effects of

(1) $O(^1D)$ relaxation

(2) R-R transfer in OH

(3) v-v transfer in OH

are contained within the f(x) function

$$f(x) = -4.225 + 7.79750x - 5.7498x^2 + 1.9579x^3 - .30916x^4 + .01831x^5$$

$x = 3 + \log(3 \times 10^{-11}[M]\tau)$

τ = FWHM laser pulse width, sec

With the present parameterization, f(x) in principle has the limits $0 \leq f(x) \leq 0.91$. The valid limits on x and f(x) which can be used in this formulation are $1.75 \leq x \leq 4.35$ and $.0166 \leq f(x) \leq .651$ because of the range of data fitted and the polynomial used.

Thus

$$[OH]^{laser}_{total} = 2 \times 0.91 \times 3.8 \times 10^{-2} \frac{[O_3][H_2O]}{[M]} \frac{E}{N_p A} \qquad (10)$$

Table 4 identifies the corresponding notation used in each of the expressions given above. The working expressions derived by the Ford and Georgia Tech Group are in effect identical. For the Harvard Group and the Ford Group the functional dependence of f(x) and F(χ) on [M] and τ(= Δt) is essentially identical. This result is not surprising since in both approaches the time dependence of the interference is controlled largely by $O(^1D)$ relaxation; i.e., the state-to-state calculation of the Harvard group employing rapid R-R relaxation is similar in effect to imposing a fixed thermal R distribution on the v = 0 OH quantum states, whereas the Ford group's approach treats only $O(^1D)$ relaxation explicitly. This correspondence is borne out by direct comparison of

$$f(x) \leftrightarrow A'_C F(\chi) = 0.7 F(\chi)$$

as illustrated in figure 4.

TABLE 4. COMPARISON OF WORKING EXPRESSIONS FOR LASER-INDUCED OH

WAYNE STATE UNIVERSITY/ FORD MOTOR CO	GEORGIA TECH	HARVARD UNIVERSITY
σ_o	σ	---
ϕ	ϕ	---
Δt	τ	τ
A	K	---
χ	$\pi\chi$	---
A'_C	$\frac{F_{interf}}{F_{nat}}$	---
$F(\chi)$	$2\left[\frac{1}{2} - \frac{1}{\pi\chi}\left(1 + \frac{\exp(-\pi\chi)-1}{\pi\chi}\right)\right]$	f(x)
E	$\frac{E}{\left(\frac{hc}{\lambda}\right) \pi \left(\frac{d}{2}\right)^2}$	$\frac{E}{N_p A}$
k	k_3	---
k_n	k_2	---
k_o	k'_2	---

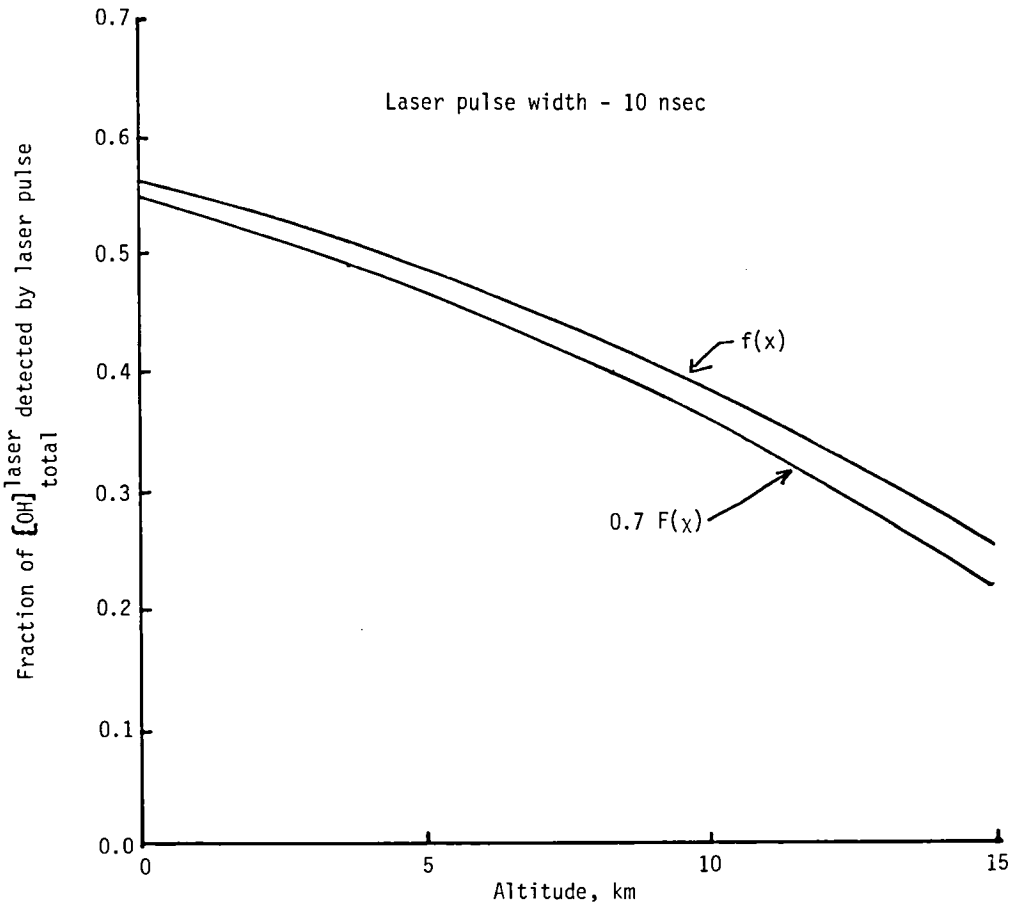

Figure 4. Comparison of f(x) and F(χ) for the Ford and Harvard formulations of laser-induced OH.

Choosing A'_C = 0.7 excludes the laser OH formed in the v = 1 and 2 levels from contributing to the interference. Thus, if A'_C = 0.7 the expressions of the Harvard, Ford, and Georgia Tech groups are in substantial agreement.

The point of contention between the two theories at present is the correct value for A'_C or the rate of R-R relaxation in the ground electronic state of OH which has yet to be measured definitively in the laboratory. The Harvard group has adopted the viewpoint that R-R relaxation is rapid; A'_C = 0.7. The Ford group favors the viewpoint that R-R relaxation is slow, or $A'_C \approx 0.15$ (Wang and Davis, 1982).

Several general comments are in order. First, the OH interference is directly proportional to the concentration of H_2O and O_3. Consequently, measurements in the boundary layer with high levels of H_2O can be severely impacted. Second, the $[OH]^{laser}$ given in each of the expressions is dependent upon the laser energy flux. From this dependence stems the rationale for the lidar approach

being pursued by the Ford and Goddard groups and the approach proposed by the Harvard group. Namely, the lidar configuration lends itself to a reduced energy density at the sample volume because of the large volume that is probed, thereby reducing E. The Harvard group proposes to reduce the energy flux by utilizing low peak pulse energies at high repetition rate. The dependence of $[OH]^{laser}$ on the laser pulse width is also included in each expression via the X parameter, and more subtly in the lifetime of $O(^1D)$. The dependence of $[OH]^{laser}$ on pressure is also through the lifetime of $O(^1D)$. The excitation pulse widths and $O(^1D)$ lifetime become comparable for excitation pulses of 1 nsec or less at atmospheric pressure. For short pulses and/or low pressures, the buildup and decay of $O(^1D)$ and consequently the OH interference lag the laser pulse shape (and consequently the OH interference) thereby minimizing its effects. Operation with short pulses is the basis of the approach that the Georgia Tech group has taken while operation at low pressures is the approach preferred by the groups from the Kernforschungsanlage (KFA) and Portland State University.

As a final comment concerning the working equations given above, it is clear that $[OH]^{laser}$ can be made as small as desired through manipulation of various system parameters (e.g., energy density). In general, however, this is done at the expense of real signal. Therefore, a comparison between the various instrumentation approaches to determine which minimizes the OH interference problem is meaningless if overall system performance is not also considered. Because of this, we now resist the temptation to utilize the above working equations for absolute numerical comparisons between the one lidar and two in situ approaches. This comparison is in fact presented along with system performance expectations for current and projected systems in a later section.

Measurement Systems

Several systems for the implementation of the basic LIF technique (see table 3) were discussed at the workshop. These systems are described in this section along with pertinent details related to the rationale for the approach and its status.

Lidar. - The basic lidar system concept consists of a laser source, transmitting optics, a receiver telescope, a detection system, and signal processing electronics. Use of the lidar configuration, in general, offers some advantages related to more efficient use of laser power by permitting a large measurement volume, and since the sample volume is located some distance away from the sample platform, uncertainties associated with platform contamination or surface losses are minimized. However, the main driving force for the lidar configuration is that it minimizes the laser-induced OH interference problem (e.g., see previous section) by permitting a large area sample beam thereby reducing the energy density, E, at the sample site. The principal disadvantages of the lidar configuration are its much greater susceptibility to interference from scattered solar flux and calibration.

Direct calibration of lidar systems is difficult at best even when dealing with stable molecules. No satisfactory approach is currently available for calibration when dealing with a short-lived species such as OH. Therefore indirect methods are generally employed to extract quantitative OH concentrations from the return signal.

Three groups are currently employing or proposing the lidar configuration for OH measurements. The group at the Ford Motor Company has pioneered the use of the lidar configuration with a number of flight tests on the NASA CV-990 aircraft. The group at Goddard is currently developing the lidar configuration for both OH and NO detection (National Aeronautics and Space Administration, 1983) and the group at the Jet Propulsion Laboratory is developing a lidar system for OH detection.

(a) Ford Motor Co.: The group at Ford Motor Co. was the first to recognize the advantages offered by the lidar configuration and, in fact, implemented the lidar approach for ambient OH measurements. Their early research and development efforts have led to the only aircraft flight tested (e.g., on NASA's CV-990) lidar system for OH measurements. A schematic of this lidar system is shown in figure 5, and is described in more detail by Wang et al. (1981). The salient features of the Ford lidar system are: (1) 282-nm excitation with detection of OH fluorescence at 309 nm, (2) broadband detection (e.g., $\simeq$ 5 nm) of OH fluorescence, (3) termination of receiver field of view (FOV) to reduce solar background, (4) normalization of the OH return signal to the nitrogen Raman scattering and (5) use of return signals from an "on" and "off" wavelength to correct for NRF.

The excitation laser beam is generated by a Nd-YAG laser pumped tunable dye laser system doubled into the ultra-violet (UV). A portion of the UV beam is split off to pass through a water vapor discharge cell where the OH fluorescence from the cell is monitored to establish that the laser is properly tuned. A Lyot depolarizer is used to depolarize the laser output. The sample volume is illuminated by an expanding beam during a preselected gate interval. The delay of the gate interval is typically chosen so that fluorescence induced by the laser pulse is monitored only for distances greater than 8 m and less than 16 m. A Newtonian telescope pointing along the path of the expanding laser beam collects the fluorescence generated. The return signal is imaged through a sequence of filters centered at 308 nm and having a spectral band pass of about 3 nm. For each laser pulse, a portion of the return signal is split from the telescope's output and directed through interference filters centered at 302 nm to a second photomultiplier. This provides a reference signal proportional to nitrogen Raman scattering for each OH fluorescence return. The OH fluorescence is referenced to the Raman signal thereby providing a methodology for indirect calibration of the lidar system. The laser system is typically tuned on and off the OH fluorescence line with a temporal separation of about

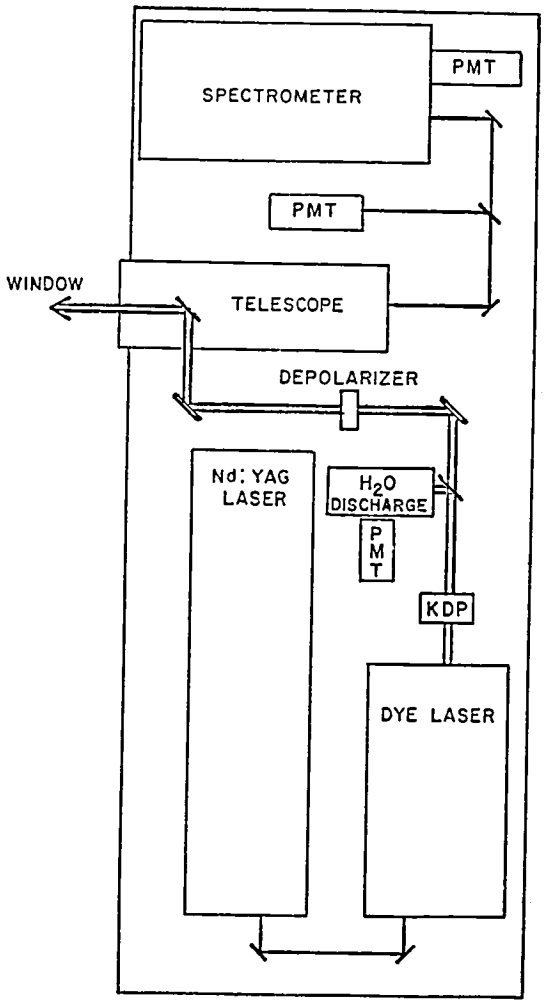

Figure 5. Wayne State Univ./Ford Motor Co. lidar system.

1 second. The on and off return signals are used to correct for NRF. To correct for the background component of the return signals that is unrelated to the laser wavelength (e.g., solar background), the detection electronics are gated on again several microseconds after each laser pulse. The resulting signal is due primarily to solar background. To minimize the solar background, the line of sight of the telescope is terminated by a backstop. Use of the backstop is one of the features that distinguishes it from the Goddard approach and increases its flexibility in that the solar background noise is not a strong function of solar zenith angle or platform altitude. On the CV-990 the backstop is provided by the wing tip of the aircraft.

The OH concentration obtained from the Ford system is subject to the uncertainties of the measurement of the OH fluorescence relative to the N_2 Raman scattering. The OH fluorescence efficiency is only known to within $\pm$ 35%. Nonethless, referencing

the OH fluorescence to nitrogen Raman scattering assures consistency from measurement to measurement, and any improvement in the accuracy of the value for OH fluorescence efficiency can be translated directly to the OH measurements.

(b) Goddard Space Flight Center: Two concepts for the lidar approach to implement the LIF technique for measurements of ambient tropospheric OH are currently under consideration at the Goddard Space Flight Center. The two system concepts differ in the bandwidth used to spectrally resolve the OH fluorescence return signal and the excitation wavelength. A broadband width (i.e., $\approx$ 5 nm) approach is currently in a brassboard configuration for aircraft test flights. A narrow-bandwidth approach with 308-nm excitation is currently in the conceptual evaluation phase although the two concepts share many common lidar components.

The similarities between the Ford and the Goddard broadband systems are 282-nm excitation with 308-nm detection and indirect calibration via N_2 Raman scattering. An aspect of the Goddard lidar concept which distinguishes it from the Ford Motor Company approach is the method used to reduce sky background. The Goddard system is pointed upward with the background filtered through an adjustable polarizer. Looking upward reduces the solar background because less atmosphere is present to scatter light toward the receiver, and the polarizer takes advantage of the fact that Rayleigh scattered light (the source of the background) is strongly polarized while fluorescence from the hydroxyl is not. Insertion of a polarizer decreases the collection efficiency for the fluorescence by a factor of two while achieving a much greater reduction in the background thereby resulting in a net improvement in the signal-to-noise ratio.

The basic lidar systems used for both the narrowband and broadband filtering concepts share many common components. The common source of both instruments is a frequency-doubled tunable dye laser pumped by a doubled neodymium-YAG laser. The frequency is checked by splitting a small amount of the 282-nm radiation off and passing it through a fluorescence cell in which OH molecules are produced by the photolysis of water with a xenon continuum lamp. For the broadband system the collected radiation is directed into a 5-nm bandwidth spectral selection system which isolates the Rayleigh scattered return at 282 nm and the OH fluorescence signal centered at 308 nm. Before processing, the 308-nm radiation is passed through a pair of adjustable multilayer dielectric Brewster angle polarizers to minimize the background of polarized scattered light and a 5-nm spectral filter centered at 308 nm. Both the 282-nm Rayleigh return and the 308-nm OH signal are detected using photomultiplier tubes and processed using either a gated photon-counting system or a gated integrator depending upon the signal levels.

Scattered solar flux is by far the most serious noise source for this system. At low altitudes much of the stray light has

been multiply scattered which decreases the polarization of the scattered light thereby increasing the solar contribution. Maximum polarization of scattered solar radiation occurs when viewing 90° to the solar direction and with the platform at the maximum available altitude. Consequently a configuration having a fixed viewing direction can best take advantage of the polarization of skylight when the sun is low in the sky and limits the usefulness of such a system to mid to upper tropospheric altitudes and early morning or late afternoon operation.

The Goddard lidar configuration tends to minimize the fluorescence interference from other sources because there are no foreign objects or sources of contamination near the measurement volume (i.e., no flow tube walls). However, because the current system has no provisions for rapid tuning or double pulsing between on-line and off-line operation, measurements in heavily loaded air (below the boundary layer or in plumes) are precluded.

The proposed narrow-bandwidth lidar system differs from the broadband system primarily in the choice of the excitation and detection wavelengths and the use of a multiple Fabry-Perot etalon for spectral discrimination. The proposed narrow-bandwidth system would use 308 nm excitation instead of 282 nm. Detection would be from the same manifold at 309 nm. Since the individual fluorescence lines arising from the hydroxyl molecule are approximately 0.001 nm wide, one could in principle build a single line detector with a bandpass 5000 times narrower than that of the broadband system (i.e., 5 nm/.001 nm = 5000).

The principal advantage for the lidar configuration gained from operating with a reduced bandpass is the reduction of the background. The 5000x reduction in bandpass would provide a comparable reduction in the scattered solar flux, and therefore in the high background limit the noise is reduced by approximately 70. In addition the $Q_1(1)$ line (307.84 nm) of the (0,0) manifold lies in an absorption feature of the solar spectrum, further reducing the intensity of the solar scatter by an altitude-dependent factor which can be as large as 10. Additional benefits arise from the fact that the absorption cross-section in the (0,0) manifold is about 3 times larger than for the (0,1) transitions. This results in a direct factor of three increase in signal. Finally, the ozone absorption cross-section at 308.6 nm is about 30x smaller than that at 282 nm, and the $O(^1D)$ quantum yield is about 0.55. These two facts combine to reduce the laser-produced OH by a factor of at least 50.

The overall benefits of the narrowband detection scheme are offset to some degree by the lower number of fluorescence photons arising from a single emission line compared to the number in a whole band. Although no studies of the yield of individual lines of OH have been performed, it is estimated that the $Q_1(1)$ line represents about 4% of the total band strength. Accounting for this reduction in fluorescence photons results in an estimated

10-fold improvement in overall performance if solar scatter continues to dominate the noise.

(c) Jet Propulsion Laboratory: To date all the field experiments using LIF and lidar systems to detect OH radicals in the atmosphere have used frequency-doubled dye lasers operating near 282 nm. The primary reason for using this excitation wavelength is that the resulting fluorescence is centered near 309 nm which is significantly red-shifted from the laser wavelength so that relatively simple filtering techniques can be used to discriminate between elastically scattered laser light and fluorescence. In this section a 308-nm excitation scheme as proposed by the JPL group (Laudenslager et al., 1980, 1981, 1982, 1984; McDermid et al., 1983a, b, c, d) will be discussed in terms of its potential for reducing NRF and laser-induced OH interferences and increasing the OH fluorescence signal. The components required for implementation of this scheme and some of their advantages are also considered.

Figures 1 and 2 illustrate schematically the 282-nm and 308-nm excitation schemes. In the 282-nm scheme OH is excited to the v'=1 level; different rotational transitions correlating with low rotational levels of the ground state can be used for excitation. In order to be detected at 309 nm the v'=1 level must be relaxed by collisions with atmospheric molecules, principally N_2 and O_2, to the v'=0 level. Both V-T and R-T processes occur with almost unity collision efficiency and with multiquantum (R) transitions showing appreciable probability, ultimately producing close to a Boltzmann population distribution in the excited state. Competing with relaxation is electronic quenching which drastically reduces the fluorescence efficiency, especially in the troposphere. It has been shown that the rate constants for electronic quenching show a dependence on the rotational and vibrational state (McDermid and Laudenslager, 1980, 1982; Copeland and Crosley, 1984). Thus, if the fluorescence intensity at 309 nm is to be used to infer hydroxyl radical concentrations, the rate constants for all the state-to-state energy transfer processes must be known and incorporated into a kinetic model of the excited state. This is an extremely complex problem and is directly impacted by the accuracy and completeness of the data set of state-to-state rate constants. For excitation at 308 nm directly into the v'=0 level the effects of vibrational relaxation can be eliminated from the analysis. Quenching and rotational relaxation must still be considered but far fewer levels are involved, allowing more detailed and precise calculations to be made (McDermid et al., 1983b).

Using excitation at 308 nm immediately realizes an increase in fluorescence since the absorption cross-section is some 3 to 4 times larger than at 282 nm. However, because of the proximity of the laser and emission wavelengths, a high-resolution, high-contrast spectral filter is required. Suitable devices have already been developed for remote sensing experiments, particularly wind

speed measurements (Rees et al., 1981a, 1982a, b; Killeen et al., 1982; Hays et al., 1981), and could readily be adapted to an OH-lidar system.

Figure 6 shows a detailed energy level diagram pertinent to the 308-nm excitation scheme envisioned by the JPL group. Excitation is carried out in the $Q_{21}1$ rotational transition at 307.847 nm to the F_2 manifold of the $^2\Sigma$ excited state. For slow rotation (low J), Hund's case (a) is an appropriate description of the $^2\Sigma$ state; for higher rotational levels in the $^2\Sigma$ state and for all levels of the $^2\Sigma$ state, Hund's case (b) is appropriate. (See Appendix A.) The consequence of this is that the so-called $Q_{21}1$ satellite line is essentially fully allowed and has a similar transition probability to the main $Q_1 1$ line. It has been observed (McDermid et al., 1983c; Stepowski and Cottereau, 1981) that the F_1 and F_2 manifolds of the $^2\Sigma$ state do not mix appreciably, even after collisional relaxation. This result is not surprising from consideration of the coupling between the angular momentum J and the spin S since the process $F_1 <-> F_2$ essentially involves a reversal of the angular momentum vector. This fact has very important consequences regarding the fraction of the total fluorescence which can be detected with a narrow spectral bandwidth filter.

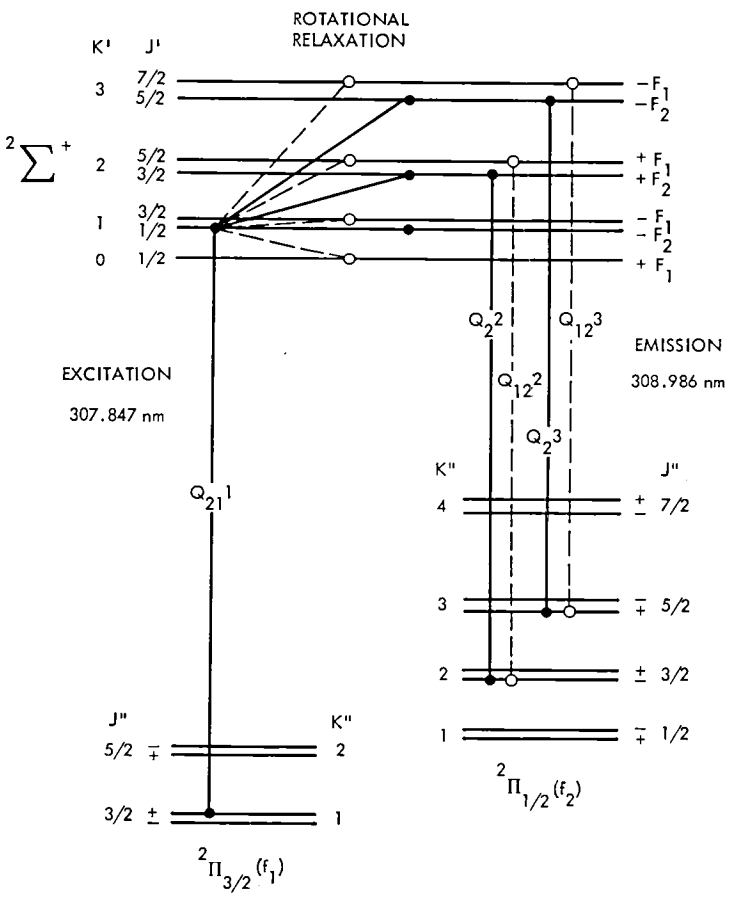

Figure 6. The 308-nm excitation scheme prepared by JPL.

There is a fortuitous overlap, within $\Delta\lambda < 0.001$ nm, of the rotational transitions $Q_2 2$, $Q_{12} 2$, $Q_2 3$, and $Q_{12} 3$ at 308.986 nm, at which wavelength the JPL group proposes to set their detector. It can readily be shown from considerations of the relative rotational transition probabilities that almost 20% of the total fluorescence from a Boltzmann distribution in the F_2 of the $^2\Sigma$ state will be detectable in a 0.001-nm spectral bandpass at 308.986 nm. However, if excitation is to the F_1 manifold then only 3% of the total fluorescence would be observed. This indicates the importance of exciting in one of the satellite branches such as Q_{21}.

A key element in the 308-nm scheme is the use of a triple Fabry-Perot etalon filter with an imaging photon detector (IPD) (Rees et al., 1980, 1981b). The spectral resolution of the filter is ≈0.001 nm and the imaging detector allows simultaneous monitoring of a number of different (relatively closely spaced) wavelengths. Thus it is possible to measure the OH fluorescence, a rotational Raman normalization signal, and the background level simultaneously on a single laser pulse. This eliminates the statistical correlation problems discussed elsewhere in this report and also avoids the need for two laser systems as in the Georgia Tech system. Also, the interferences caused by broadband spectral sources, such as NRF and solar scatter, are greatly reduced. For example, detector bandwidths of approximately 5 nm have been used in the 282-nm scheme. By employing a 0.001-nm filter these interferences would be reduced by a factor of 5000. It is interesting to note that, due to the presence of OH in the Sun, all OH fluorescence lines correspond to absorption features in the solar spectrum. The absorption in the solar spectrum at 308.986 nm is particularly strong because of the overlapping of a number of lines and this leads to an additional reduction in the level of solar scatter by a factor of ≈10 thus giving a total reduction in the interference level from solar radiation of 5×10^4.

The artificial generation of OH through photolysis of ozone as noted for 282-nm excitation can occur in the 308-nm scheme but at a significantly reduced level. The absorption cross section for ozone at 308 nm is 1.28×10^{-19} cm^2 and at 282 nm is 3.7×10^{-18} cm^2. The quantum yield for production of $O(^1D)$ is also reduced at 308 nm, $\phi[O(^1D)] = 0.7$, compared with 282 nm, $\phi[O(^1D)] = 0.9$, at 295 K. At higher altitudes (lower temperatures) the quantum yield at 308 nm falls rapidly. Thus the net interference level is reduced by a factor of ≈40 in the 308-nm scheme and this eliminates the need for special techniques to control this interference. For the same level of artificial OH interference some 40 times more laser energy can be used, within the limits posed by saturation effects (see Appendix B), with a proportional increase in laser-induced fluorescence.

In the 308-nm scheme the energy gap between the excitation and detection wavelengths is ≈100 cm^{-1} and thus vibrational Raman scattering by any atmospheric component is not a potential interference. However, rotational Raman scattering by nitrogen and oxygen has been considered even though the scattering cross-sections are very small (≈10^{-29} cm^2 sr^{-1}). (There is some

uncertainty regarding the absolute magnitude of the Raman cross-section for N_2 at wavelengths shorter than 350 nm.) For excitation in low Q_1, Q_{21}, or P_1 rotational lines there are no overlaps in the proposed detection region near the Q_2 bandhead. The use of nearby Raman lines for normalization is attractive, as noted above.

A promising coherent source for excitation at 308 nm is the XeCl excimer laser. Excimer lasers represent a new class of laser which operates directly in the UV and has good efficiency (>2%). Excimer lasers are high-pressure (typically 1 to 5 atmospheres) transversely excited electric discharge lasers somewhat similar to the TEA CO_2 laser. Transversely excited gas lasers are inherently very rugged and reliable devices if designed properly. To date, several excimer lasers have been operated for many pulses with little loss of output energy on a sealed gas system using fast gas recirculation. Some chemical and particulate cleanup may be necessary, and for the case of the rare-gas/fluoride lasers some gas makeup may also be required. Lasing occurs from bound excited molecules to the ground states of the rare-gas/halide molecules which are unbound or, as is the case for XeCl, very weakly bound. The bound-free transition gives rise to a broad spectral gain bandwidth, typically 1 to 2 nm wide for the excimer lasers. These lasers are scalable to high pulse energies in the ultraviolet (0.1 to 40 J) and with gas recirculation can be operated at high repetition rates (1 to 1000 Hz). The temporal pulse widths of excimer lasers can also be varied from picoseconds to several hundred nanoseconds.

Excimer lasers can be tuned directly over their gas bandwidth using intracavity dispersive optics to obtain narrow spectral output (Pacala et al., 1982, 1984). Table 5 lists the tuning ranges and operational characteristics of the most efficient excimer lasers. Although the various developed excimer lasers do not offer total wavelength coverage in the UV, the high energy output from the excimer laser allows for efficient stimulated Raman shifting of the tuned output to other UV, visible and VUV wavelengths. At JPL the XeCl excimer laser has been operated with narrow spectral bandwidths (<0.001 nm) (Pacala et al., 1984) and has demonstrated direct tuning to several absorption lines of the OH, A-X, 0-0 transition including the $Q_{21}1$ line discussed above. A continuous tuning range from 307.5 to >308.5 nm has been demonstrated at JPL for XeCl. It is interesting to note that the XeBr laser operates in the spectral region suitable for 282 nm excitation of OH. The XeBr laser has a gain region from 281.3 to 282.3 nm and pulse energies of 100 mJ $pulse^{-1}$ have been obtained from such a laser (Sze and Scott, 1978).

The excimer laser source should be customized to meet the needs of atmospheric measurements. In order to achieve long-lived operation on a self-contained gas mixture the laser body must be constructed from the proper materials and some means of gas cleanup should be incorporated into the flow system. To obtain high-repetition-rate operation the design of the electronic

TABLE 5. WAVELENGTH RANGE AND OPERATIONAL CHARACTERISTICS OF SELECTED EXCIMER LASERS

TYPE OF LASER	WAVELENGTH (nm)	EFFICIENCY (%)	ENERGY (J)	PULSE WIDTH (ns)	REPETITION RATE (Hz)	COMMENTS
EXCIMER LASERS						
DISCHARGE						
ArCl	175					MANY λ's EACH TUNABLE OVER 1.0 TO 2.0 nm. NARROW SPECTRAL WIDTH. SINGLE MODE HAS BEEN DEMONSTRATED, FROM OSCILLATOR-AMPLIFIER, 1 kHz REPETITION RATE REQUIRES GAS RECIRCULATION.
ArF	193-194					
KrCl	221-223					
KrF	248-249	0.1-4	0.1-40	1-250	1-1000	
XeBr	282-282					
XeCl	307-309					
XeF	351-353					
EXCIMER PUMPED DYE (XeCl-308 nm)						
FUNDAMENTAL	320-800	0.1-0.2	<0.12	1-100	1-1000	A LONGER VISIBLE WAVELENGTH EXCIMER WOULD BE MORE EFFICIENT AS A DYE PUMP.
FREQUENCY DOUBLED	220-320	0.01	<0.08	1-50	1-1000	
RAMAN SHIFTING OF (XeCl LASER 308 nm)	**STOKES SHIFTS** 1ST	2ND	3RD			
H_2	353	414	499			TUNING OF EXCIMER LASER PRODUCES TUNABLE STOKES OUTPUT.
D_2	339	377	426			
CH_4	338	375	422			
N_2	337	359	392	<50		ANTI-STOKES SHIFTS ALSO POSSIBLE AT LOWER EFFICIENCY.
Tl		405				
Pb		459				RAMAN OSCILLATOR-AMPLIFIER CONFIGURATION IMPROVES EFFICIENCY.
Ba		475				
Bl		475				

circuitry is critical. The concept of magnetic saturable reactor switches has been developed at JPL to solve this problem. In order to obtain narrow-bandwidth tunable operation, an excimer laser oscillator-amplifier arrangement is necessary. Several excimer lasers with Raman shifting cells will probably be suitable for field measurements of multiple species. The design of these components is very much constrained by the parameters required for the particular atmospheric measurement.

In summary, compared to the 282-nm scheme, the 308-nm scheme as proposed by the JPL group would yield an increased fluorescence signal and a reduction in the level of interferences by $>10^4$ thus providing a realistic sensitivity at the [OH] = 1×10^5 molecule cm^{-3} level. Also, the availability of simple, compact and efficient tunable XeCl excimer lasers operating near 308 nm offers advantages for the field instrument. Detection of OH in laboratory experiments has been accomplished using these lasers. The ability to tailor the energy, repetition rate and pulse length of these lasers made them especially suitable for application to the OH measurement problem.

In Situ Systems at Atmospheric Pressure. Three systems or approaches for implementing the in situ LIF technology at ambient pressures for measurements of OH were discussed as part of the workshop. These systems are now described.

(a) Georgia Institute of Technology:

In situ sampling at atmospheric pressures represents one of the most direct and earliest approaches for implementing the LIF technique for OH measurements. One of the first groups to initiate this approach from both ground based and airborne platforms was from the University of Maryland and is now at Georgia Tech. This section will describe the current state of technology of the Georgia Tech LIF in situ system.

The basic excitation scheme of the Georgia Tech approach consists of 282-nm excitation with detection of OH fluorescence at 309 nm using an ≈ 5-nm narrow-bandwidth filter. The LIF system at Georgia Tech has been designed to minimize two of the dominant noise sources plaguing in situ ambient pressure systems; i.e., laser-generated OH and broadband nonresonant fluorescence. The method used for reduction of OH interference has been that of reducing the laser pulse duration as was first suggested by Wang et al. (1976) and Hanabusa et al. (1977) and then again by Davis et al. (1981b). The rationale for short pulses was discussed in the previous section. In particular, if the excitation pulse can be made sufficiently short, then the lifetime of the $O(^1D)$ (and consequently the OH) produced by photolysis of O_3 lags the laser pulse. The approach to minimize broadband nonresonant fluorescence is, in part, based upon results obtained by Davis et al. (1981a, b) during the GAMETAG missions which clearly indicated that one of the dominating noise sources was temporally uncorrelated background fluorescence. One obvious approach to correct for a broadband background noise source is to measure the signal + background at λ_{on} = 282 nm and the background only for λ_{off}, slightly different from λ_{on}. However, because of the uncorrelated nature associated with this background noise, the λ_{off} signal must be obtained close enough in time to effectively freeze the atmospheric component contributing to the fluorescence.

The optical hardware for the Georgia Tech system is illustrated in top and side views in figure 7. The sample probe is illustrated in figure 8. The salient features of this configuration are (1) the use of two Nd:YAG laser pumped, frequency-doubled dye laser systems for generation of λ_{on} and λ_{off} wavelengths; (2) pockel cells to achieve short pulses; (23) 282-nm excitation with 308-nm detection and (4) an OH calibration system. The two complete laser systems provide the mechanism for obtaining the λ_{on} signal (e.g., OH signal plus background) and the λ_{off} signal (e.g., background only) with control of the temporal separation of the two signals down to less than 1 msec. With the use of the pockel cells, UV excitation pulses in the range of 0.15 ns to 4.5 ns can be achieved starting from a basic laser pulse width of 9

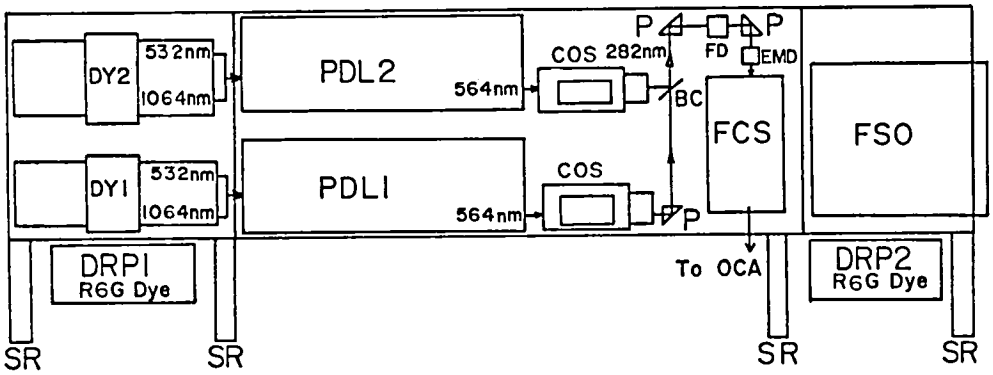

DRP - Dye Reservoir and Pump
DY - Frequency Doubled Nd:YAG Laser
EMD - Energy Monitor Diode
FCS - Frequency Calibration System
FD - Fast Diode
FSO - Fast Sampling Oscilloscope
OCA - Optical Coupling Arm
P - 90° Prism
PDL - Pulsed Dye Laser
SR - Seat Rail
BC - Beam Combining Mirror
COS - Complex Optical System

(a) Top view.

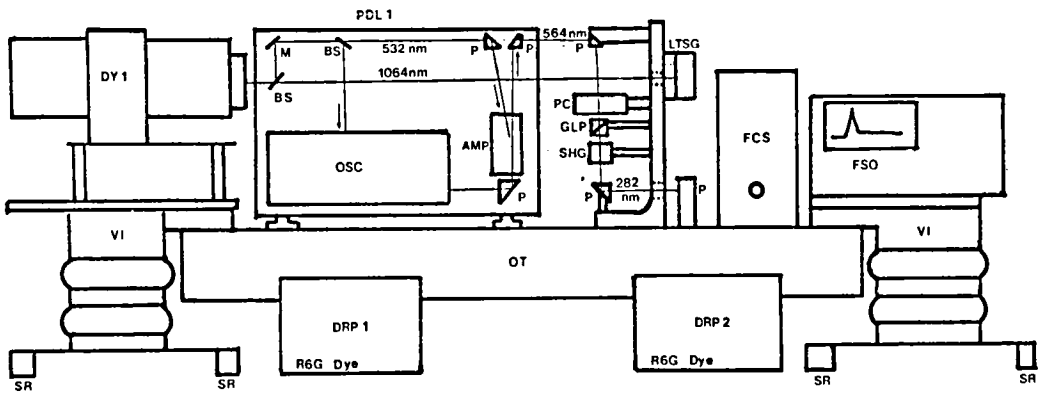

AMP - Dye Laser Amplifier
BS - Beam Splitter
DY - Frequency Doubled Nd:YAG Laser
DRP - Dye Reservoir and Pump
FCS - Frequency Calibration System
FSO - Fast Sampling Oscilloscope
GLP - Glan Laser Polarizer
LTSG - Laser Triggered Spark Gap
M - Mirror
OSC - Dye Laser Oscillator
OT - 2' x 6' Optical Table
P - 90° Prism
PC - Pockel Cell
PDL - Pulsed Dye Laser
SHG - Second Harmonic Generation Crystal
SR - Seat Rail
VI - Vibration Isolator

(b) Side view.

Figure 7. Georgia Tech OH system.

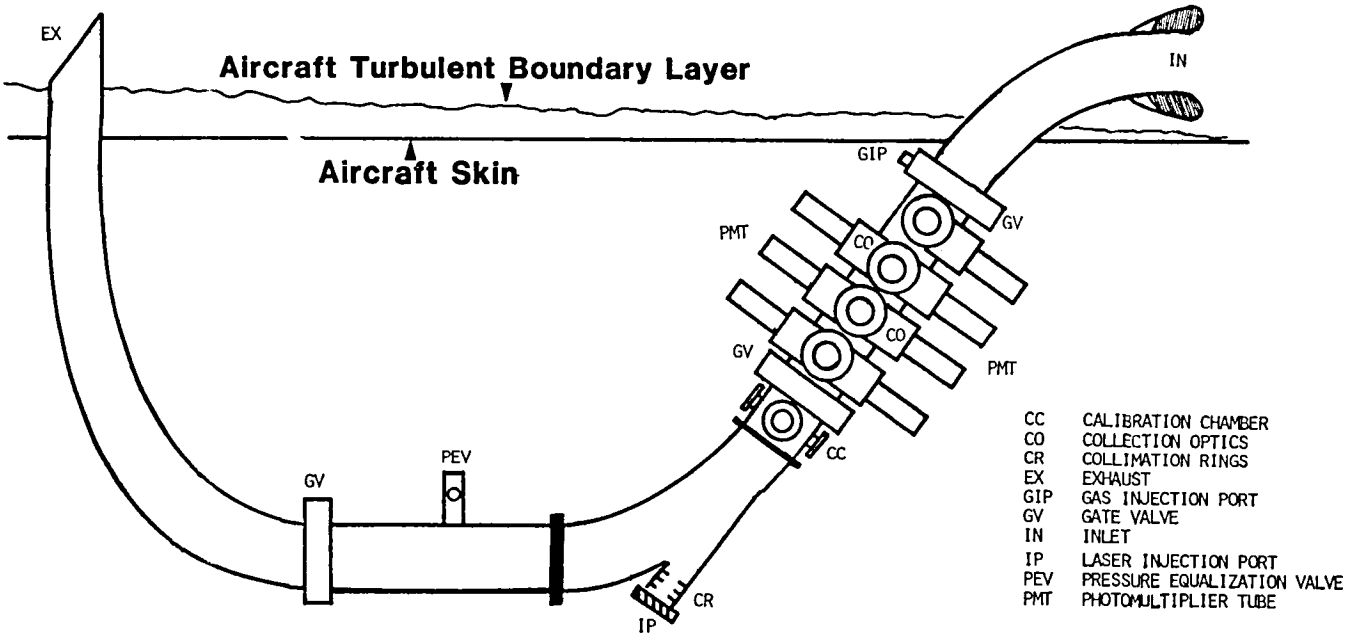

Figure 8. Georgia Tech OH sample chamber.

ns. The currently demonstrated reduction in the laser-generated OH O_3/H_2O interference utilizing a pulsewidth of 0.5 ns is a factor of 10 relative to that observed from a 9-ns pulse.

An important component of any in situ sampling system is the sample chamber and associated inlet plumbing. This is particularly true for a reactive trace species such as OH. The Georgia Tech OH sampling manifold shown in figure 8 has been designed for aircraft operation and can be completely sealed off from the aircraft cabin. Full aperture gate valves on both ends of the OH fluorescence chamber permit the isolation of the chamber while the aircraft is on the ground, thus preventing excessive contamination of the chamber liner. These gate valves also serve to isolate the fluorescence chamber from rain and snow while operating under severe flying conditions. In the latter regard when water droplets do appear on the laser injection window, a third gate valve can be closed and a pressure equilibration valve opened. At this point, the laser injection window can be taken off and cleaned without disrupting the aircraft cabin pressure. The intake manifold consists of a 3.5-in. i.d. black anodized pipe (Teflon coated) which is bent through an arc of ~ 50°. For typical tropospheric conditions the lifetime of OH is on the order of 1 to 2 sec and the radial diffusion time at tropospheric pressures is on the order of 90 to 200 msec. Since the time of transit of an OH molecule to the point of sampling for an aircraft air speed of 130 knots is 30 ms, OH losses due to homogeneous chemistry are negligible. Note also that the fluorescence chamber shown in figure 8 has been designed to handle as many as 12 PM

tubes and associated optics thereby permitting efficient use of the available excitation energy. The use of multiple PMT's is, in effect, similar to the use of a multipass excitation chamber, but, based on the Georgia Tech group's experience, results in lower total noise levels than a multipass system.

One of the more attractive features of the in situ sampling systems is the potential for direct absolute calibration in terms of known OH concentrations. Figure 8 also shows the position of a calibration chamber in which known amounts of OH can be generated, although at levels well above ambient for calibration. A gas injection port (GIP) for injection of a gas to scavenge ambient OH from the air stream is also available.

Although several noise sources contribute to defining the operational signal-to-noise ratio for the aircraft system, fluorescence from the walls of the sample chamber is an important one directly associated with the design of the chamber. This noise source is derived from scattered 282-nm radiation being absorbed by small amounts of contaminants on the walls of the chamber. The photon noise from N_2 and CH_4 Raman scattering and aerosol fluorescence is normally much lower than that of wall fluorescence under clean tropospheric air conditions. However, when sampling in continental boundary layer air over geographical regions where significant anthropogenic sources are present, the atmospheric aerosol loading is at least 10-50 times higher than in remote tropospheric boundary layer air, and the corresponding noise signal approaches, and in some cases exceeds, that from wall fluorescence. The solar flux noise source is typically three orders of magnitude lower than that resulting from wall fluorescence. This is a direct result of both the design characteristics of the collection optics and the use of time gating on the signal processing electronics.

(b) Harvard University:

As with the other LIF systems discussed in this report, a central concern of the Harvard group is the need to minimize photochemical OH interference while providing a system that can be directly calibrated for response to known amounts of OH and for evaluating system and background noise in the absence of OH. The basic scheme utilizes 282-nm excitation with detection of the 309-nm fluorescence in an in situ sampling configuration. The distinguishing features of the system proposed by the Harvard group are (1) the use of a high pulse rate, low pulse energy copper (Cu) vapor laser source; and (2) a system configuration for calibration and noise measurements.

Figure 9 illustrates the system proposed by the Harvard group. As noted earlier, laser-induced OH is, among other parameters, dependent upon the laser pulse width and the peak flux. In particular, it is generally recognized that to minimize this OH interference, a short laser pulse and/or low peak flux is desirable. Conversely, to maximize system sensitivity, high average powers and/

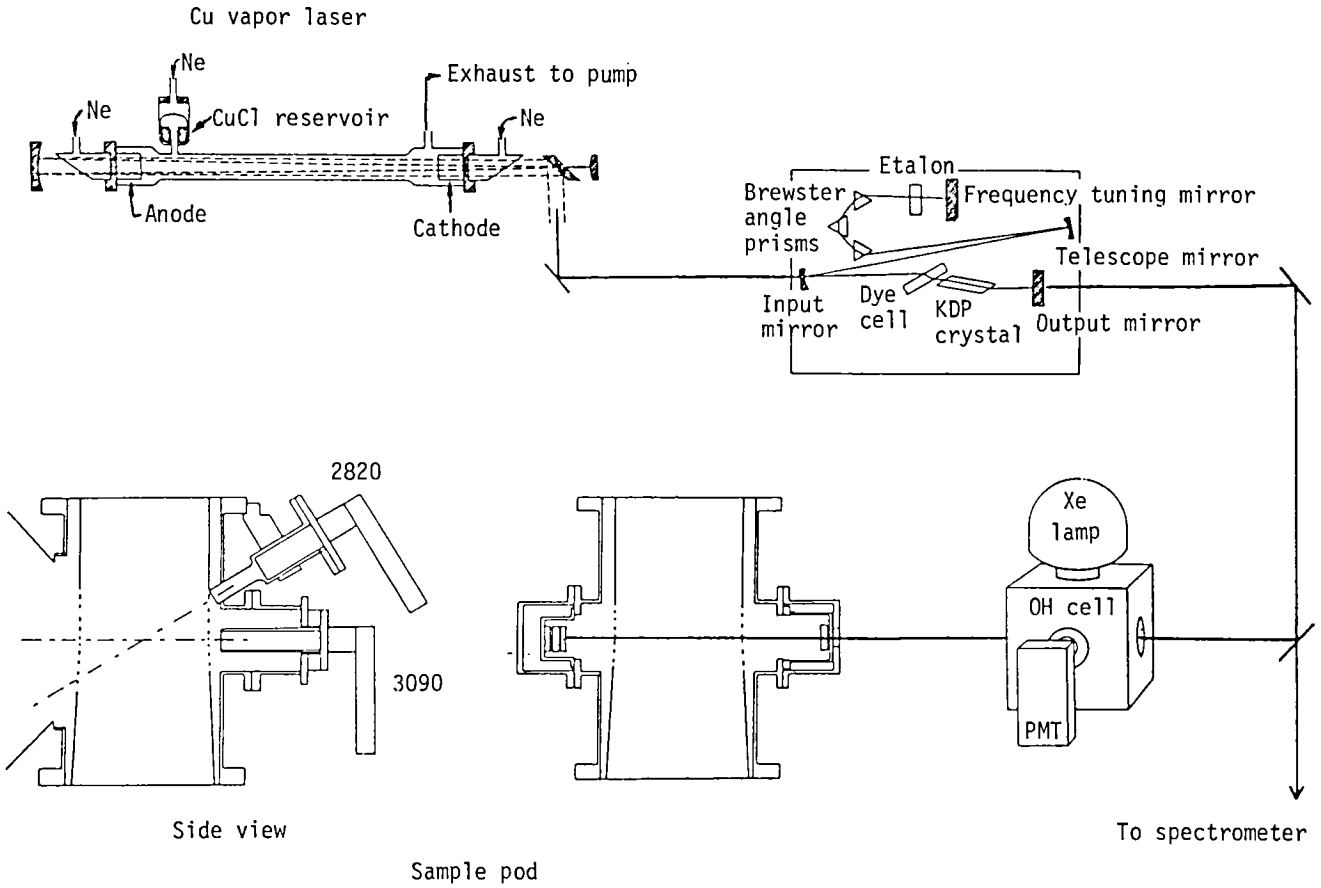

Figure 9. Schematic drawing of proposed Harvard Univ. optical system.

or high peak flux are desirable. To accommodate these conflicting goals, the system approach suggested by the Harvard group is the use of a high-repetition-rate pulsed laser to provide high average powers with low peak flux. In particular an atomic copper vapor laser is proposed as the source to pump a dye laser which is in turn doubled into the ultraviolet spectral region. This is in fact the approach that has been developed by the Harvard group for balloon-borne stratospheric OH measurements. The proposed Cu-laser system would operate at rates in the 15 to 20 kHz range at 510.6 nm. This system would provide an average output power of 20 W, corresponding to 1 mJ/pulse and a peak power of 50 kW with a 20-nsec pulse width. This would be used to pump a dye laser for a projected output at 282 nm with a spectral bandwidth of <5 GHz and an average power of 50 mW.

The advantages expected from such a system are illustrated in figure 10 (Stimpfle and Anderson, 1982), where R, the ratio of the fluorescence from OH formed photochemically in the laser pulse to that from ambient OH, is plotted against the pulse repetition frequency at a fixed average power. The values of R shown here

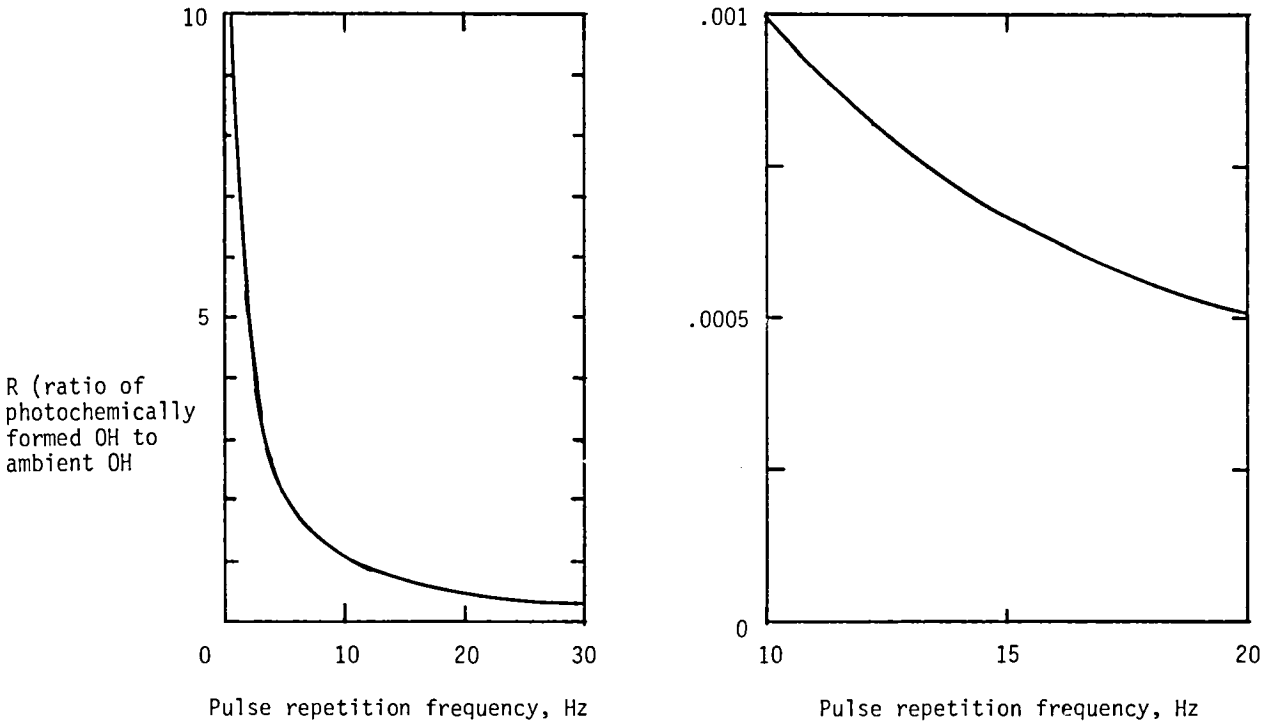

Figure 10. Influence of varying the pulse repetition at a fixed average energy.

are calculated assuming that each pulse interrogates a different sample volume element. Note that for a fixed average power, the peak laser flux must decrease with increasing repetition rate. It is clear that under the assumed conditions, the fluorescence from laser-induced OH is drastically reduced at the higher repetition rates. The dependence of the OH interference for the Harvard approach was discussed in the previous section and given by equation (10). It was noted in the previous section that the OH interference could be reduced as much as desired (e.g., E approaching 0) but at the expense of the signal-to-noise ratio. Accordingly it is important to realize that the results illustrated in figure 10 are constrained by the requirement that each laser pulse interrogate a new sample volume element. To realize this the characteristic sample element length and the laser repetition rate must be consistent with the time required for the sample air flow through the sample chamber.

The sample chamber proposed in the Harvard system is an aerodynamic pod mounted exterior to the aircraft fuselage. The proposed design of the pod would include a multipass cell for increasing traversals of the UV beam through the scattering volume and PMT's with interference filters for wavelength discrimination. The proposed pod would permit injection of C_3H_6, O_3 and H_2O at the entrance of the pod during flight. Injection of the C_3H_6 would be designed to scavenge ambient OH from the airstream there-

by permitting inflight background noise measurement in the absence of ambient OH. Injection of O_3 and H_2O would provide the possibility of evaluating the susceptibility of the system to laser-induced OH. And finally, a Lyman α lamp coupled with a light trapping cell would be located upstream of the detection axis as a means to photodissociate H_2O to produce OH. This would provide a mechanism to demonstrate that the OH detection system was operating and give a rough check on the OH sensitivity.

In Situ Systems at Low Pressure. One of the approaches that is currently being pursued at Portland State University and Institut für Chemie, KFA, Julich, for minimizing background noise is referred to as baric filtering. The group at Portland State University refers to this technique as fluorescence assay with gas expansion (FAGE). (See, e.g., Hard et al., 1979, 1980.) In this mode of operation the basic OH excitation scheme can utilize either the 282-nm or the 308-nm excitation scheme described above. The salient feature of the baric filtering is that the excitation of OH occurs in a partial vacuum. Because of this, one of the more interesting aspects of this approach is that there is typically a time delay between the excitation and the fluorescence event. This offers the potential for temporal discrimination between the OH fluorescence and background noise. Much of the background interference occurs simultaneously with the laser pulse while the temporal behavior of the OH fluorescence is controlled by radiative lifetime and collisional quenching. At low pressure, the OH fluorescence is delayed with respect to the excitation pulse. Moreover for most molecules nonradiative deactivation processes dominate at atmospheric pressures, and under these conditions the fluorescence efficiency is low. If the gas sample is excited at low pressures, the increase in fluorescence efficiency compensates for the decrease in density of the target species thereby leaving the fluorescence per unit excited volume nearly constant. For OH the radiative lifetime of the $A^2\Sigma$ state is approximately 700 nsec. In the pressure range of a few torr, net lifetimes of 100 to 300 nsec are achieved, permitting the use of time-delayed detection to suppress the early background due to Rayleigh, Mie and Raman scattering and rapidly decaying NRF. This time delay reduces the need for spectral filtering, especially with 308-nm excitation, where the required spectral resolution would otherwise be high but where the excitation cross section is largest.

Figure 11 illustrates a typical timing sequence for the baric filtering approach. The PMT is gated off during the laser excitation pulse to avoid saturating effects. After the laser pulse departs from the excitation cell, the PMT is switched on. Still later, after a total delay that is adjustable, the gated charge integrator or gated photon counter is switched on for an adjustable duration. The optimal gate time is dependent upon the signal strength for the background and the OH fluorescence. The best SNR that can be achieved by gating out a single fluorescence background is

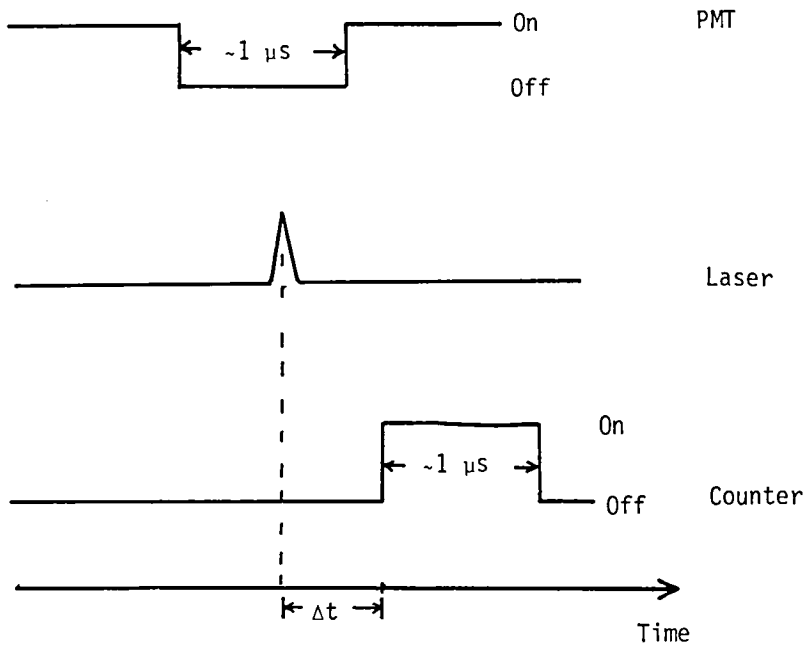

Figure 11. Typical timing sequence for baric filtering.

$$SNR_{max} = S\left(\frac{2k_B/k_S - 4}{2k_B/k_S - 3}\right)^{1/2}$$

where the k's are the observed fluorescence decay rates for the background (B) and signal (S), and S is the OH signal strength. This reduces to the signal-limited case ($SNR = S^{1/2}$) for $k_B >> k_S$. It is significant that this limit can always be theoretically reached, whenever $k_B >> 2k_S$. Furthermore, the maximum SNR rises very rapidly with k_B/k_S, as shown in figure 12, reaching 80% of the limiting value when the rate constant ratio R has increased from 2 to 3.

Another advantage of baric filtering is the reduction of photolytic interference, caused by laser-induced photolysis of other molecules to produce OH. While laser-induced OH interference is still present, transient kinetic effects (e.g., excitation photons leaving the detection zone before an appreciable quantity of OH is produced) reduce its dominating characteristics. The Portland State University group has experimentally verified the absence of photolytic interference in their system by sampling room air at 45% RH, enriched with ozone to a concentration of 3.9 ppm. After expansion to 4 torr, no OH signal was observed at the 10^6 cm^{-3} level, with or without delayed gating. When the delay was removed and the final pressure was raised to 150 torr, photolytic interference equivalent to an ambient OH concentration of 8×10^7 cm^{-3} was observed. From the latter observation, a worst-case interference at 4 torr is calculated to be equivalent to 1×10^5 OH cm^{-3}

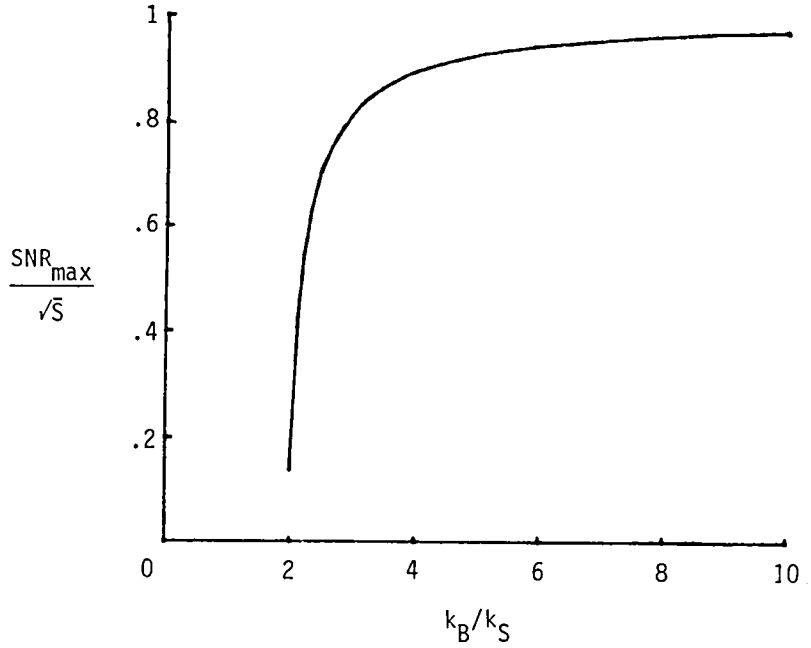

Figure 12. Effectiveness of optimally delayed gating vs. ratio of first-order decay rate constants of a fluorescent background B and signal S.

in ambient air containing 5×10^{12} O_3 cm^{-3} and 2.5×10^{17} H_2O cm^{-3}. Tests have also been conducted using H_2O_2 and HONO; these gases are weaker absorbers at 282 nm, but they offer less temporal suppression of this interference (Hard et al., 1980). H_2O_2 at ~ 100 ppm and HONO at ~ 0.1 atm, with subsequent dilution by a factor not greater than 1000, give detectable interference equivalent to 10^7 OH cm^{-3}. This translates to negligible interference for the baric filtering technique at ambient concentrations of these gases. Finally, since there are other possible photolytic parents, air from a propene/NO_x smog chamber reaction was sampled in the NO, NO_2 and O_3 regimes, and in each case the OH signal disappeared after the lights were turned off.

A particularly attractive feature of the baric filtering technique is the possibility of calibration of the overall system. Because the inlet flow rate in the baric filtering approach is relatively low, absolute calibration can be obtained by sampling from a chamber containing a known amount of OH. In a closed chamber irradiated by UV fluorescent lamps or sunlight, the OH concentration can be measured by the rate of disappearance of a more abundant species with which only OH reacts, provided the reaction rate constant is available from other work. One approach that has been used by the Portland State University group involves the use of an irradiated 150-liter Teflon bag containing a propene/NO/H_2O starting mixture. The propene concentration is measured repetitively by gas chromatography with flame ionization detection. Because propene is also removed by reaction with ozone, the calibration is restricted to the NO-rich regime. The calibration procedure suggested by the group from Institut für Chemie consists

of generating known amounts of OH in the vicinity of the inlet orifice through photodissociation of H_2O by Lyman α radiation. Careful design of a calibration flow system would permit a direct calibration of a low-pressure sampling system.

The main disadvantage of the expansion method is the loss of OH by wall reactions. About 50% of the measured species is currently estimated to be lost in the sampling process. Uncertainties in the many factors entering this calculation illustrate the importance of an absolute calibration as well as proper aerodynamic design.

Comparison of LIF Measurement Techniques

A significant portion of the time at the workshop for those participants cognizant of the LIF techniques was devoted to two activities: (1) the development of a central equation describing the LIF process and the various systems for implementation of the LIF technique and (2) the estimation of the performance of each of the systems described above. The results of these activities are presented in this section.

Central LIF Equation. - The variety of LIF techniques (as well as others) that are currently under development or have been proposed is a testimony to the importance as well as the difficulty of obtaining valid measurements of tropospheric OH. While the mathematical basis for LIF detection has been reasonably well understood for many years, the participants of the workshop felt that the development of a "central equation" which encompassed the different nomenclatures/forms of equations used to describe different OH LIF sensors would prove valuable both to those groups directly involved in such measurements as well as to the broader atmospheric chemistry scientific community. Moreover, the development of a "central equation" from which the working expression for each LIF instrument could be extracted as a specialized case would provide a common basis for comparisons of current and future LIF systems.

The approach used was first to provide a spectroscopic description of the energy levels and transitions employed in the LIF methods for the structural details of the OH radical. Second, the so-called central equation was derived by relating the expected count rate in a LIF system to the absolute OH concentration. Finally, the assumptions and/or approximations necessary to extract a working expression for each LIF approach from the central equation were explicitly stated. This then related the approach and observed quantities of an LIF technique described in the previous section to the central LIF equation. This effort resulted in agreement among the participants on the values of all parameters to be used relative to the spectroscopic details of the OH radical and provided a common language for the discussion of system details. A detailed discussion of the development of the fundamental equation resulting from this effort is presented in Appendix A. The central equation and the working expression for each LIF technique are given in figure A7 and will not be repeated here.

It was also recognized that these fundamental equations did not address the issue of saturation phenomena in LIF measurements. Since saturation effects are very complex and mathematical analysis quite difficult, it was decided that a brief discussion should be included with a particular emphasis on the status of work in this area. This discussion is presented in Appendix B.

Performance Estimates. As a result of the workshop activities related to agreement upon the central LIF equation (discussed in the previous section) and the development and comparison of the working expressions for OH interference (discussed in an earlier section), the anticipated and in some cases the achieved performances of several LIF techniques were compared for common sample atmospheric conditions. Since the implementation approaches were in different stages of development, one estimate was made for current capability and another was based upon anticipated technology improvements or proposed systems. Tables 6 and 7 present these performance estimates in the form of signal-to-noise ratios. Two test atmospheres were postulated, each of which contained a concentration of 5×10^6 OH cm^{-3}. A tropical marine boundary layer was assumed with 1 atm total pressure, 25 ppbv ozone, and 25 torr water vapor. A middle tropospheric condition was assumed with 0.5 atm total pressure, 60 ppbv ozone, and 0.3 torr water vapor.

It has been noted earlier that the OH interference and OH fluorescence signals are both a function of the laser energy. Since the OH interference is a corrective term, the SNR can in principle be made as large as desired by increasing the laser energy. In practice however the laser-generated OH becomes too large to be realistically correct. Accordingly, a ground rule for this comparative evaluation was established such that the level of laser-induced OH must be less than 20 percent of the true OH concentration. The level of interference calculated for each LIF approach is given at the head of each column along the row denoted "Laser-Generated OH". The basis of comparison is the expected signal-to-noise ratio for the assumed conditions. Integration times of 1 and 20 minutes (e.g., column 1) were assumed for this evaluation. Two levels of background NRF noise (e.g., column 2) were assumed. While the nature of its origin and its meteorology have not been established, its magnitude was assumed to be proportional to detector bandwidth, and values of 10^7 to 10^8 equivalent hydroxyl radicals cm^{-3} for a 2.7-nm bandwidth are typical for both boundary layer and midtropospheric atmospheres, with the smaller figure applying to over-ocean midtropospheric observations. The variance of NRF background exceeds Poissonian by a "Degradation Factor" (column 3) which depends upon the design of the instrument, specifically the time interval between "on-line" and "background only" measurements. This degradation factor is expected to be unity when this interval is short, and at 1 sec the Ford group has observed a value of 5 (unpublished results).

TABLE 6. SIGNAL-TO-NOISE RATIOS ([OH] = 5×10^6 cm^{-3}) BASED UPON CURRENT TECHNOLOGY

INTEGRATION TIME (min)	OH EQUIVALENT BACKGROUND (molec cm^{-3})	DEGRADATION FACTOR	FORD (SNR)	GEORGIA TECH (SNR)	PORTLAND STATE (SNR)
	MARINE BOUNDARY LAYER (1 atm, 25 ppb O_3, 25 torr H_2O)				
	Laser-Generated OH (molec cm^{-3})		3.5×10^5	5×10^5	4×10^4
1	10^7	1	----	11.0[a]	2.2
		5	----	b	0.4
		20	----	b	0.1
	10^8	1	----	3.8[a]	1.9
		5	----	b	0.4
		20	----	b	0.1
20	10^7	1	----	49.0[a]	9.8
		5	8[c]	b	2.0
		20	----	b	0.5
	10^8	1	5[c]	17.0[a]	8.5
		5	----	b	1.7
		20	----	b	0.4
	MIDDLE TROPOSPHERE (0.5 atm, 60 ppb O_3, 0.3 torr H_2O)				
	Laser-Generated OH (molec cm^{-3})		2.2×10^4	3×10^4	3×10^2
1	10^7	1	----	16.0[d]	2.2
		5	----	b	0.4
		20	----	b	0.1
	10^8	1	----	5.3[d]	1.9
		5	----	b	0.4
		20	----	b	0.1
20	10^7	1	----	69.0[d]	9.8
		5	16[e]	b	2.0
		20	----	b	0.5
	10^8	1	----	24.0[d]	8.5
		5	10[e]	b	1.7
		20	----	b	0.4

[a] For the background levels given, the minimum detectable concentration (MDC) for a S/N = 2 ranges from 2.6×10^5 cm^{-3} to 8.3×10^5 cm^{-3}. However, based upon information from GAMETAG flights as to the background levels, the Georgia Tech group feels a more conservative MDC for a S/N = 2 ranges from 8×10^5 cm^{-3} to 1.5×10^6 cm^{-3} for 20-minute integrations.

[b] Poisson statistics are applicable due to short on/off resonance time; therefore no degradation due to NRF is expected.

[c] Actual performance level for ground-based operation with integration time of 30 minutes.

[d] For the background levels given, the minimum detectable concentration (MDC) for a S/N = 2 ranges from 1.8×10^5 cm^{-3} to 5.8×10^5 cm^{-3}. However, based again on information from the GAMETAG flights as to the background levels, the Georgia Tech group feels a more conservative MDC for a S/N = 2 ranges from 3×10^5 cm^{-3} to 6×10^5 cm^{-3} for 20-minute integrations.

[e] Projected performance level based on actual ground-based performance with integration time of 30 minutes.

TABLE 7. SIGNAL-TO-NOISE RATIOS ([OH] = 5×10^6 cm^{-3}) BASED UPON ANTICIPATED TECHNOLOGY IMPROVEMENTS

INTEGRATION TIME (min)	OH EQUIVALENT BACKGROUND (molec cm^{-3})	DEGRADATION FACTOR	FORD (SNR)	GEORGIA TECH (SNR)	GODDARD BROADBAND (SNR)	GODDARD NARROWBAND (SNR)	HARVARD (SNR)	PORTLAND STATE (SNR)
MARINE BOUNDARY LAYER (1 atm, 25 ppb O_3, 25 torr H_2O)								
	Laser-Generated OH (molec cm^{-3})			2.5×10^5	1×10^6	1×10^6	1×10^6	1×10^5
1	10^7	1	---	25.0[a]	b	b	12.0	3.5
		5	---	c	b	b	6.1	0.7
		20	---	c	b	b	3.1	0.2
	10^8	1	---	8.5	0.1	4.8	4.4	3.0
		5	---	c	d	d	2.0	0.6
		20	---	c	d	d	1.0	0.1
20	10^7	1	---	110.0[a]	b	b	5.6	15.5
		5	16	c	b	b	2.7	3.1
		20	---	c	b	b	1.4	0.8
	10^8	1	---	38.0[a]	0.5	22.0	1.9	13.4
		5	10	c	d	d	8.8	2.7
		20	---	c	d	d	4.4	0.7
MIDDLE TROPOSPHERE (0.5 atm, 60 ppb O_3, 0.3 torr H_2O)								
	Laser-Generated OH (molec cm^{-3})			1.5×10^4	1×10^6	1×10^6	2.6×10^4	7.5×10^3
1	10^7	1	---	36.0[e]	2.7	8.1	35.0	3.5
		5	---	c	d	d	7.0	0.7
		20	---	c	d	d	1.8	0.2
	10^8	1	---	12.0[e]	b	b	12.1	3.0
		5	---	c	b	b	2.4	0.6
		20	---	c	b	b	0.6	0.1
20	10^7	1	---	154.0[e]	12.2	36.0	157.0	15.5
		5	32	c	d	d	31.4	3.1
		20	---	c	d	d	7.9	0.8
	10^8	1	---	54.0[e]	b	b	55.0	13.4
		5	20	c	b	b	11.0	2.7
		20	---	c	b	b	2.8	0.7

[a] Based upon GAMETAG flight information relative to the background levels, the Georgia Tech group believes a more realistic estimate of the minimum detectable concentration (SNR = 2) to be in the range of 3.5×10^5 cm^{-3} to 7×10^5 cm^{-3} for a 20-minute integration time.

[b] Background dominated by solar noise, results for 10^7 and 10^8 background are the same.

[c] Poisson statistics are applicable due to short on/off resonance time; therefore no degradation due to NRF is expected.

[d] Background dominated by solar noise, Poisson statistics are applicable.

[e] For the same reason noted in footnote (a) the minimum detectable concentration (SRN = 2) is estimated to be in the range of 1.4×10^5 cm^{-3} to 3×10^5 cm^{-3} for a 20-minute integration time.

With the exception of the entries in table 6 by the Ford group, the SNR's are computed from the working signal expressions given for each group in Appendix A. Appendices C - G were provided by the respective groups to describe the numerical calculations leading to the entries in tables 6 and 7.

Among the groups providing entries for table 6, only Ford and Georgia Tech have systems that are aircraft ready and have in fact been flight tested. The LIF techniques not specifically listed are not sufficiently developed to warrant comparison in the "Current Technology" table. The performance levels given for the Ford system are based upon measurements obtained from a ground-based platform and for a 30 minute integration time. Also, the Ford entries are given only for a degradation factor of 5, corresponding to the actual degradation noted by the Ford group with a 1-second delay between their λ_{on} and λ_{off} wavelengths. It is important to note that the SNR's given for the Ford system have not been achieved under flight conditions. Entries are given for the Georgia Tech system only for a degradation factor equal to 1. Recall that the Georgia Tech system utilizes two laser systems, which permits λ_{on} and λ_{off} signals with temporal separations of less than 1 msec. The NRF between λ_{on} and λ_{off} is expected to be correlated, resulting in no degradation in SNR with integration time (e.g., see footnote b to table 6). Note also that the SNR calculated for the test conditions established by the workshop is considerably larger than that actually expected by members of the Georgia Tech Group (e.g., see footnote a to table 6). The performance given in footnote a for the Georgia Tech system is based upon flight experience and in particular reflects the fact that the Georgia Tech Group considers the background noise adopted for this comparison as too optimistic. It is of interest to note that the predicted laser-generated OH interference is comparable for the two atmospheric LIF systems but is about an order of magnitude lower for the Portland State system which employs low-pressure excitation.

The anticipated improvements in the performance of those systems listed in table 6 as well as the anticipated performance of proposed systems are given in table 7. The improvements in performance for the three systems also listed in table 6 are typically less than a factor of 2. In general the new technology improvements represent higher laser pulse frequency, providing more signal per unit integration interval, shorter pulse width, and improved spectral resolution for better background discrimination. The Ford group also included improvements in optical configuration which will provide higher signal throughput. The additional three systems included in table 7 represent approaches that are anticipated with in the next 2 to 5 years. Note that the Goddard approaches included in table 7 are uniquely limited by solar scattering rather than NRF background.

Summary Comments. Although the literature is sizable and rapidly growing, the LIF technique is still young as a means of making

hydroxyl measurements under ambient conditions. This fact is reflected most strongly in the uncertainty which exists on the question of whether or not the best variant of the technique has been identified. Remote (lidar) and in situ (atmospheric and low pressure) variants which are being investigated have been described. The agreement on the mathematical formalism developed at this workshop should, through its usage by workshop participants and other investigators in their future work, aid in the presentation and understanding of current and new ideas for the advancement of the LIF techniques. From the performance intercomparisons some maturity seems evident in the nearness with which several variants are approaching a common standard of performance. The temptation is to conclude that perhaps each of them has been nearly optimized by adjustment of instrument parameters to offer results as good as that variant of technique permits. The temptation to reach this conclusion should probably be resisted a little longer.

Indirect Methods

Indirect methods for determination of ambient OH concentrations are based upon the reaction of OH with a given tracer gas. The abundance of the tracer gas must be known before and after reaction with OH and the reaction rates must be known. Two indirect approaches were discussed during the workshop. The first, referred to here as the global average approach, relies principally on the global mass balance of certain trace constituents and accordingly provides a globally averaged estimate of tropospheric OH. The second approach referred to here as the radiochemical approach is an in situ sampling technique that relies on measuring the production of $^{14}CO_2$ via reaction of ^{14}CO and OH. Details of both of these approaches are discussed below.

Global Average. Effective utilization of this approach for OH determination requires that the tracer species satisfy a number of conditions:

- Its atmospheric abundance in time and space must be accurately defined.
- It must be known that removal occurs predominantly by reaction with OH and the rate constants must be accurately determined.
- The sources and source distributions in time and space must be accurately known.

Within this framework the uncertainties are further reduced if reaction with OH has modest or low activation energy and the molecule is reasonably long lived.

Over the last decade attempts have been made with tracer chemicals that are either predominantly natural in origin or pre-

dominantly anthropogenic in origin. ^{14}CO and ^{12}CO are two of the naturally occurring tracers that have been utilized to estimate OH levels. The ^{12}CO sources however are so complex and varied that such an approach is at best unreliable. The problem of complex sources is minimized, although not eliminated, when ^{14}CO is utilized. The dominant source of ^{14}CO is cosmic rays and this source is independent of season and latitude. Compared to the cosmic ray production rate ($\approx 20 \times 10^{25}$ molec yr^{-1}) anthropogenic sources are negligible. ^{14}CO is also produced in significant but uncertain quantities (2 to 10 $\times 10^{25}$ molec yr^{-1}) by the oxidation of organic matter. Current atmospheric ^{14}CO data are all taken at ground level, but seasonal (figure 13) and latitude gradients have been noted. These limited data have been fitted with the help of a 2-D model (Volz et al., 1981) to suggest an average tropospheric OH abundance of $7 \pm 3 \times 10^5$ molec cm^{-3}. These values are a factor of 3 lower than those estimated by Weinstock and Niki (1972) almost a decade ago, largely because of their underestimation of ^{14}CO abundance. It must be realized, however, that the lifetime of ^{14}CO is short (5 $\pm$ 2 months), and a finer resolution of the organic source term and vertical gradients is needed to further refine these estimates.

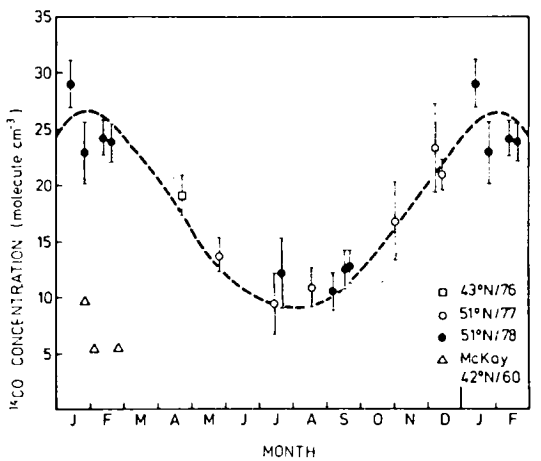

Figure 13. Seasonal variation of ^{14}CO at 15°N. (From Volz et al., 1981)

Recently Singh et al. (1983) have suggested that simpler and more easily measured molecules such as propane can be used to study the seasonal behavior of OH, provided the source term is adequately characterized. Indeed, a poorly characterized source function provides a major element of uncertainty when OH estimates are derived from mass balances of naturally occurring chemicals.

In recent decades, synthetic organic chemicals have been injected into the air environment in such large amounts that measurable background levels are present. Because of the exclusive man-made source of such chemicals, the uncertainties associated with

the source term could, in principal, be eliminated. A preliminary screening led to the selection of methyl chloroform (Singh, 1977a, b; Lovelock, 1977) as the most suitable molecule for the following reasons:

- Its atmospheric concentration was high enough and could be accurately measured
- The usage was such that emissions were virtually identical to production
- An agreed-upon OH rate constant was available

Synthetic organic chemicals thus could be monitored for their removal rate in laboratory-like conditions.

Although a good deal of methyl chloroform data is now available (figures 14 and 15), the earlier results (Singh 1977a, b) have not changed significantly:

- The tropospheric lifetime of methyl chloroform is 8 to 10 years, corresponding to a mean OH concentration of 6×10^5 molec cm^{-3} (table 8)
- The north/south gradient of methyl chloroform is too large to be accounted for by the distribution of its sources and therefore an assymetry of OH distribution must be invoked

To best interpret methyl chloroform data, one must use a 2-D model, even though the basic features of OH distribution can be adequately obtained with the help of a multibox model.

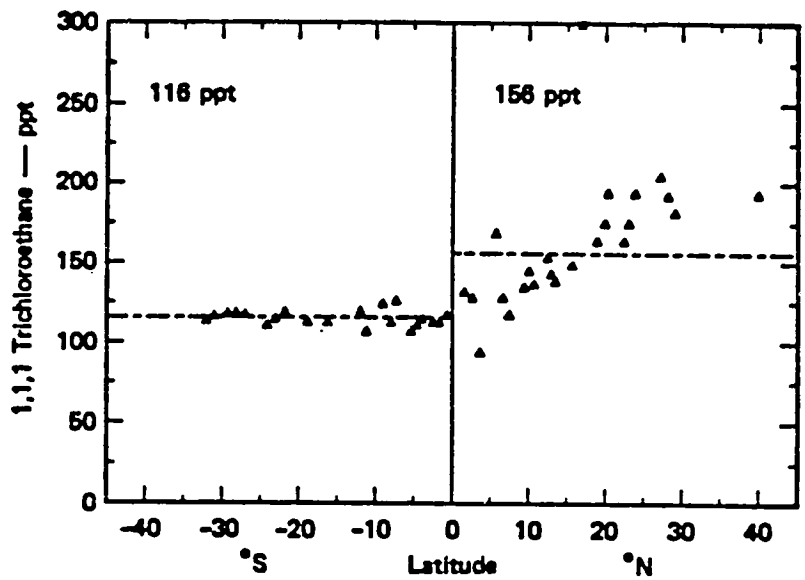

Figure 14. Latitudinal distribution of methyl chloroform. (From Singh et al., 1983)

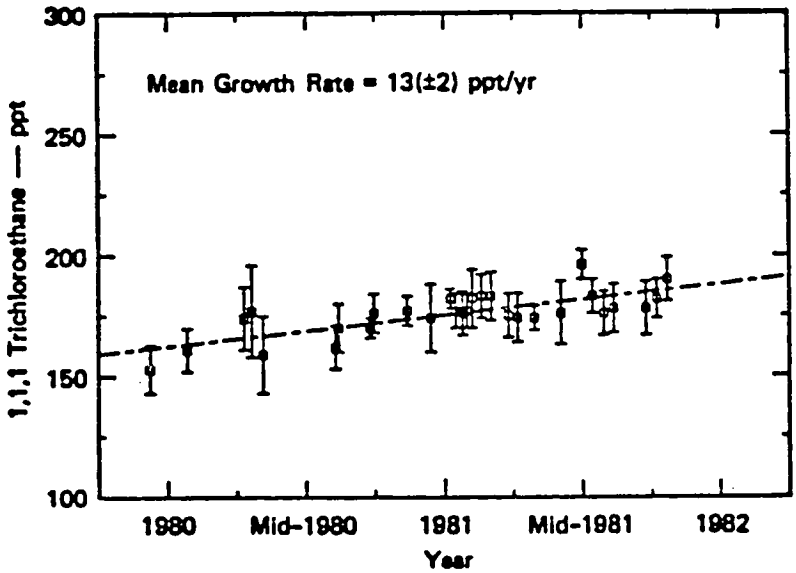

Figure 15. Growth of methyl chloroform at 40°N. (From Singh et al., 1983)

TABLE 8. ESTIMATION OF RESIDENCE TIMES, INTERHEMISPHERIC EXCHANGE RATE AND HYDROXYL RADICAL ABUNDANCE FROM COMPARISONS OF MEASURED AND PREDICTED RESULTS

Compounds	Measured Parameters - Dec. 1981		Predicted best values from emissions data and a 2-box model				Estimated mean OH concentration (T=265 K)	
	Global average concentration $\bar{X}$ (ppt)	Weighted average NH/SH concentration ratio $\bar{R}$	T_a* (year)	T_c* (year)	X_p (ppt)	R_p*	$k_{OH} \times 10^{12}$† (cm^3 $molec^{-1}$ s^{-1})	OH, 10^5 (molec cm^{-3})
Fluorocarbon 12	294	-	69	1.2	294	1.07±0.01	—	—
Fluorocarbon 11	179	1.08	55	1.2	179	1.08±0.01	—	—
Methylene Chloride	29	1.81	0.9	1.0	29	1.96±0.12	4.27exp(-1094/T)	5.1
1,2 Dichloroethane	25	2.64	0.6	1.2	24	2.63±0.25	8.86exp(-1094/T)	3.7
1,1,1 Trichloroethane (Methyl Chloroform)	136	1.34	9.3	1.2	136	1.21±0.02	5.40exp(-1810/T)	5.8
Tetrachloroethane	17	5.80	0.6	1.2	17	2.71±0.27	9.44exp(-1199/T)	5.2

* T_a and T_c respectively are mean atmospheric residence time and mean interhemispheric exchange rate. The errors in R_p are based on a value of a = 0.96 ± 0.04.

† Recommended rate constants from Hampson (1980); 1,2 dichloroethane rate constant is from Howard and Evenson (1976). The temperature dependence is assumed to be that of methylene chloride (R. Atkinson, private communication).

Although methyl chloroform was the best initial choice of anthropogenic traces to study atmospheric OH removal, other choices can now be made. Molecules such as dichloromethane, 1, 2 dichloroethane and tetrachloroethane are three other anthropogenic molecules suited for this purpose (Singh et al., 1983). A two-box model (table 8) shows that removal rates of these molecules are consistent with average OH concentrations of 4 to 5 $\times 10^5$ molec cm^{-3}. Because of their relatively short lifetimes compared to methyl chloroform (table 8), these chemicals can show OH latitudinal gradients with greater sensitivity. There is no doubt that atmospheric removal rates of OH levels which are deduced from these additional chemicals can provide strong support for the reliability of indirect techniques outlined above.

Uncertainties in such methods are not inherent to the technique but are often due to differences in measurements associated primarily with calibration problems. Although these differences have been resolved substantially over the years, further work is necessary. Another source of uncertainty is in the emissions data. Because of often complex sources of naturally occurring gases (^{14}CO, ^{12}CO, C_3H_8 etc.), synthetic organic molecules offer a superior opportunity. To date, the synthetic molecule most commonly employed for OH determination has been methyl chloroform. Other similar molecules should be employed to gain further confidence in the predictive capabilities of the global average. Molecules such as dichloromethane, 1, 2 dichloroethane and tetrachloroethane are strong candidates for this purpose. These somewhat more reactive molecules may provide additional information on the seasonal and latitudinal behavior of OH concentrations. Two-dimensional models would be ideally suited for the interpretation of these data.

Radiochemical Method. The radiochemical technique developed at Washington State University consists of a measurement of the rate of carbon monoxide oxidation. This rate is an important atmospheric chemistry parameter in its own right, but current models indicate that it is also a direct measure of hydroxyl concentration. Species other than hydroxyl are known to oxidize carbon monoxide (for example, CH_3O), but are not expected in sufficient concentration in the atmosphere to cause more than 5% of the total oxidation. In what follows we will tacitly neglect these other oxidants.

Two rather different approaches have, for technical reasons, been used in a ground-based (Campbell et al., 1979) and airborne radiochemical instrument. This discussion centers on the airborne instrument, but a brief discussion of the ground-based instrument is included for completeness.

The ground-based instrument illustrated schematically in figure 16 maintains the normal atmospheric chemistry with as little perturbation as possible. A known small increment (10%) is made in the ambient carbon monoxide concentration, using carbon-14 monoxide, and the resulting rate of production of carbon-14 dioxide

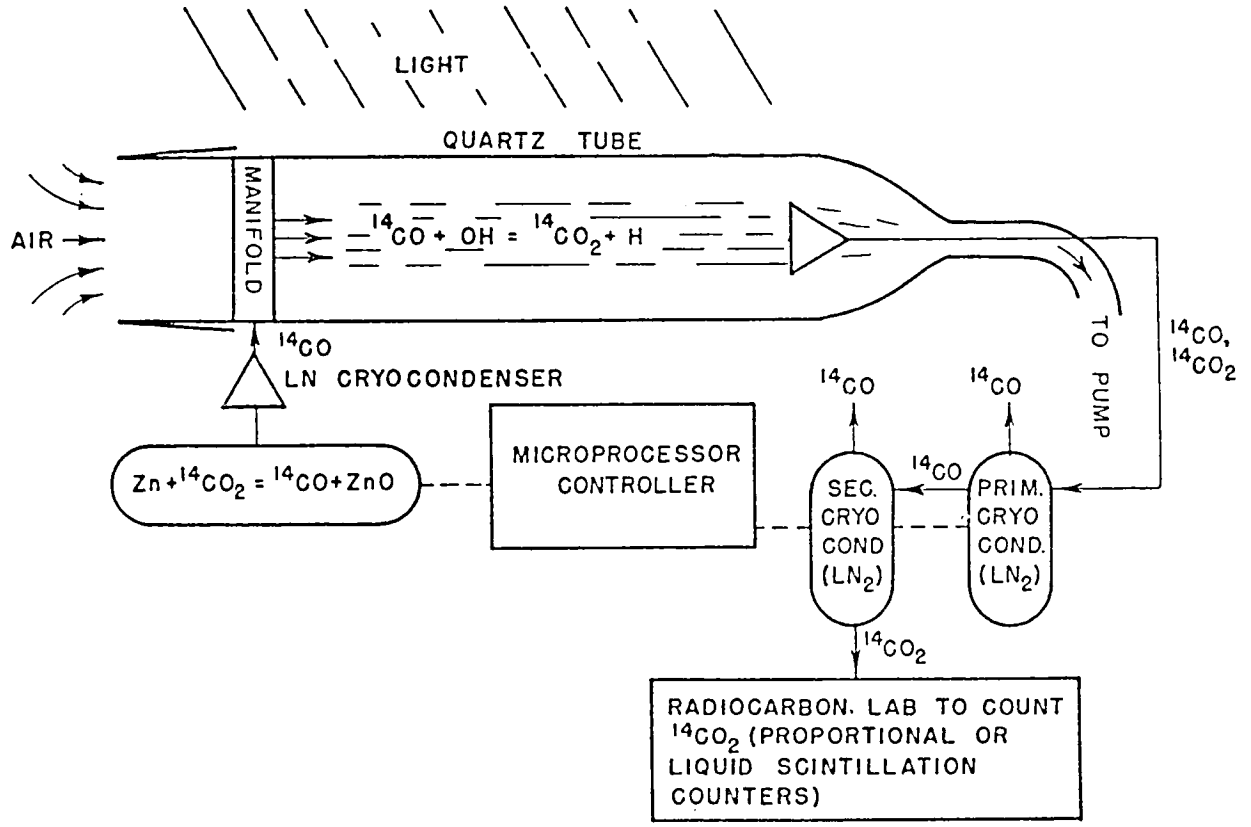

Figure 16. WSU flow reactor for measurements of hydroxyl radical concentrations in tropospheric air.

is measured over an interval of about 7 seconds. By assuming steady-state unperturbed chemistry in the instrument the hydroxyl concentration can be immediately deduced, given the value of the rate coefficient for the OH + CO reaction.

The crux of the technique lies in ensuring that the chemistry is unperturbed. The sampled air is pulled into a quartz-walled flow reactor, where the turbulence in the flow external to the instrument is allowed to partially decay, and then carbon-14 monoxide of very high purity is quickly mixed into the stream from an array of nozzles. The flow, by then almost laminar, proceeds down the reactor tube for 7 seconds. The central region of the flow, which has not been in diffusive contact with the walls of the reactor, is then diverted for extraction of the carbon dioxide. After separation from the unreacted carbon-14 monoxide (which is in considerable excess), the carbon dioxide is transferred to a beta counting system to determine its carbon-14 content.

Perturbations to the ambient chemistry can arise from changes in photolytic insolation (minimized by the use of the quartz reactor, which is transparent to all photolytic radiation), from loss of reactive species from the flow to the walls of the reactor

(a subject studied extensively both by numerical flow modeling and by wind tunnel tests), from the increment in carbon monoxide (model studies indicate a somewhat less than first-order dependence), and from the effects of the beta particles emitted by the carbon-14 monoxide (which can be simulated by use of an external source of beta radiation). In practice the cumulative error due to all of these effects can be kept small (<20%) provided the atmospheric turbulence intensity is not too high.

A different configuration is needed for an instrument to be mounted on an aircraft, especially a high-speed aircraft, and this has required a change in the principle of operation. Superficially the airborne instrument resembles the ground-based one. The incoming air is decelerated to a relatively low velocity, the carbon-14 monoxide is mixed into it, and after a delay to permit reaction, the carbon dioxide is trapped out and separated for counting. There is, however, a major difference in approach caused by the impossibility of admitting sunlight to the deceleration and reaction regions of the airborne instrument; the operation no longer assumes steady state to be obtained in the chemistry. In place of the assumption of steady state we substitute a general objective of converting each hydroxyl radical in the collected air stream into a molecule of carbon-14 dioxide employed. Actual conversions range from 5% to 30%. Nevertheless the idealization remains a useful way of viewing the instrument's operation.

In practice the operating conditions are chosen less with the idea of maximizing the conversion of hydroxyl to carbon-14 dioxide than with that of maximizing the signal-to-noise ratio and minimizing those errors whose magnitude cannot be determined independently. We include in these errors uncertainties in the details of the chemistry which occurs between the time the air enters the instrument and the time it leaves the reaction chamber, where steps are deliberately taken to quench any remaining radicals and bring all chemical changes to a halt.

Figure 17 shows the major flows in the instrument and the methods of measuring them. The air is twice decelerated before it fully enters the inlet, once by passage close to the stagnation point on an axisymmetric airfoil mounted externally to the aircraft's boundary layer, and again by passage through a second quasi-stagnant region just inside the mouth of the inlet. At this second deceleration point the central part of the flow proceeds down the inlet, while the air entering further from the axis is reflected by the pressure gradient and forms a reverse flow region immediately adjacent to the inside wall of the inlet. For both of these deceleration steps, which reduce the velocity from as much as 250 m s^{-1} to a nominal 27.4 m s^{-1}, the associated boundary layers are very thin (because of the short development times). In particular, they are much thinner than the 'insulating' air layer between the airstream actually being sampled and potential radical sinks, such as the metal face of the decelerating airfoil or the metal walls of the end of the inlet tube. Consequently, negligible radical losses (<1%) are expected up to

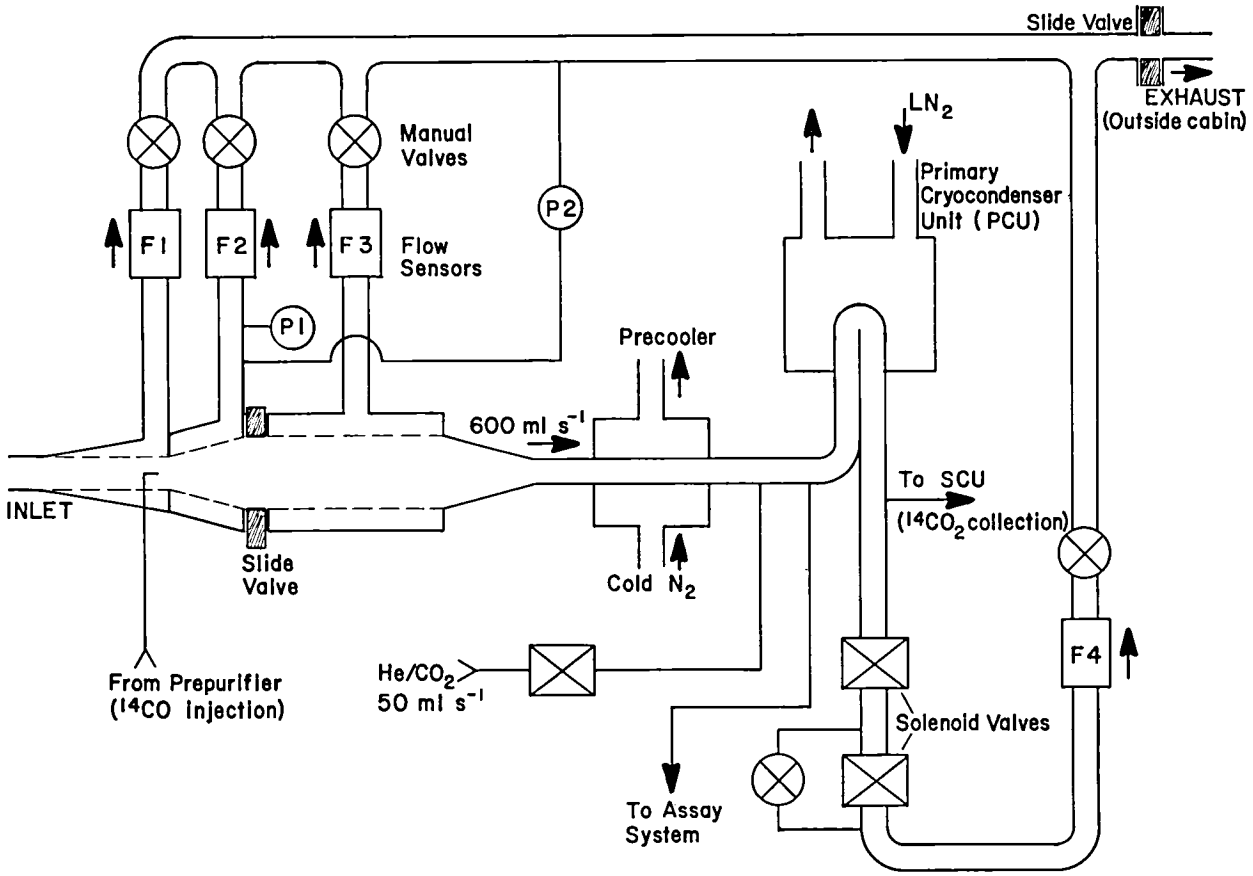

Figure 17. WSU hydroxyl instrument MK III. Principal flow path schematic.

this point, provided only that the flow not be grossly turbulent. Note that upper limits for these losses can be measured by the same techniques employed for measuring losses in the other parts of the apparatus (see below), and such measurements will be made when an opportunity offers.

As the sample traverses the length of the inlet to the point of injection of the carbon-14 monoxide, a distance of 26.7 cm, the flow is still further decelerated by graded suction through the inlets's porous wall. The final velocity at the injector is reduced to 11.1 m s^{-1}. The loss of hydroxyl by chemical decay during transit through this section, which requires 0.0149 s, is small, even if not entirely negligible. Chemical lifetimes in the incoming air in reasonably unpolluted regions can be expected to be in the range from about 0.67 s at sea level (150 ppbv carbon monoxide content) to about 3.4 s at 13 km altitude. The corresponding losses due to decay during transit through the inlet range from 2.2% to 0.4%.

Wall losses are minimized by the suction. Air which has come close enough to the wall to have suffered loss of radicals

by diffusion and surface recombination also has a high probability of being removed from the flow by being sucked through the porous wall. Laboratory measurements have put upper bounds on these losses of about 4%, provided the flow is reasonably stable. (Early measurements on the CV-990 aircraft in August 1983 disclosed much higher losses, on the order of 15%, associated with grossly turbulent flow in the inlet. Consultations with Pratt and Whitney indicated that the source of the problem was misalignment of the major axis of the external deflecting airfoil from the direction of the airflow prevailing in its location.)

The admixing of the carbon-14 monoxide into the airstream is the next step in the process. Mixing occurs at the throat of the diffuser section with a diametrical expansion ratio of 1.91. The walls of this diffuser are also porous and subjected to graded suction which removes 17% of the incoming flow, again minimizing the losses of reactive species from the main part of the flow. The injector itself consists of four nozzles of 0.1 mm tubing. Measurements of the turbulence intensity and scale length in the region immediately downstream indicate prompt and thorough dispersion of the carbon-14 monoxide, which is typically supplied at a mixing ratio of several hundred ppm in helium carrier gas. The exit velocity of the carrier gas from the individual nozzles (about 30 m s^{-1}) is chosen to give a well-developed, rapidly broadening jet behind each nozzle, without adding significantly to the momentum flux in the main flow.

Losses of radicals to the injector nozzles themselves may be calculated from the extensive data compiled for heat transfer from small cylinders in a flowing gas. These calculations show a maximum loss at low aircraft altitudes of about 2%, falling to less than 1% at 13 km.

From the diffuser the air passes into a reactor section, where sufficient time is allowed for the OH + CO reaction to proceed part way to completion. Again the walls are porous, with a graded suction which reduces the mean axial velocity from 2.54 m s^{-1} at the inlet end to 0.51 m s^{-1} at the exhaust. At the exhaust end a screen is interposed to quench any remaining radicals and more sharply define the reaction time, which has a nominal value of 0.218 s. Laboratory studies of the wall losses, which are greatest in this section because of the lowered axial velocities, put upper bounds of about 5% under conditions of reasonably stable flow.

The subsequent operations focus on efficiently collecting all the carbon dioxide in the sampled air and separating from it the unreacted carbon-14 monoxide, which is in excess of the desired carbon-14 dioxide by factors ranging from 10^6 to 10^9. Stringent precautions must be taken to prevent spurious (especially surface catalytic) conversion of carbon-14 monoxide to the labeled dioxide. Separation ratios of 10^9 are attained in practice by means of a three-stage freezing/sublimation process. A corresponding requirement is that the carbon-14 monoxide injected be free of contami-

nant carbon-14 dioxide; proportions of less than 10^{-9} can now be consistently obtained for periods of a few seconds after final purification.

In addition to the collection of the carbon dioxide, an aliquot of the reactor effluent is collected in such a way as to represent an integrated sample over the duration of the measurement, which is typically 100 s. This aliquot is both measured in quantity (moles) and counted to determine the mixing ratio of the carbon-14 monoxide in the reactor. The flow rate out of the reactor (and also out of each suction chamber) is measured, together with the pressure and temperature of the airstream in the reactor.

The sensitivity of this technique (see Appendix H for a detailed discussion) is limited by two sources of noise: counting errors and separation inefficiencies. Counting errors arise from the finite background of the carbon-14 beta counting system, and require that sufficient activity be collected (as carbon-14 dioxide) to provide at least 0.25 counts per minute. In general this can be achieved using practical run durations of about 2 minutes, even for very low ambient hydroxyl concentrations.

Separation inefficiencies in practice are the limiting factor in the attainable sensitivity. Equations (H8) and (H9) relate the ratio of carbon-14 dioxide to carbon-14 monoxide to the ambient hydroxyl concentration; values of this ratio less than 2×10^{-9} may not be presently measurable. The corresponding ambient hydroxyl concentrations are 5 to 10×10^{4} cm^{-3}.

Long-Path UV Absorption

Absorption spectroscopy has, in general, been a versatile approach for direct detection of many atmospheric species. This is a technique that is implemented by measuring the change in the radiance from a source that is due to absorption occurring as the radiance is directed over a known path length. The major advantages of this approach have been its simplicity of implementation and its versatility for detection of a wide range of species. The disadvantages are associated with interference from the absorption features of other atmospheric molecules and the difficulty of extracting small signal changes embedded in the source radiance. In addition, for trace species, the optical path must be on the order of 1 to 10 km, thereby presenting difficult implementation problems from other than ground-based platforms.

Traditionally, the IR spectral region has been characterized as the fingerprint region for atmospheric measurements. This characterization stems from the fact that most polyatomic molecules have vibrational-rotational bands in this region, and indeed the OH radical exhibits absorption features in the near IR as well as in the UV. However, the IR absorption has not proven suitable for detection of ambient OH, due primarily to the excessive interference from ambient water vapor. Implementation of the long-path absorption technique for measurement of OH utilizes the

strong, narrow, and well-resolved rotational absorption lines in the near UV. The intense $Q_1(2)$ line in the (0-0) band of the $(A^2\Sigma \leftarrow X^2\Pi)$ transition at 307.9951 nm has been selected as most suitable for the detection of OH because (a) it is one of the strongest lines, and (b) there is a second weaker line, the $Q_{21}(2)$, at 308.0006 nm in its immediate vicinity which can also be recorded to give a uniquely characteristic absorption spectrum for OH. The presence of atmospheric OH would therefore be identified by two spectral features, which lends much higher confidence to its observation. An instrument utilized by Hübler et al. (1982) is described schematically in figure 18. A laser system, consisting of a mode-locked argon ion laser which pumps a frequency-doubled dye laser, serves as the light source. The emitted UV is pulsed with a pulse duration of less than 50 psec and a repetition rate of 82 MHz with an output power of 2 mW. The spectral half-width of the UV output is about 0.1 nm. For comparison, the pressure-broadened width of the $Q_1(2)$ line is 0.002 nm. The resolution of the monochromator used here is 0.002 nm. To reduce both the UV flux density and the divergence, the laser beam is expanded in a Cassegrain type telescope to a diameter of 0.3 m. The light path length was determined by a mirror 1.5 to 5 km away. The reflected light is focused on the entrance slit of a Spex double monochromator with a 0.05-nm-wide portion of the spectrum scanned repetitively by 1092 slits (10 μm wide, 10 mm high) placed radially around the periphery of a rotating metal disc (200 mm diameter). A stationary mask with a rectangular opening insures that light passes through only one slit at a time. The spectrum is scanned at a repetition rate of 6 kHz and the wavelength-dependent intensity distribution is monitored by a photomultiplier. This signal is amplified and converted to digital signals corresponding to wavelength intervals of 0.0003 nm. The 180 segments of each scan are stored and averaged separately in a

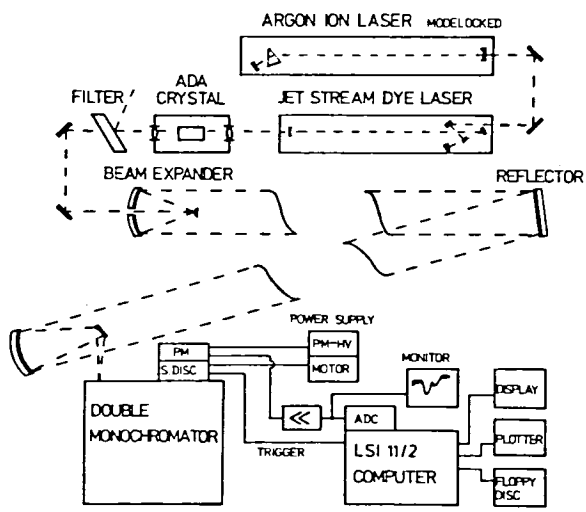

Figure 18. Principle of apparatus for long-path optical absorption using laser light. (From Hübler et al., 1982)

fast signal averager, which is synchronized by an infrared light barrier. The scans are further integrated over 5-minute intervals and then stored.

A calibration for the position of the OH lines in the spectrum is repeated every 5 minutes. This is achieved by recording the strong absorption from OH radicals in an acetylene-air flame placed in the unexpanded laser beam. Whenever the spectral position of the $Q_1(2)$ line has changed more than 0.0006 nm the data of the previous 5 minutes are discarded to avoid deterioration of the spectral resolution.

To detect an OH concentration of 10^6 molecules cm^{-3}, a measurement accuracy sufficient to resolve a differential absorption on the order of 10^{-4} is required. Because of noise introduced mainly by light intensity fluctuations, a noise level as low as 10^{-4} has not as yet been achieved with a 5-minute measuring interval. Therefore a number of integrated scans are superimposed with respect to the $Q_1(2)$ reference line from the flame. In this way compensation for any long-term wavelength drift of the spectrograph is achieved. Absorption features with an optical density of about 10^{-4} have been extracted from the integrated data via correction for the baseline profile. In general, the resulting spectrum is a superposition of spectra from several constituents such as SO_2, CH_2O, etc. Deconvolution has yielded characteristic OH spectra; an example is shown in figure 19 for an optical path of 9.7 km. The average OH concentration inferred from these data is 3×10^6 OH molecules cm^{-3}.

The spectra from long-path UV absorption spectroscopy can provide convincing evidence of the presence of atmospheric OH, even after correction for the contribution from other atmospheric constituents. The minimum detectable OH level is a function of the optical path length that can be used, and this in turn is strongly influenced by the atmospheric conditions. Demonstrated sensitivities on the order of 1×10^6 OH molecules cm^{-3} for path

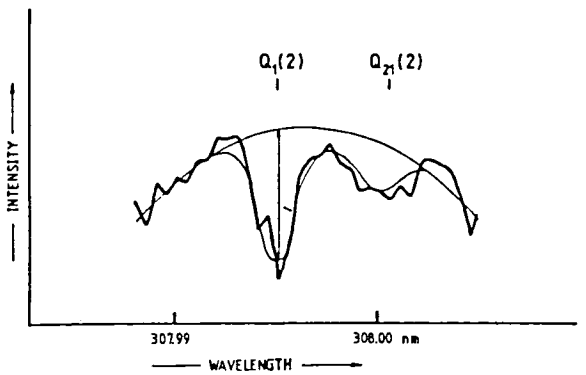

Figure 19. Atmospheric OH UV absorption measurement at Deuselbach on Sept. 24, 1980. (From Hübler et al., 1982)

lengths of 3 km have been achieved. It should be noted that direct scaling with the path length is often not realizable because of the increased turbulent noise or transmission losses experienced with increases in the optical path.

Measurement Validation

Validation of measurements of trace atmospheric species is clearly an important phase in the development of any given instrument. Validation of atmospheric measurements, however, has, in general, an extra dimension of difficulty as compared to the normal laboratory measurements encountered in many scientific fields. This new dimension is the inability to control the environmental parameters surrounding a given measurement. This leads to an inherent lack of repeatability of the measurement conditions and hence a loss of one traditional method for validation (i.e., repeatability). Under such circumstances certification and/or validation of a measurement technique (and results) must rely upon comparison with model results, calibration standards, and/or intercomparisons of measurements made by instruments using different principles of detection. Of these three, the latter two are more desirable since the purpose of many atmospheric measurements is model input or model verification.

Calibration. The use of standards in the field calibration of a given instrument provides a measure of the basic response and linearity of the instrument. Such a calibration generally entails the introduction of known amounts of the desired species into the sample chamber or volume used by the instrument and preferably at concentration levels expected to be encountered in the atmosphere. For OH, the establishment of a known calibration source is not a trivial task, particularly at ambient atmospheric levels. Moreover, the range of sampling geometries that have been employed for OH instrumentation (e.g., remote vs. in situ) and the variations with a given geometry (e.g., ambient vs. low pressure) indicate the range of difficulties that might be expected in establishing calibration procedures for OH. It is clear that no universally accepted calibration procedure currently exists for OH, and each instrument approach has in most cases been "calibrated" using procedures uniquely applicable to the given instrument. These various "calibration" approaches have been discussed in the previous sections.

Notwithstanding these individual approaches, it was the consensus of the workshop participants that a more unified approach to OH calibration should be considered. Such an approach should be able to accommodate the variety of sample geometries and conditions, and in particular the lidar and in situ sampling geometries. One possible approach to a "universal" calibration station is being considered by the Ford group for their lidar system. Their approach entails the use of a number of medical UV lamps arranged around the circumference of a 20- to 30-cm-diameter, 10-meter-long tank. A multipass absorption cell configuration would be included in the design to provide means to measure the OH con-

centration within the cell via UV absorption. Direct calibration of the lidar approach appears to present the more difficult of the calibration tasks because of the large sampling volume.

The possibility has been raised of modifying the design of this device so that other instruments could also be calibrated. While there appear to be no problems in calibrating these instruments with such a device, the feasibility of modifying the device to supply the relatively large flows required by the in situ techniques requires further study. It was agreed that the availability of such a device at Ford may materially assist in obtaining a uniform calibration of all instruments in use.

Beyond the calibration of individual instruments, questions were raised about the stability of any and all calibrations. Determination of the stability of the individual instruments must be relegated to the investigators and little information is available at the present time. Should an instrument have problems in this area there are a number of steps which can be taken to rectify the lack of stability, to the extent justified by the current accuracy requirements. These steps include, for example, laser frequency stabilization, and do not add greatly to the complexity or cost of the instrument.

Instrument Intercomparisons. No two hydroxyl instruments have ever made measurements at the same place at the same time, and so no intercomparison data can be presented. Notwithstanding the short history of hydroxyl measurements and the paucity of instruments, it may still be contended that this unusual situation should not persist longer than necessary. The techniques are exacting and often novel, so a certain scepticism of the data produced by any one instrument by the scientific community is only to be expected (and even, indeed, to be hoped for). This scepticism is unlikely to abate until the extent of agreement of measurements made by different instruments on the same samples of the real atmosphere is established. It is a reasonable, although not necessarily correct, presumption that initial instrument intercomparisons will disclose disagreements attributable to stability, interference or other problems. The existence of these problems should be ascertained at an early time by instrument intercomparisons, which may also serve as a convincing validation of the instrument calibrations.

Any intercomparisons should be carried out in real atmospheres representative of the atmospheres to be encountered during global measurement programs. There is no reason to anticipate that species present in heavily contaminated atmospheres will affect hydroxyl concentration measurements (i.e., act as interfering species in the broad sense of the word), but data showing divergences between different types of instruments in unrepresentative atmospheres will not be discounted until such time as they are shown to occur also in more representative atmospheres. Within this restriction, a reasonable variety of atmospheres should be employed during instrument validation.

The calibration stability of instruments should not escape scrutiny during intercomparisons. For this reason it may be desirable to operate instruments for longer periods between recalibrations than would normally be the case in actual field measurement programs, in order to disclose drifts in calibration more clearly.

Collection of data from intercomparisons, in the face of time-varying hydroxyl concentrations and differing integration times/sensing times from one instrument to another, will require reasonably good signal-to-noise ratios in the measurements. Most instruments have a signal-to-noise ratio which is proportional to the first or higher power of the hydroxyl concentration over the range of concentations to be found in the atmosphere. This dictates a minimum desirable OH concentration for intercomparisons, such as a concentration which gives an expected standard deviation of no more than 15% in the ratio of the concentrations measured by any two instruments. Such an intercomparison will require a minimum concentration, under the atmospheric conditions of the first section of table 6, of 5×10^6 cm^{-3}, and more if conditions are rendered less favorable by higher concentrations of ozone or NRF (presumably aerosol) species.

Intercomparisons must be carried out between instruments mounted on the same aircraft. However, it also appears highly desirable to intercompare instruments on the ground, especially early in their development. It may furthermore prove desirable to make intercomparisons between an instrument on the ground (perhaps on a tower or a mountain top) and an instrument on an aircraft flying nearby. This last type of intercomparison may provide more robust calibration of aircraft instruments than can otherwise be obtained, especially for in situ instruments where inlet losses need consideration, and may provide a check on the stability of instruments when installed on aircraft.

Ground intercomparisons could also profit from the inclusion of systems which are inherently incapable of or not ready for airborne operation. This could include the long-path UV absorption methods and the Washington State University ground-based indirect OH instrument.

Sites for any intercomparison will need to be carefully considered from the point of view of spatial homogeneity of hydroxyl concentrations (including the gradient near the ground and variations in the UV albedo of the underlying surfaces) and temporal variability (which will make comparisons of instruments with differing sensitive times more difficult). The minimum concentration for adequate statistics must also be considered.

MEASUREMENT OF PEROXIDES

The major emphasis of this workshop has been on the evaluation of techniques for detection of OH. This of course is a

consequence of its importance in atmospheric chemistry and the lack of reliable measurements. The following sections, however, describe results of the workshop activities concerning other H_xO_y related molecules of atmospheric interest. The deliberation given to these constituents is admittedly brief and by no means as complete as the preceding sections on OH. This should not be construed as a lack of importance of any of the remaining H_xO_y species but more a comment on the development status of many of the techniques.

The group was aware of three HO_2-related measurement techniques, of which two (Stedman, University of Denver; Cambell, Washington State University) measure all species which react with NO to produce OH, and give a value which is the equivalent HO_2 concentration. In fact the limited rate constant data available show all peroxyl radicals to react with NO at similar rates, so these measurements would produce something close to the sum of concentrations of peroxyl species.

The one technique which measures HO_2 explicitly is a frozen radical technique developed at KFA in Julich (Mihelcic et al., 1978). This is a working instrument which is relatively portable but has limited sensitivity (about 10^8 cm^{-3}) which may limit its use.

The Stedman technique uses "radical multiplication" in the presence of large concentrations of NO and CO; the detected species is NO_2. It has high sensitivity and is an operating, compact instrument. It requires calibration and its calibration stability has not been assessed.

The Washington State University instrument is a modification of the radiochemical hydroxyl instrument. An additional injection of NO is made, converting RO_2 to OH, which is then measured. This is a simple modification of any radiochemical hydroxyl instrument. Sensitivities of less than 10^6 cm^{-3} with accuracies of 30% are expected.

The group was addressed by George Dawson of the University of Arizona, who reported upon a promising condensation wet-chemical technique, and Mike Rodgers of the Georgia Tech group, who reported upon a unique differential photofragmentation method. The NCAR group (Kok and Lazrus) was also reported to be making good progress towards an improved wet-chemical method. A brief discussion of the wet-chemical and photofragmentation techniques will be given below.

Wet Chemical

Hydrogen peroxide is a highly soluble gas and therefore should be collected with high efficiency by condensation sampling. And indeed, readily detectable concentrations of H_2O_2 have been found in condensate (Farmer and Dawson, 1982). Quantitation of the method, however, requires further work. The problems in the

measurement of gas phase hydrogen peroxide (H_2O_2) are not with the analytical techniques for detecting H_2O_2 but in the use of aqueous solutions for trapping gas phase H_2O_2. The problem with trapping gaseous samples of H_2O_2 in the aqueous solution is the reactions of ozone (O_3) with the solution to both produce and destroy H_2O_2. For example,

$$O_3 + HO \rightarrow H_2O_2 + O_2$$

$$O_3 + H_2O_2 \rightarrow H_2O + 2\ O_2$$

The predominance of one reaction over the other depends on the concentrations of the reactants. Recent papers by Heikes et al. (1982) and Zika et al. (1982) detail these reactions more completely. These reactions make the accurate measurement of gas phase H_2O_2 in ambient air questionable at this point in time. While the first reaction has specifically been identified as producing H_2O_2 in aqueous solution, other reactions involving ambient air species are also possible.

The most sensitive analytical techniques currently available for H_2O_2 determination, luminol chemiluminescence (Kok et al., 1978) and peroxidase enzyme fluorescence (A. L. Lazrus, private communication, 1982), both use aqueous solutions as the medium for H_2O_2 analysis. These techniques can quantitate less than 1×10^{-8} M of H_2O_2 in 1 mL of aqueous solution.

To accurately collect and analyze ambient gas phase H_2O_2 using trapping techniques, methods must be found to remove the ozone from the air stream and/or reduce the activity of the collected H_2O_2 and H_2O. This is a very difficult task since H_2O_2 is very reactive and can be decomposed easily. Preliminary investigations are under way to examine various techniques to accomplish this. Concurrently the development of a gas phase H_2O_2 source is also under development.

Photofragmentation/Differential Fluorescence

Detection of H_2O_2. Given that the LIF approach to monitoring hydroxyl radical concentrations under atmospheric conditions proves successful, then LIF offers the potential for the development of sensitive detectors for other H_xO_y species. Many H_xO_y species (such as H_2O_2) produce OH radicals during UV photolysis; accordingly a detection scheme might consider utilizing the OH produced from photofragmentation of a parent species to establish its concentration. As an example of this approach, we consider the detection of H_2O_2:

$$H_2O_2 + h\nu_1 \rightarrow 2\ OH$$

$$OH + h\nu_2 \rightarrow OH^*$$

$$OH^* \rightarrow OH + h\nu_3$$

Since H_2O_2 is present in concentrations far in excess of naturally occurring OH, even a small fractional photolysis of H_2O_2 would produce OH concentrations much greater than the naturally occurring OH concentrations. Consequently this approach for H_2O_2 detection would suffer negligible interference from the natural concentration of OH. Large interferences could potentially occur, however, from the photolysis of other H_xO_y species. For H_2O_2 detection the following interferences must be considered:

(a) $HNO_3 + h\nu \rightarrow OH + NO_2$

(b) $H_2O + h\nu \rightarrow OH + H \quad (\lambda < 242)$

(c) $HCOOH + h\nu \rightarrow HCO + OH$

(d) $CH_3OOH + h\nu \rightarrow CH_3O + OH$

(e) $O_3 + h\nu \rightarrow O(^1D) + O_2$

$O(^1D) + M \rightarrow O(^3P) + M$

$O(^1D) + H_2O \rightarrow 2\ OH$

Examination of the absorption cross section data along with typical concentration ratios indicates that there is no spectral region where H_2O_2 may be detected without interference by one or more of the above processes. Thus, in order to establish the concentration of H_2O_2, some means of correcting for this interference must be developed. The proposed method, differential fluorescence, utilizes the fact that near the peak of the ozone absorption cross section, process (e) dominates over all other means of producing OH radicals. By comparing the OH produced by photolysis in this region (for example, $\lambda_1 = 266$ nm) with that produced in some other wavelength region where process (e) and the primary process are the major processes ($\lambda_2 = 222$ nm) one can correct for the interference from process (e) by the following relation:

$$[H_2O_2] = \frac{1}{2\sigma_{H_2O_2} F_2} \left([OH]_2 - \frac{F_2\ \sigma_2}{F_1 \sigma_1} [OH]_1 \right)$$

where σ_1 and σ_2 are the absorption cross sections for ozone at $\lambda_1 = 266$ nm and $\lambda_2 = 222$ nm, respectively; $\sigma_{H_2O_2}$ is the absorption cross section for H_2O_2 at $\lambda_2 = 222$ nm; F_1 and F_2 are the laser fluences at 266 and 222 nm; and $[OH]_1$ and $[OH]_2$ are the OH concentration levels resulting from the photolysis of atmospheric air samples at 266 and 222 nm.

The limit of our ability to determine the H_2O_2 concentration is set by the precision to which this interference can be corrected for. It is in this regard that the extreme sensitivity of exist-

ing LIF OH sensors can be utilized to the fullest extent. The OH concentration produced by the photolysis of these species is fully three orders of magnitude greater than the detection limit of current OH sensors.

Detection of CH_3OOH. Unlike H_2O_2 described above, CH_3OOH can be detected with little or no interference from other atmospheric gases. The detection of CH_3OOH would begin with the primary process

$$CH_3OOH + h\nu_1 \rightarrow CH_3O + OH$$

with the subsequent detection of CH_3O by:

$$CH_3O + h\nu_2 \rightarrow CH_3O^*$$

$$CH_3O^* + M \rightarrow CH_3O + M$$

$$CH_3O^* \rightarrow CH_3O + h\nu_3$$

The laser-induced fluorescence detection of CH_3O has been reported by several investigations (Inoue et al., 1979, 1980; Ohbayashi et al., 1977). The principal interferences to the detection of CH_3O are believed to be:

$$\text{(a)}\ CH_3ONO + h\nu \rightarrow CH_3O + NO$$

$$\text{(b)}\ CH_3ONO_2 + h\nu \rightarrow CH_3O + NO_2$$

ASSESSMENT OF TECHNIQUES

In this section the findings of the workshop participants relative to the measurement capabilities of the techniques considered will be summarized. As noted above, the largest percentage of the workshop's discussion was focused on techniques to measure OH in general and on the various LIF techniques in particular. Accordingly, this section will address the status of the OH techniques first and then techniques for the remaining species as a group.

Table 9 reviews the OH techniques that were considered by the workshop participants. Under the "Techniques" heading the spectrum of instruments is identified by key words or acronyms that are intended to highlight the measurement concept and a particularly distinguishing feature in the implementation of each concept. The group developing the instrument is also identified primarily as an additional method to characterize the particular technique. It is recognized that other laboratories may also be pursuing one or more of the concepts listed here. The comments that are given are directed primarily at the operational status of the technique at the time the workshop was convened. Footnotes on these comments attempt to update this status.

TABLE 9. STATUS OF OH TECHNIQUES CONSIDERED AT WORKSHOP

Techniques	Group	Comments
• LIF/Lidar	Ford Motor Co.	A/C tested with with measurements[a]
• LIF/In Situ	Georgia Tech.	A/C tested with measurements[b]
• LIF/Low Pressure	Portland State University	Ground-based measurements
• Radiocarbon Tracer (photostationary & flow reactor)	Washington State University	Ground-based measurements
• Long-Path UV Absorption	Institut für Chemie KFA, Julich	Ground-based measurements
• Global Average	SRI	Global Average
• LIF/Lidar	NASA Goddard	A/C test planned
• Radiocarbon Tracer/ flow reactor	Washington State University	A/C tests planned[c]
• LIF/Low-Pressure	Institut fur Chemie KFA, Julich	Lab tests under way
• LIF/High-rep-rate laser	Harvard University	Lab tests under way
• LIF/308-nm excitation	Jet Propulsion Laboratory	Lab tests under way

a Additional flight tests in October 1984 and April 1985 as part of NASA's Global Tropospheric Experiment (GTE).
b Additional flight tests in April 1985 as part of NASA's GTE.
c Flight test in April 1985 as part of NASA's GTE.

The grouping of the techniques listed in table 9 is intended to highlight those techniques that had been developed to the point that tropospheric OH measurements were reported to the workshop (e.g., first six) or flight tests were planned (e.g., middle two) or were in an early development phase (e.g., last three). Of the six systems reporting OH measurements, only the LIF/lidar system developed by the Ford group and the LIF/in situ system developed by the Georgia Tech group had undergone some level of flight testing. The long-path UV absorption developed by the KFA group (and also the ERL Aeronomy Laboratory group), the LIF/low-pressure system developed by the Portland State group (development by the KFA group also under way), and the radiocarbon tracer systems developed by the WSU group had also reported measurements of OH from ground-based instruments. Of these three instruments only the LIF/low-pressure system appears to be compatible with future aircraft measurements. The global average approach represents the last of the six concepts that reported tropospheric OH

measurements to the workshop. The specific question of aircraft compatability for this method is moot since no OH instrument as such is involved, although it clearly must rely upon global measurements of selected tracers from both ground and aircraft platforms. Of the remaining five techniques, two had definite plans for aircraft tests and the last three were deemed compatible with future aircraft missions.

The majority of the techniques listed in table 9 employ some variation of the LIF concept. This in itself reflects a general consensus of the participants relative to the techniques available for OH measurements, namely, that some variant of LIF offers the potential for providing sufficient sensitivity and specificity in an aircraft-compatible instrument to meet the needs for measuring tropospheric OH. At this point, however, the participants felt that it was premature to attempt to provide a more in-depth assessment or ranking of the OH techniques. Each of the aircraft-compatible techniques offered the potential for providing measurements under some conditions that would be useful to atmospheric models. This assessment is due in part to a lack of OH measurements in general, which tends to elevate any valid measurement to a status that might not otherwise be offered. Notwithstanding the current state of OH measurements, the various measurement techniques do in fact possess sufficient merit for continued consideration. As is often the case, those that are less well developed (i.e., low-pressure sampling and 308-nm excitation coupled with narrow-bandwidth detection) seem to offer advantages to circumvent the shortcomings of the more developed techniques. To realize those advantages, however, will require application of new technologies (e.g., excimer laser and high-resolution filters) and adaptation of instrument system to aircraft environment. While there appears to be no insurmountable technological obstacle, implementation of these new techniques in an aircraft environment will be no mean feat.

The participants reviewing the LIF techniques recognized that each variant of the techniques must address interference from laser induced OH and nonresonant fluorescence. It was further agreed that techniques utilizing 282 nm excitation had a potentially larger interference problem than the 308 nm schemes. However, it was recognized that this interference was understood sufficiently well to permit correction for a significant level of the interference. It was also recognized that such corrections are at best a last resort effort. A more desirable approach is to use an instrument configuration (e.g., lidar, low-pressure sampling) and/or implementation (e.g., short pulse, low pulse energy, 308-nm excitation, narrow-bandwidth detector) to minimize the noise source. The NRF background represents a noise source that is less well understood although it appears to be related to aerosol fluorescence and is assumed to be proportional to detector bandwidth. This results in an order of magnitude difference between boundary layer and free troposphere noise levels. At the present NRF cannot be predicted and LIF systems must rely solely on instrument design and/or operational methods to minimize its

impact. Because of the apparent dependence of NRF on aerosol loading some of the LIF techniques listed in table 9 may ultimately be restricted to operation in a relatively clear environment.

An aircraft-compatible radiocarbon tracer instrument is scheduled for flight test as part of NASA's GTE. The sensitivity of this technique will depend upon the use of materials with low catalytic activity. The long-path UV absorption instruments show no promise of being adaptable to aircraft use. Nonetheless, these instruments should remain as important ground-based techniques which can act as secondary calibration standards.

The workshop discussions related to techniques for measurement of H_xO_y species other than OH were, at best, brief. Because of this, specific recommendations cannot be presented. As a general comment, however, it was clear that there are few if any instruments available for field application. There is a clear need for additional funding to encourage new approaches as well as to bring the few existing techniques to a point that field experience can be gained.

CONCLUDING REMARKS AND RECOMMENDATIONS

Before listing recommendations that have emerged from the workshop discussion, it is worth noting that while the workshop was charged with rather broad objectives, in actual fact the major focus of its deliberations was an assessment of a single measurement concept (i.e., LIF) for a single species (i.e., OH). This single concept currently includes a wide range of variants which do, in fact, exhibit fundamental differences even though they stem from the same basic phenomena. For the most part, the LIF variants that have emerged have done so because there has been no clear demonstration of the superiority of any one technique or LIF variant for measuring OH. This is an important result which emerges as the basis for the more specific recommendation noted below. Another important result that emerges from the workshop is the realization that the LIF concept is perhaps the only direct detection scheme that offers the potential for combining sufficient sensitivity and selectivity for tropospheric OH measurements from an airborne platform. This realization is manifested by the continued interest in developing one or more of the LIF variants.

The discussions of the various LIF concepts have resulted in a better understanding of factors that have affected their successful implementation. Laser-induced OH, for example, is a noise source that plagued the credibility of early LIF OH measurements. It is now believed that this is one of the noise sources that is understood and can be predicted to an extent that correction for a significant fraction of this interference should be feasible. The non-resonant fluorescence is a noise source that has only recently been recognized. It is one that can totally dominate LIF instruments and its origin and meteorology are not

well understood although methods for minimizing or eliminating its impact now appear to be in hand. A major accomplishment of the workshop has been the development of a common format for describing the relationship between observed signal and hydroxyl concentration. Such a formalized format should provide a mechanism for a common repository of fundamental spectroscopic constants for OH, as well as a common format for evaluating current and future LIF systems.

SPECIFIC RECOMMENDATIONS

1. Alternate techniques for OH measurement should continue to be explored and supported if they are found to offer significant advantages. These include the following:

    a) LIF measurement with sample expansion to low pressures

    b) LIF measurement using higher repetition rates

    c) LIF measurement using narrower band detectors

    d) LIF measurement using 308-nm excitation in the 0-0 band

    e) LIF measurement using short laser pulse widths

    f) Measurement techniques analogous to the radiochemical method but using other, possibly non-radioactive, reagent species.

2. A better understanding, at least at the empirical level, is needed of the dynamics of the OH radical, in order to assess the improvements to be expected in reducing interference in the LIF method from ozone photolysis.

3. NASA should encourage the assembly of carefully reviewed compilations of data, such as quenching constants for OH* and NO_2*, of interest to experimentalists. This effort could parallel similar efforts on behalf of modellers.

4. There should be coordinated studies, and dissemination of results of studies, of the nature of the nonresonant fluorescent background to LIF measurements. Features of interest include its meteorology, on which some data may already be available, its spectrum, and its two-point autocorrelation function.

5. Development of OH calibration techniques should be expedited, including exploration of common calibration systems such as that proposed by the Ford group, and improvements in the open-air long-path absorption technique.

6. Intercomparison of OH instruments at an early time should be encouraged. NASA should endeavor to see that the best calibration feasible is utilized in each field expedition, and both the relative calibration factors and calibration stabil-

ities of all instruments should be determined and treated as part of the record of the field expedition.

7. Through this report and otherwise, NASA should request the community to consider possible techniques for aircraft measurement of HO_2, H_2O_2 and CH_3OOH.

REFERENCES

Bradshaw, J. D., M. O. Rodgers, and D. D. Davis, Second Conference on the Composition of the Nonurban Troposphere, Williamsburg, Va., May 1982.

Campbell, M. J., J. C. Sheppard and B. B. Au, Measurement of hydroxyl concentrations in boundary layer air by monitoring CO oxidation, Geophys. Res. Lett., 6, 175-178, 1979.

Chameides, W. L. and D. D. Davis, The free radical chemistry of cloud droplets and its impact on the composition of rain, J. Geophys. Res., 87, 4863-4877, 1982.

Copeland, R. A. and D. R. Crosley, Rotational level dependence of electronic energy transfer in the $A^2\ \Sigma^+$, v'= 0 state of OH and OD, International Conference on Radiationless Transitions, Irvine, CA, 1984.

Crutzen, P. J., Gas phase nitrogen and methane chemistry in the atmosphere, in Physics and Chemistry of the Upper Atmospheres, edited by B. M. McCormac, pp. 110-124, D. Reidel Pub. Co., Boston, MA, 1973.

Davis, D. D., M. O. Rodgers, S. D. Fischer and K. Asai, An experimental assessment of the O_3/H_2O interference problem in the detection of natural levels of OH via laser induced fluorescence, Geophys. Res. Lett., 8, 69-72, 1981a.

Davis, D. D., M. O. Rodgers, S. D. Fischer and W. S. Heaps, A theoretical assessment of the O_3/H_2O interference problem in the detection of natural levels of OH via laser induced fluorescence, Geophys. Res. Lett., 8, 73-76, 1981b.

Farmer, J. C., and G. A. Dawson, Condensation of soluble atmospheric trace gases, J. Geophys. Res., 87, 8931-8942, 1982.

Hampson, R. F., Chemical kinetic and photochemical data sheets for atmospheric reactions, Rep. FAA-EE-80-17, U.S. Dep. Transp., Washington, D. C., 1980.

Hanabusa, M., C. C. Wang, S. Japar, D. K. Killinger and W. Fisher, Pulsewidth dependence of ozone interference in the laser fluorescence measurement of OH in the atmosphere, J. Chem. Phys., 66., 2118, 1977.

Hard, T. M., R. J. O'Brien, T. B. Cook, and G. A. Tsongas, Interference suppression in HO fluorescence detection, Appl. Opt., 18, 3216-3217, 1979.

Hard, T. M., R. J. O'Brien, and T. B. Cook, Pressure dependence of fluorescent and photolytic interferences in HO detection by laser-excited fluorescence, J. App. Phys., 51, 3459-3464, 1980.

Hays, P. B., T. L. Killeen and B. C. Kennedy, The Fabry-Perot interferometer on Dynamics Explorer, Space Sci. Instr., 5, 395, 1981.

Heikes, B. G., A. L. Lazrus, G. L. Kok, S. M. Kunen, B. W. Gandrud, S. N. Gitlin and P. D. Sperry, Evidence for aqueous phase synthesis of hydrogen peroxide in the tropsphere, J. Geophys. Res., 87, 3045-3051, 1982.

Howard, C. J. and K. M. Evenson, Rate constants for the reaction of OH with ethane and some halogen substituted ethanes at 296 K, J. Chem. Phys., 64, 4304-4306, 1976.

Hübler, G., D. Perner, U. Platt, A. Toennissen and D. H. Ehhalt, Groundlevel OH radical concentration: New measurements by optical absorption, Second Symposium on the Composition of the Nonurban Troposphere, AMS, Washington, D. C., 1982.

Inoue, G., H. Akimoto and M. Okuda, Laser-induced fluorescence spectra of CH_3O, Chem. Phys. Lett., 63, 213-216, 1979.

Inoue, G., H. Akimoto and M. Okuda, Spectroscopy of the CH_3O A^2A_1-X^2E system by laser-excited fluorescence method, J. Chem. Phys., 72, 1769-1775, 1980.

Keafer, L. S., Jr. (Ed.), Tropospheric Passive Remote Sensing, NASA CP-2237, 1982.

Killeen, T. L., P. B. Hays, B. C. Kennedy and D. Rees, Stable and rugged etalon for the Dynamics Explorer Fabry-Perot interferometer. 2. Performance, Appl. Opt., 21, 3903, 1982.

Kok, G. L., T. P. Holler, M. B. Lopez, H. A. Nachtrieb, and M. Yuan, Chemiluminescent technique for the determination of hydrogen peroxide in the ambient atmosphere, Environ. Sci. Technol., 12, 1072-1076, 1978.

Laudenslager, J. B., R. W. Svorec, I. S. McDermid and T. J. Pacala, Development and application of excimer lasers for remote sensing, Tenth International Laser Radar Conference, Silver Springs, MD, 1980.

Laudenslager, J. B., T. J. Pacala and I. S. McDermid, Scanning, tunable XeCl laser: Characteristics and application to LIF detection of OH, Conference on Lasers and Electro-Optics (CLEO), Washington, D. C., 1981.

Laudenslager, J. B., I. S. McDermid and T. J. Pacala, Development of compact excimer lasers for remote sensing, Workshop on Optical and Laser Remote Sensing, Monterey, CA, 1982. (Also Springer Series on Optical Sciences: Optical and Laser Remote Sensing, D. K. Killinger and A. Mooradian, eds., Springer Verlag, 1983, Part 6.1, p. 236, 1982.)

Laudenslager, J. B., I. S. McDermid, T. J. Pacala and D. M. Rider, Applications of excimer lasers for atmospheric species measurements, New Lasers for Analytical and Industrial Chemistry, A. Bernhardt, ed., Proc. SPIE 461, 34, 1984.

Levine, J. S. and D. R. Schryer (Eds.), Man's Impact on the Troposphere - Lectures in Tropospheric Chemistry, NASA RP-1022, 1978.

Levy, H., II, Normal atmosphere: Large radical and formaldehyde concentrations predicted, Science, 173, 141-143, 1971.

Lovelock, J. E., Methyl chloroform in the troposphere as an indicator of OH radical abundance, Nature, 267, 32, 1977.

McDermid, I. S. and J. B. Laudenslager, Radiative lifetimes and quenching rate constants relevant to remote sensing of hydroxyl radicals with 308 nm excitation (XeCl), Topical Meeting on Spectroscopy in Support of Atmospheric Measurements, Sarasota, FL, 1980.

McDermid, I. S. and J. B. Laudenslager, Radiative lifetimes and quenching rate coefficients for directly excited rotational levels of OH ($A^2\Sigma^+$,v' = 0), J. Chem. Phys., 76, 1824, 1982.

McDermid, I. S., J. B. Laudenslager and T. J. Pacala, Application of new technological developments to the remote detection of atmospheric hydroxyl radicals using 308 nm excitation, Topical Meeting on Optical Techniques for Remote Probing of the Atmosphere, Lake Tahoe, NV, 1983a.

McDermid, I. S., J. B. Laudenslager and T. J. Pacala, The hydroxyl radical: Verification of lidar experiment, Jet Propulsion Laboratory Document JPL D-493, 1983b.

McDermid, I. S., T. J. Pacala and J. B. Laudenslager, The hydroxyl radical: Verification of lidar experiment. II. Nuclear radiation and resolved fluorescence experiments, Jet Propulsion Laboratory Document JPL D-1067, 1983c.

McDermid, I. S., J. B. Laudenslager and T. J. Pacala, New technological developments for the remote detection of atmospheric hydroxyl radicals, Appl. Opt., 22, 2586, 1983d.

Mihelcic, D., D. H. Ehhalt, J. Klomfass, G. F. Kulessa, U. Schmidt and M. Trainer, Measurements of free radicals in the atmosphere by matrix isolation and electron paramagnetic resonance, Ber. Bunsenges. Phys. Chem., 82, 16-19, 1978.

National Aeronautics and Space Administration, Applying Modeling Results in Designing a Global Tropospheric Experiment, NASA CP-2235, 1981.

National Aeronautics and Space Administration, Assessment of Techniques for Measuring Tropospheric N_xO_y, NASA CP-2292, 1983.

Ohbayashi, K., H. Akimoto and I. Tanaka, Emission spectra of CH_3O, C_3H_5O, and i-C_3H_7O radicals, J. Phys. Chem., 81, 798-802, 1977.

Ortgies, G., K. H. Gericke and F. J. Comes, Is UV laser induced fluorescence a method to monitor tropospheric OH, Geophys. Res. Lett., 7, 905-908, 1980.

Pacala, T. J., I. S. McDermid and J. B. Laudenslager, A wavelength scannable XeCl oscillator-ring amplifier laser system, Appl. Phy. Lett., 40, 1, 1982.

Pacala, T. J., I. S. McDermid and J. B. Laudenslager, Ultranarrow linewidth, magnetically switched, long pulse, xenon chloride laser, Appl. Phys. Lett., 44, 658, 1984.

Rees, D., I. McWhirter, P. A. Rounce, F. E. Barlow and S. J. Kellock, Miniature imaging photon detectors, J. Phys. E.: Sci. Instrum., 13, 763, 1980.

Rees, D., I. McWhirter, P. B. Hays and T. Dines, A stable, rugged, capacitance stabilized piezoelectric scanned Fabry-Perot etalon, J. Phys. E: Sci. Instrum., 14, 1320, 1981a.

Rees, D., I. McWhirter, P. A. Rounce and F. E. Barlow, Miniature imaging photon detectors. II. Devices with transparent photocathodes, J. Phys. E: Sci. Instrum., 14, 229, 1981b.

Rees, D., P. A. Rounce, I. McWhirter, A. F. D. Scott, A. H. Greenaway and W. Towlson, Observations of atmospheric absorption lines from a stabilized balloon platform and measurements of stratospheric winds, J. Phys. E: Sci. Instrum., 15, 191, 1982a.

Rees, D., T. J. Fuller-Rowell, A. Lyons, T. L. Killeen and P. B. Hays, Stable and rugged etalon for the dynamics explorer Fabry-Perot interferometer. 1. Design and construction, Appl. Opt., 21, 3896, 1982b.

Rodgers, M. O., J. D. Bradshaw, K. Liu and D. D. Davis, Sequential two-photon laser-induced fluorescence detection of mercury, Opt. Lett., 7, 359-361, 1982.

Schryer, D. R. (Ed.), Heterogeneous Atmospheric Chemistry, Geophysical Monograph 26, AGU, Washington, D. C., 1982.

Seinfeld, J. H., F. Allario, W. R. Bandeen, W. L. Chameides, D. D. Davis, E. D. Hinkley, and R. W. Stewart, Report of the NASA Working Group on Tropospheric Program Planning, NASA RP-1062, 1981.

Singh, H. B., Atmospheric halocarbons: Evidence in favor of reduced average hydroxyl radical concentrations in the troposphere, Geophys. Res. Lett., 4, 101-104, 1977a.

Singh, H. B., Preliminary estimation of average tropospheric OH concentrations in the northern and southern hemispheres, Geophys. Res. Lett., 4, 453-456, 1977b.

Singh, H. B., L. J. Salas and R. E. Stiles, Selected man-made halogenated chemicals in the air and oceanic environment, J. Geophys. Res., 88, 3675-3683, 1983.

Stepowski, D. and M. J. Cottereau, Time resolved study of rotational energy transfer in $A^2\Sigma^+$ (v' = 0) state of OH in a flame by laser induced fluorescence, J. Chem. Phys., 74, 6674, 1981.

Stimpfle, R. M. and J. G. Anderson, Tropospheric OH observations: Application of the high repetition rate atomic copper vapor laser, Second Symposium on the Composition of the Nonurban Troposphere, AMS, Washington, D. C., 1982.

Sze, R. C. and P. B. Scott, High energy lasing in XeBr in an electric discharge, Appl. Phys., 32, 479, 1978.

Volz, A., D. H. Ehhalt and R. G. Derwent, Seasonal and latitudinal variation of ^{14}CO and the tropospheric concentration of OH radicals, J. Geophys. Res., 86, 5163-5171, 1981.

Wang, C. C., L. I. Davis, Jr., C. H. Wu and S. Japar, Laser-induced dissociation of ozone and resonance fluorescence of OH in ambient air, Appl. Phys. Lett., 28, 14-16, 1976.

Wang, C. C., L. I. Davis, P. M. Selzer and R. Munoz, Improved airborne measurements of OH in the atmosphere using the technique of laser-induced fluorescence, J. Geophys. Res., 86C, 1181, 1215, 1981.

Wang, C. C. and L. I. Davis, Jr., Comments on "Theoretical and Experimental Assessment of the O_3/H_2O Interference Problem in the Detection of OH ..." by Davis et al., Geophys. Res. Lett., 8, 98, 1982.

Weinstock, B. and H. Niki, Carbon monoxide balance in nature, Science, 176, 290-292, 1972.

Wofsy, S., J. C. McConnell and M. B. McElroy, Atmospheric CH_4, CO and CO_2, J. Geophys. Res., 77, 4477-4495, 1972.

Zika, R. and E. S. Saltzman, Production of H_2O_2 in the aqueous phase via aeration of water samples with ambient air, Geophys. Res. Lett., 9, 231-234, 1982.

APPENDIX A

FUNDAMENTAL EQUATIONS OF THE LIF HYDROXYL MEASUREMENTS

INTRODUCTION: OBJECTIVES AND ORGANIZATION

The primary objective of this appendix is to define the equation relating OH concentration to the observed detector count rate for a given laser flux. That equation, which will be referred to henceforth as the "central equation" for absolute sensitivity, will be cast in terms of standard spectroscopic quantities such as oscillator strengths, Hönl-London factors, rotational and vibrational quantum numbers, etc., such that it may be tested directly under laboratory conditions.

A second objective will be to relate the working expressions used by each of the OH LIF groups to this central equation, thereby establishing a common language for the comparison of experimental results and the definition of LIF system performance.

Three sections comprise this appendix. The first details the relevant structural details of the OH radical via a spectroscopic description of the energy levels and transitions employed in the LIF method. Second, the central equation relating observed count rate to absolute concentration will be derived, and third, that equation will be related to the observed quantities cited by each of the experimental groups engaged in the measurement of OH in the Earth's atmosphere.

SPECTROSCOPY OF THE OH RADICAL

This section describes the structure of the $A^2\Sigma - X^2\Pi$ transition of the OH molecule. The electronic spin of the hydroxyl radical is 1/2, which produces a doublet structure. The selection rule, $\Delta J = 0 \pm 1$ for the total angular momentum quantum number, means that each component of the doublet has three main branches. Two vector coupling schemes are of importance here. The first (Herzberg, 1950), conventionally called Hund's case (a), assumes that the interaction between nuclear rotation and electronic motion is very weak. The electronic motion is coupled to the internuclear axis, as shown in figure A1. The electronic angular momentum, Ω (angular momentum will be referred to in units of h), is defined as the sum of Λ and Σ, the electron orbital angular momentum and the electron spin, respectively. The total angular momentum, J, then assumes the values $J = \Omega, \Omega + 1, \Omega + 2, \ldots$, and need not be an integer.

If, however, $\Lambda = 0$, as in the A state of OH, the spin vector, S, is not coupled to the internuclear axis and Ω is not defined. Hund's case (a) then becomes meaningless, and is replaced by Hund's case (b). In this case, the angular momenta, Λ, and N form a resultant K, which is shown in figure A2. The quantum number, K, is the total angular momentum apart from spin, and may assume the values Λ, $\Lambda + 1$, $\Lambda + 2$, etc. It must be an integer. The two components of the doublet structure thus correspond to $J = K \pm 1/2$. The coupling cases are simply conceptual devices and represent limiting cases; for instance, as J

(or K) increases, a molecule that was originally close to case (a) may approach case (b).

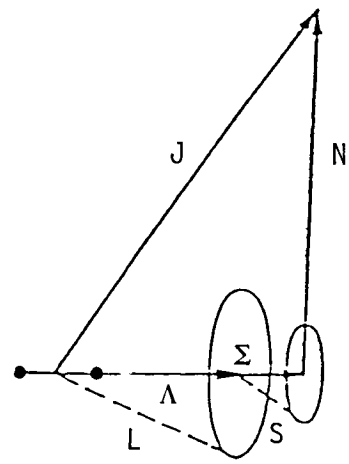

Figure A1. Vector diagram of Hund's case (a).

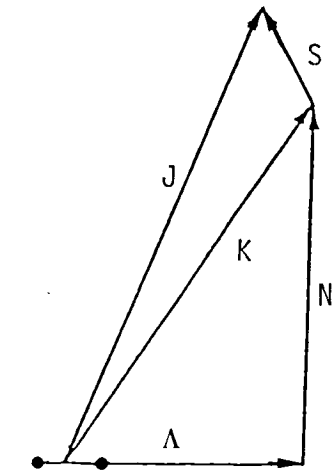

Figure A2. Vector diagram of Hund's case (b).

There exist, then, six main branches: R_1, R_2, Q_1, Q_2, P_1, and P_2, for $\Delta J = \pm 1, 0, -1$, respectively. There are also six satellite branches for which $\Delta K \neq \Delta J$. These are shown in figure A3, along with the main branches. The superscript indicates the ΔK of the transition, and the subscript indicates the upper to lower doublet transition. Figure A3 assumes that the $^2\Pi$ state conforms to case (a) for which we can effectively divide each of the bands into two subbands: $^2\Pi_{1/2} - {}^2\Sigma$, and $^2\Pi_{3/2} - {}^2\Sigma$.

The rotational term values for the $X^2\Pi$ state have been calculated by Hill and Van Vleck (1928):

$$F_1(J) = B_v[(J + 1/2)^2 - \lambda^2 - 1/2\sqrt{4(J + 1/2)^2 + Y(Y - 4)\lambda^2}] - D_v J^4$$

$$F_2(J) = B_v[(J + 1/2)^2 - \lambda^2 - 1/2\sqrt{4(J + 1/2)^2 + Y(Y - 4)\lambda^2}] - D_v(J + 1)^4$$

where Y A/B_v with A ≡ coupling constants which measure the strength of the coupling between the spin and the projection of the orbital angular momentum on the internuclear axis

F_1 refers to the components with $J = K + 1/2$

F_2 refers to those with $J = K - 1/2$, as summarized here:

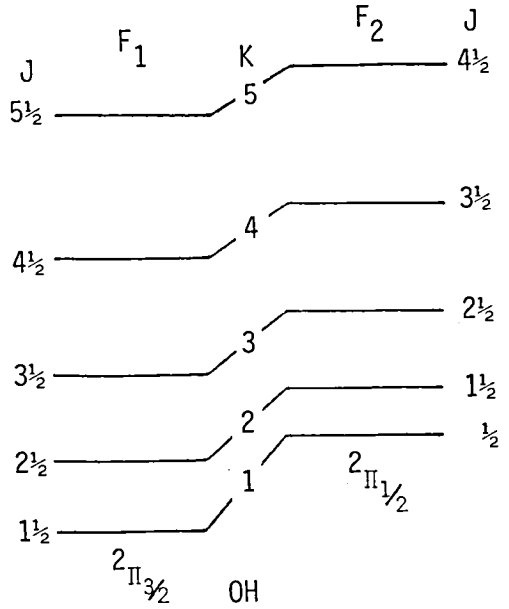

Molecular constants for OH have been reviewed recently by Huber and Herzberg (1979). That review is included here in table A1 to provide the spectroscopic data base for this and subsequent sections.

State	T_e	ω_e cm^{-1}	$\omega_e\chi_e$ cm^{-1}	B_e cm^{-1}	α_e cm^{-1}	D_e $10^{-4}cm^{-1}$	r_e Å	Observed Transitions	
$C^2\Sigma^+$	89459.	1232.9	19.1	9.247	0.078	2	2.046	C → A C → X	55820.7 (88223)
$D^2\Sigma^-$	82130	2954		15.2179		16.16	1.0809	D ↔ X	81759.7
$B^2\Sigma^+$	69774	660		5.086		9.29	1.869	B → A	35965.5
$A^2\Sigma$	32684.1	3178.8	92.91	17.358	0.786	20.39	1.0121	A ↔ X	32402.3
$X^2\Pi$	0	3737.76	84.881	18.910	0.7242	19.38	0.96960	1/2 ← 3/2	126.23

Summary with complete literature search can be found in Huber and Herzberg (1979).

Table A1. Spectroscopic constants for $^{16}O^1H$.

Figure A3 (Anderson, 1971) shows that both F_1 and F_2 are double. The rotational term values given previously do not reflect this, as the interaction between the rotation of the nuclei and the projection of λ on the internuclear axis L has been neglected. This interaction increases with increasing rotation. The components correspond to the opposite symmetry with respect to inversion at the origin of coordinates and are usually designated Π_i^+ and Π_i^- where i can be 1 or 2, depending on the doublet in question.

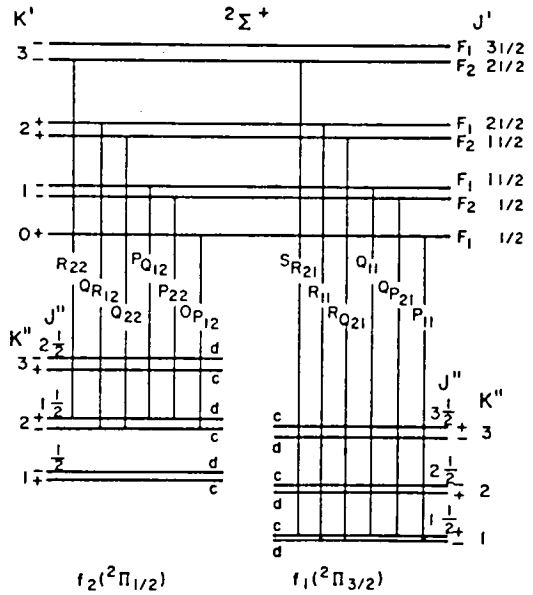

Figure A3. The transition array including satellite branches for $A^2\Sigma$-$X^2\Pi$ transition of the hydroxyl radical.

The relative transition probabilities or line strengths for the $^2\Sigma$ - $^2\Pi$ transition have been expressed for an arbitrary coupling constant by Earls (1935). His expressions represent specialized cases of formulas derived by Hill and Van Vleck (1928). Earls' expressions are given by the equations below. The upper sign in the expression always refers to the main branch, and the lower sign represents the satellite branch.

$$S = \left(\frac{2J + 1}{J}\right)\left(\frac{(2J + 1) \pm U[(2J + 1)^2 - 2A]}{32}\right) \qquad \begin{matrix} P_1 \\ O_{P_{12}} \end{matrix}$$

$$S = \left(\frac{2J + 1}{J + 1}\right)\left(\frac{(2J + 1)^2 - 2 \pm U[(2J + 1)^3 - 8J + 2(A - 4)]}{32}\right) \qquad \begin{matrix} Q_1 \\ P_{Q_{12}} \end{matrix}$$

$$S = \left(\frac{2J + 1}{J + 1}\right)\left(\frac{(2J + 1) \pm U[(2J + 1)^2 + 2(A - 4)]}{32}\right) \qquad \begin{matrix} R_1 \\ Q_{R_{12}} \end{matrix}$$

$$S = \left(\frac{2J + 1}{J}\right)\left(\frac{(2J + 1) \pm U[(2J + 1)^2 + 2(A - 4)]}{32}\right) \qquad \begin{matrix} Q_2 \\ Q_{P_{21}} \end{matrix}$$

$$S = \left(\frac{2J + 1}{J + 1}\right)\left(\frac{(2J + 1)^2 - 2 \pm U[(2J + 1)^3 - 8J - 2A)]}{32}\right) \qquad \begin{matrix} Q_2 \\ R_{Q_{21}} \end{matrix}$$

$$S = \left(\frac{2J + 1}{J + 1}\right)\left(\frac{(2J + 1) \pm U[(2J + 1)^2 - 2A)]}{32}\right) \qquad \begin{matrix} R_2 \\ S_{R_{21}} \end{matrix}$$

$$\text{where } U = \frac{1}{\sqrt{(2J + 1)^2 + A(A - 4)}}$$

The values of J are those of the $^2\Pi$ state.

The basic parameters in the structure of the transition discussed in this section will be used in the sections that follow to calculate the observed count rate for a given laser flux, pumping transition, scattering geometry, pressure, and OH concentration.

THE CENTRAL EQUATION FOR

LASER-INDUCED FLUORESCENCE ABSOLUTE CALIBRATION

In the spirit of writing an equation relating observed signal-to-OH concentration, we begin by assuming that the radiation field used to induce fluorescence is capable of pumping any combination of rovibronic transitions. Given the capability of modern lasers to select a single rovibronic transition, however, the resulting summation over pumped transitions will collapse to a single term in the equation defining the kinetics of mixed radiation and collisional energy transfer appropriate to this problem.

A fully detailed treatment of this problem would require the solution of a coupled set of time-dependent equations of the form:

$$\frac{dN(J',v',E)}{dt} = P_{laser} + P_{v',J'} - L_{v',J'} - L^{X^2\Pi}_{v',J'} - L_{rad}$$

- P_{laser}: Production rate to quantum level J',v' in electronic state E' from laser excitation
- $P_{v',J'}$: Production rate from v,J energy transfer into v',J' from all other levels
- $L_{v',J'}$: Removal by v,J energy transfer within $A^2\Sigma$ state
- $L^{X^2\Pi}_{v',J'}$: Collisional deactivation to $X^2\Pi$ state from v'J' level of $A^2\Sigma$
- L_{rad}: Removal by radiation to lower rovibronic state

Examples of the functional form of these terms are indicated below following standard kinetic and spectroscopic notation. (See Steinfeld, 1978, and Herzberg, 1950.)

The state-to-state energy transfer terms into v',J' from all other levels v_i,J_j in the $A^2\Sigma$ state will be of the form:

$$P_{v',J'} = \sum_{i,j} k^{II}(v',J';v_i,J_j)[M][OH(v_i,J_j,A^2\Sigma)]$$

where the $k^{II}(v',J';v_i,J_j)$'s are the bimolecular rate constants representing the rates of collisional energy transfer and [M] is the bath gas. Because of the distinct difference in rates for O_2 and N_2, a full solution will require two such sums, one for $M \equiv N_2$ and one for $M \equiv O_2$.

The rate of laser-induced excitation will take the form:

$$P_{laser}(v_x,J_x,X^2\Pi;v_A,J_A,A^2\Sigma) =$$

$$N(v_x,J_x,\theta)f_{v_x \to v_A}\left(\frac{S(J_x,J_A)}{2J_A + 1}\right)\frac{\pi e^2}{mc}\left[\int_{-\infty}^{\infty} F(\nu)g(\nu)d\nu\right][OH(X^2\Pi)]$$

where all quantities have been previously defined. We will adopt the convention for quantum levels such that for laser-induced excitation followed by collisional redistribution and radiation, the sequence in quantum numbers is:

$$(v_x,J_x,X^2\Pi) \xrightarrow[\text{excitation}]{\text{laser-induced}} (v_A,J_A,A^2\Sigma) \xrightarrow[\text{transfer}]{\text{collision}}$$

$$(v',J',A^2\Sigma) \xrightarrow[\text{quenching}]{\text{radiation}} (v'',J'',X^2\Pi)$$

The two major candidates for laser-induced fluorescence in the atmosphere are indicated in figure A4; specifically,

Option 1:

$$(v_x = 0,J_x,X^2\Pi) \xrightarrow[\text{absorbed}]{282\text{ nm}} (v_A = 1,J_A,A^2\Sigma)$$

followed by

$$(v' = 0,J_x,A^2\Sigma) \xrightarrow[\text{emitted}]{309\text{ nm}} (v'' = 0,J'',X^2\Pi)$$

or

Option 2:

$$(v_x = 0,J_x,X^2\Pi) \xrightarrow[\text{absorbed}]{309\text{ nm}} (v_A = 0,J_A,A^2\Sigma)$$

followed by

$$(v' = 0, J', A^2\Sigma) \xrightarrow[\text{emitted}]{309\ \text{nm}} (v'' = 0, J'', X^2\Pi)$$

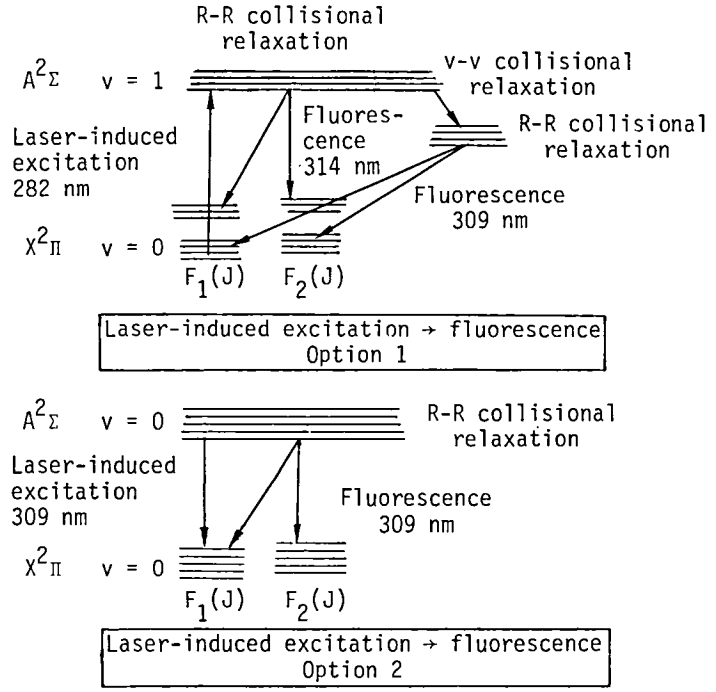

Figure A4. Two possible options for laser-induced fluorescence of hydroxyl radical.

Given that option 2 is much simpler to treat because of the absence of v_A - v' transfer in the upper electronic state, we will write our "central equation" for the more complicated case represented by option 1.

For tropospheric OH measurements (and in fact for stratospheric measurements down to a total pressure of ∿10 torr), rotational and vibrational relaxation rates are so fast in the time scale of fluorescence that, to an excellent degree of approximation, we can represent the process of laser-induced fluorescence as:

1. A rate of excitation from the $(v_X, J_X, X^2\Pi)$ level pumped by the laser to $(v_A, J_A, A^2\Sigma)$

2. Fraction of molecules which (a) collisionally relax from $(v_A, J_A, A^2\Sigma) \rightarrow (v' = 0, J', A^2\Sigma)$ to (b) those which leave the $(v_A, J_A, A^2\Sigma)$ level by collisional relaxation but remain in the $A^2\Sigma$ state, leave the $(v_A, J_A, A^2\Sigma)$ level by radiation to the $X^2\Pi$ state, and those which are rovibronically quenched by collision

3. Fraction of molecules in $(v' = 0, J', A^2\Sigma)$ which radiate in competition with collisional quenching of the $A^2\Sigma$ state

That is, to an adequate level of accuracy, the number of photons observed per pulse, S_{OH}, in a specific $(v',J',A^2\Sigma) \rightarrow (v'',J'',X^2\Pi)$ rovibronic transition is a product:

$$S_{OH} = \left\{\begin{array}{l}\text{Rate of excitation}\\ \text{from } (v_X,J_X,X^2\Pi) \text{ to}\\ (v_A,J_A,A^2\Sigma) \text{ integrated}\\ \text{over a laser pulse}\end{array}\right\} \times \left\{\begin{array}{l}\text{Fraction of molecules}\\ \text{collisionally coupled from}\\ (v_A,J_A,A^2\Sigma) \rightarrow (v',J',A^2\Sigma)\\ \text{relative to all other removed}\\ \text{terms from } (v_A,J_A,A^2\Sigma)\end{array}\right\}$$

$$\times \left\{\begin{array}{l}\text{Fraction of molecules}\\ \text{in } (v' = 0,J',A^2\Sigma) \text{ which}\\ \text{radiate in competition}\\ \text{with collisional}\\ \text{quenching of the A state}\end{array}\right\} \times \left\{\begin{array}{l}\text{Fraction of the total}\\ \text{number of photons emitted}\\ \text{within the detection vol-}\\ \text{ume which are collected}\\ \text{by detection optics}\end{array}\right\}$$

$$\times \left\{\begin{array}{l}\text{Volume of scattering}\\ \text{region defined by the}\\ \text{overlap of the laser}\\ \text{beam and the detector's}\\ \text{field of view}\end{array}\right\}$$

We proceed to write the explicit expressions for each of these terms in order of their appearance above:

Step 1:

$$\left\{\begin{array}{l}\text{Rate of excitation}\\ \text{from } (v_X,J_X,X^2\Pi) \text{ to}\\ (v_A,J_A,A^2\Sigma) \text{ integrated}\\ \text{over a laser pulse}\end{array}\right\} = N(v_X,J_X,\theta) f_{v_X \rightarrow v_A} \left(\frac{S(J_X,J_A)}{2J_A + 1}\right)$$

$$\times \frac{\pi e^2}{mc}\left[\int_0^{\Delta t} dt \int_{-\infty}^{\infty} F(\nu,t)g(\nu)d\nu\right][OH(X^2\Pi)]$$

where Δt is sufficiently long to encompass the full width of the laser pulse.

Step 2:

$$\left\{\begin{array}{l}\text{Fraction of molecules}\\ \text{collisionally coupled}\\ \text{from } (v_A,J_A,A^2\Sigma) \rightarrow\\ (v',J',A^2\Sigma)\end{array}\right\} = \frac{k^I_{v_A \rightarrow v'}}{k^I_{v_A \rightarrow v'} + k^I_Q + k^I_R}$$

where $k^I_{v_A \to v'}$ is the first-order rate constant for vibrational relaxation from v_A to v'

k^I_Q is the first-order rate constant for collisional deactivation from the $A^2\Sigma$ state

$k^I_R = \sum_{J''} A(v' = 0,J';v'' = 0,J'')$ is the first-order rate for radiation from v',J' to all allowed lower levels in the $X^2\Pi$ state

Step 3:

$$\left\{\begin{array}{l}\text{Fraction of molecules}\\ \text{in } (v' = 0,J',A^2\Sigma) \text{ which}\\ \text{radiate in competition}\\ \text{with collisional quenching}\\ \text{of the A state}\end{array}\right\} = \frac{\sum_{\substack{\text{allowed}\\ J''}} A(v' = 0,J';v'' = 0,J'')}{\sum_{\substack{\text{allowed}\\ J''}} A(v' = 0,J';v'' = 0,J'') + k^I_Q}$$

where the $A(v' = 0,J';v'' = 0,J'')$'s are the Einstein A coefficients for emission from J' to all available J"s.

Summarizing, we have:

$$S_{OH}(v_x,J_x,X^2\Pi;v_A,J_A,A^2\Sigma;v',J',A^2\Sigma;v'',J'',X^2\Pi) =$$

$$N(v_x,J_x,X^2\Pi,\theta) f_{v_x \to v_A} \left(\frac{S(J_x,J_A)}{2J_A + 1}\right) \frac{\pi e^2}{mc} \left[\int_0^{\Delta t} dt \int_{-\infty}^{\infty} F(\nu,t)g(\nu)d\nu\right]$$

$$\times [OH(X^2\Pi)] \left[\frac{k^I_{v_A \to v'}}{k^I_{v_A \to v'} + k^I_Q + k^I_R}\right] \left[\frac{\sum_{\substack{\text{allowed}\\ J''}} A(v' = 0,J';v'' = 0,J'')}{\sum_{\substack{\text{allowed}\\ J''}} A(v' = 0,J';v'' = 0,J'') + k^I_Q}\right]$$

$$\times \left[\int_{\substack{\text{scattering}\\ \text{volume}}} \varepsilon dV\right] [T\eta]$$

We proceed to explicitly define the quantities required to determine the rate of laser excitation from the $X^2\Pi$ state to the $A^2\Sigma$ state.

Given the λ doubling of the $^2\Pi$ state and the symmetry rule for dipole transitions, the detailed definition of $N(v_x,J_x,\theta)$ is important. We will use the convention that the normalized population refers to the fractional population which can absorb laser radiation at a single frequency.

Table A2 specifies the term values for the $F_1(K)$ and $F_2(K)$ components of the $X^2\Pi$ state.

K	$F_1(K)$	J	$F_2(K)$	J
1	0.0 cm^{-1}	1-1/2	127 cm^{-1}	1/2
2	84	2-1/2	188	1-1/2
3	202	3-1/2	290	2-1/2
4	355	4-1/2	430	3-1/2
5	544	5-1/2	608	4-1/2
6	768	6-1/2	824	5-1/2
7	1028	7-1/2	1077	6-1/2
8	1322	8-1/2	1366	7-1/2
9	1651	9-1/2	1692	8-1/2
10	2016	10-1/2	2053	9-1/2

Table A2. Rotational term values for the doublet components of the $X^2\Pi$ state.

The normalized population in each of $F_1(K)$ and $F_2(K)$ components is tabulated in table A3, with explicit account taken of the λ doublet structure.

System	K	J	$N^+(v_x,J_x,\theta)$	$N^-(v_x,J_x,\theta)$
$^2\Pi_{3/2}$	1	1-1/2	.099	.099
	2	2-1/2	.099	.099
	3	3-1/2	.075	.075
$F_1(K)$	4	4-1/2	.044	.044
	5	5-1/2	.021	.021
	6	6-1/2	.009	.009
J = K + 1/2	7	7-1/2	.003	.003
$^2\Pi_{1/2}$	1	1/2	.027	.027
	2	1-1/2	.040	.040
	3	2-1/2	.037	.037
$F_2(K)$	4	3-1/2	.025	.025
	5	4-1/2	.013	.013
	6	5-1/2	.006	.006
J = K - 1/2	7	6-1/2	.002	.002

Table A3. Normalized population in each rotational level up to K = 7 in both doublet components.

Table A4a summarizes the literature values of the band oscillator strengths for the $v_X - v_A$ transitions of interest. At the present time, the only vibrational bands of interest to this subject are those

of the 0 → 0 and 0 → 1 bands; for completeness, the 1 → 1 band is given for subsequent steps in this document.

Band Oscillator Strength	Value	References
$f_{0 \to 0}$	9.5×10^{-4}	Huber and Herzberg (1979). See table A1.
$f_{0 \to 1}$	2.7×10^{-4}	Huber and Herzberg (1979). See table A1.
$f_{1 \to 1}$	4.5×10^{-4}	References in table A1.

Table A4a. Summary of band oscillator strengths.

Table A4b presents the dependence of the oscillator strength in the rotational level from the work of Wang and Killinger (1979). Results

	$q(0,0,J',J'')$			$T_{J'J''}$		
J''	P	Q	R	P	Q	R
1	0.9145	0.9136	0.9118	1.0002	0.9982	0.9943
2	0.9150	0.9132	0.9105	0.9986	0.9947	0.9889
3	0.9154	0.9127	0.9091	0.9953	0.9894	0.9817
4	0.9156	0.9120	0.9074	0.9902	0.9825	0.9728
5	0.9156	0.9111	0.9056	0.9834	0.9738	0.9623
6	0.9155	0.9101	0.9036	0.9749	0.9634	0.9500
7	0.9151	0.9088	0.9013	0.9647	0.9513	0.9362
8	0.9147	0.9074	0.8989	0.9528	0.9377	0.9208
9	0.9140	0.9058	0.8962	0.9393	0.9224	0.9038
10	0.9131	0.9039	0.8933	0.9242	0.9056	0.8853
11	0.9121	0.9109	0.8902	0.9076	0.8873	0.8654
12	0.9109	0.8997	0.8868	0.8894	0.8675	0.8441
13	0.9095	0.8972	0.8832	0.8698	0.8464	0.8215
14	0.9079	0.8946	0.8794	0.8488	0.8239	0.7976
15	0.9061	0.8917	0.8753	0.8265	0.8001	0.7725
16	0.9041	0.8886	0.8709	0.8028	0.7751	0.7463
17	0.9020	0.8852	0.8660	0.7780	0.7491	0.7190
18	0.8996	0.8816	0.8613	0.7520	0.7219	0.6908
19	0.8970	0.8778	0.8561	0.7250	0.6938	0.6617
20	0.8941	0.8737	0.8506	0.6970	0.6648	0.6319
21	0.8911	0.8693	0.8447	0.6681	0.6351	0.6014
22	0.8878	0.8646	0.8386	0.6384	0.6046	0.5703
23	0.8842	0.8597	0.8321	0.6080	0.5736	0.5387
24	0.8805	0.8545	0.8254	0.5770	0.5421	0.5068
25	0.8764	0.8490	0.8182	0.5456	0.5102	0.4747

Table A4b. Values of the Franck-Condon factors q(0,0,J',J") and the correction factor $T_{J',J''}$ for the P, Q, and R branch transitions of OH. The following spectroscopic data are used: $D_1/B_1 = 1.20 \times 10^{-4}$, $D_2/B_2 = 1.01 \times 10^{-4}$, $r_{10} = 1.0121$Å, $r_{20} = 0.9706$Å, $\alpha_1 = 0.897 \times 10^{18}$ cm^{-2}, $\alpha_2 = 1.056 \times 10^{13}$ cm^{-2}. (From Wang and Killinger, 1979)

are summarized in terms of a correction factor $T_{J',J''}$ for the P, Q, and R branch transitions of OH. This should not be confused with the term values in the previous development.

The Hönl-London factors defining the rotational line strength have been tabulated by Dieke and Crosswhite (1961). Although more recent treatments are available, what we seek is a self-consistent treatment relating absolute OH concentration, measured absorption, band oscillator strength, and normalized line strength. This question has been addressed directly in the OH band oscillator strength measurement by chemical technique (Golden et al., 1964).

Table A5 presents the tabulated Hönl-London factors which are correctly normalized for:

$$\sum_{J'} S_{J',J''} = 4(2J'' + 1)$$

K	P_1	P_2	Q_1	Q_2	R_1	R_2	O_{12}	P_{12}	Q_{21}	Q_{12}	R_{21}	S_{21}
1	9·4		0·0	5·3	2·6	2·7		5·3	6·3	2·8	3·9	0·8
2	12·7	4·4	17·0	11·0	6·1	5·7	1·3	6·0	5·1	3·8	5·1	1·2
3	16·5	8·6	25·3	18·2	10·1	8·9	1·7	6·3	5·3	4·2	5·4	1·4
4	20·5	12·9	33·7	26·1	14·2	12·8	1·8	6·2	4·9	4·2	5·3	1·4
5	24·5	17·4	42·2	34·4	18·4	16·7	1·8	5·9	4·4	4·0	5·1	1·4
6	28·6	21·8	50·6	42·6	22·7	20·7	1·7	5·5	4·0	3·7	4·8	1·4
7	32·7	26·1	59·1	51·0	26·9	24·8	1·6	5·1	3·7	3·5	4·4	1·3
8	36·8	30·5	67·5	59·3	31·1	28·8	1·5	4·7	3·4	3·2	4·1	1·2
9	40·9	34·8	75·8	67·7	35·3	32·9	1·4	4·3	3·1	3·0	3·8	1·1
10	44·9	39·0	84·1	76·0	39·5	37·0	1·3	4·0	2·8	2·8	3·6	1·1
11	49·0	43·3	92·4	84·2	43·7	41·0	1·2	3·7	2·6	2·6	3·4	1·0
12	53·1	47·5	100·6	92·5	47·8	45·1	1·1	3·5	2·5	2·4	3·2	0·9
13	57·1	51·6	108·8	100·7	51·9	49·1	1·0	3·3	2·3	2·3	3·0	0·9
14	61·2	55·8	117·0	108·9	56·0	53·2	1·0	3·1	2·2	2·1	2·8	0·9
15	65·2	59·9	125·2	117·1	60·2	57·2	0·9	2·9	2·0	2·0	2·6	0·8
16	69·3	64·0	133·3	125·2	64·2	61·3	0·9	2·7	1·9	1·9	2·5	0·8
17	73·3	68·1	141·5	133·4	68·3	65·3	0·8	2·6	1·8	1·8	2·4	0·7
18	77·3	72·2	149·6	141·5	72·4	69·3	0·8	2·4	1·7	1·7	2·3	0·7
19	81·4	76·3	157·7	149·6	76·5	73·4	0·7	2·3	1·7	1·6	2·2	0·7
20	85·4	80·4	165·8	157·7	80·5	77·4	0·7	2·2	1·6	1·6	2·1	0·6
21	89·4	84·5	173·9	165·8	84·6	81·4	0·7	2·1	1·5	1·5	2·0	0·6
22	93·4	88·5	182·0	173·9	88·7	85·4	0·6	2·0	1·4	1·4	1·9	0·6
23	97·5	92·6	190·1	182·0	92·7	89·5	0·6	1·9	1·4	1·4	1·8	0·6
24	101·5	96·7	198·2	190·1	96·8	93·5	0·6	1·9	1·3	1·3	1·8	0·5
25	105·5	100·7	206·7	198·2	100·8	97·5	0·6	1·8	1·3	1·3	1·7	0·5
26	109·5	104·8	214·3	206·2	104·9	101·5	0·5	1·7	1·2	1·2	1·6	0·5
27	113·5	108·8	222·4	214·3	108·9	105·5	0·5	1·7	1·2	1·2	1·6	0·5
28	117·5	112·9	230·4	222·4	112·9	109·6	0·5	1·6	1·2	1·2	1·5	0·5
29	121·6	116·9	238·4	230·4	117·0	113·6	0·5	1·6	1·1	1·1	1·5	0·5
30	125·6	120·9	246·5	238·4	121·0	117·6	0·5	1·5	1·1	1·1	1·4	0·4
31		125·0		246·0		121·6	0·5	1·5		1·0		

Table A5. Rotational-transition probabilities for a $^2\Sigma \rightarrow {}^2\Pi$ transition with the coupling constant $\alpha = -7.55$. (The K values are those of the final state.) (From Dieke and Crosswhite, 1961)

We turn next to the question of the overlap integral:

$$\int F(\nu)g(\nu)d\nu$$

In order to standardize the nomenclature, we review briefly the relationship between peak absorption cross section, integrated absorption cross section, integrated flux, and the above integral. Toward this end, we consider the case of two Gaussian envelopes summarized in figure A5. The Doppler width of OH absorption, $\Delta\nu_D$, is somewhat less than the FWHM of the laser emission envelope, $\Delta\nu_L$.

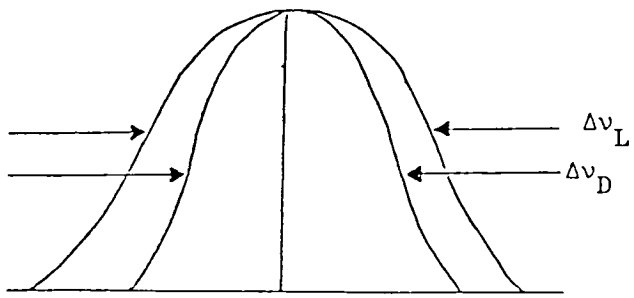

Figure A5. Illustrative Gaussian envelopes.

We define the Gaussian absorption line shape (see, for example, Killinger, 1978):

$$\sigma(\nu) = \sigma_o p(\nu) = \sigma_o \left(\frac{4\ \ln\ 2}{\pi}\right)^{1/2} \Delta\nu_D^{-1}\ \exp\left[-4(\ln\ 2)\ \frac{(\nu - \nu_D)^2}{\Delta\nu_D^2}\right]$$

noting that:

$$\int \left(\frac{4\ \ln\ 2}{\pi}\right)^{1/2} \Delta\nu_D^{-1}\ \exp\left[-4(\ln\ 2)\ \frac{(\nu - \nu_D)^2}{\Delta\nu_D^2}\right] d\nu = 1$$

Thus,

$$\int \sigma(\nu)d\nu = \sigma_o \int p(\nu)d\nu = \sigma_o$$

Note that:

$$\sigma_o = \frac{\pi e^2}{mc}\ f_{v',v''}\left(\frac{S_{J',J''}}{4(J'' + 1)}\right)$$

The frequency dependence of the laser flux is given by:

$$F(\nu) = F_o\left(\frac{4\ \ln\ 2}{\pi}\right)^{1/2} \Delta\nu_L^{-1}\ \exp\left[-4(\ln\ 2)\ \frac{(\nu - \nu_L)^2}{\Delta\nu_L^2}\right]$$

If the positions of the Doppler profile ν_D and the laser line width ν_L are coincident (which is typically the case), the integral is straightforward:

$$\int F(\nu)\sigma(\nu)d\nu = F_o\sigma_o\left(\frac{4\ \ln\ 2}{\pi}\right)\left(\frac{1}{\Delta\nu_D}\right)\left(\frac{1}{\Delta\nu_L}\right)$$

$$\times \int_{-\infty}^{\infty} \exp\left[-4(\ln\ 2)\left(\frac{(\nu - \nu_D)^2}{\Delta\nu_D^2} - \frac{(\nu - \nu_L)^2}{\Delta\nu_L^2}\right)\right] d\nu$$

$$= F_o\sigma_o\ 2\left(\frac{\ln\ 2}{\pi}\right)^{1/2}\left(\frac{1}{\Delta\nu_L^2 + \Delta\nu_D^2}\right)^{1/2}$$

It is frequently of interest to relate this expression to the absorption at the peak of the absorption line:

$$\sigma(\nu)_{\nu_{peak}} = \sigma_o\left(\frac{4\ \ln\ 2}{\pi}\right)^{1/2}\left(\frac{1}{\Delta\nu_D}\right) = \sigma_{peak}$$

So,

$$\sigma_o = \left(\frac{\pi}{4\ \ln\ 2}\right)^{1/2} \Delta\nu_D\sigma_{peak}$$

Thus,

$$\int F(\nu)\sigma(\nu)d\nu = F_o\sigma_{peak}\ \left(\frac{\Delta\nu_D^2}{\Delta\nu_L^2 + \Delta\nu_D^2}\right)^{1/2}$$

This provides a simple means of comparison given the laser line width, spectral character of the laser, and total flux.

RELATIONSHIP BETWEEN THE CENTRAL EQUATION AND THE WORKING EXPRESSIONS FOR EACH RESEARCH GROUP

The objective of this section is first to link the central equation to each of the published working expressions used by each group, and second to link each of the equations used by the various groups to each other to eliminate ambiguities. Schematically, both objectives are shown in figure A6.

$$S_{OH}(v_x,J_x,X^2\Pi;v_A,J_A,A^2\Sigma;v',J',A^2\Sigma;v'',J'',X^2\Pi) =$$

$$N(v_x,J_x,X^2\Pi,\theta)f_{v_x \rightarrow v_A}\left(\frac{S(J_x,J_A)}{2J_A+1}\right)\frac{\pi e^2}{mc}\left[\int_0^{\Delta t} dt \int_{-\infty}^{\infty} F(\nu,t)g(\nu)d\nu\right]$$

$$\times [OH(X^2\Pi)]\left[\frac{k^I_{v_A \rightarrow v'}}{k^I_{v_A \rightarrow v'} + k^I_Q + k^I_R}\right]\left[\frac{\sum_{\substack{\text{allowed}\\J''}} A(v'=0,J';v''=0,J'')}{\sum_{\substack{\text{allowed}\\J''}} A(v'=0,J';v''=0,J'') + k^I_Q}\right]$$

$$\times \left[\int_{\substack{\text{scattering}\\\text{volume}}} \epsilon dV\right][T\eta]$$

- *Ford* — $S = A[OH]\frac{\sigma_o(OH)}{\Delta\nu}\eta\,(\Delta n/n)$
- *Georgia Tech* — $D = E_{\lambda_1} \times E_f \times E_d \times E_e \times V \times [OH]$
- *Harvard* — $S_{OH} = \left[\int F(\lambda)\sigma(\lambda)d\lambda\right][OH][\epsilon T\eta]VQ = C_{OH}\bar{E}Q[OH]$
- *Goddard* — $S = I\bar{n}\bar{\sigma}\eta\epsilon\frac{A_t}{4\pi}\int_{z_1}^{z_2} T_1T_2\frac{O}{z^2}dz$
- *Portland State* — $S_{OH} = [OH]T_c(P_f/P_{amb})N_pGL\sigma_o(OH)(n_1/n)YO_1O_m\Omega T_aT_m\eta T_gT_d$

Figure A6. Schematic representation of relationship between the central equation and the working expressions for each research group.

Ford Research Group (See Wang et al., 1981.)

The working expression used by the Ford group is expressed in terms of the observed count rate:

$$S = A[OH] \frac{\sigma_o(OH)}{\Delta\nu} \eta(\Delta n/n)$$

where A instrumental parameter determined by overall excitation and collection efficiency

[OH] hydroxyl concentration, cm^{-3}

$\sigma_o(OH)$ integrated absorption cross section for OH; specifically,

$$\sigma_o(OH) = r_o c f_{v_x \rightarrow v_A}$$

where $r_o = e^2/(mc)^2 = 2.8 \times 10^{-13}$ cm

and $f_{v_x \rightarrow v_A}$ is the band oscillator

$\Delta\nu$ effective line width of the transition which takes into account the ratio of the laser line "envelope" to the Doppler width of the transition; for all the laser systems currently in use, the envelope of longitudinal modes from the doubled output of the dye laser is equal to or somewhat broader than the Doppler line width of the absorption, as noted in figure A5

η fluorescence efficiency under ambient conditions

$\Delta n/n$ fraction of OH population in rotational level from which excitation originates

We proceed next to the specifications of the correlation between each of the terms in the central equation and the quantities cited above. The identification is straightforward:

$$(\Delta n/n) = N(v_x, J_x, \theta) = \frac{(2J_x + 1) \exp[-(hc/k\theta)T(v_x, J_x)]}{\sum_v \sum_{J_x} (2J_x + 1) \exp[-(hc/k\theta)T(v_x, J_x)]}$$

$$\eta = \left[\frac{k^I_{v_A \rightarrow v'}}{k^I_{v_A \rightarrow v'} + k^I_Q + k^I_R}\right]\left[\frac{\sum_{J''} A(v' = 0, J'; v'' = 0, J'')}{\sum_{J''} A(v' = 0, J'; v'' = 0, J'') + k^I_Q}\right]$$

$$\sigma_o(OH) = \pi r_o c f_{v_x \rightarrow v_A}$$

The quantity

$$A\frac{\sigma_o(OH)}{\Delta\nu} = f_{v_x \to v_A}\left(\frac{S(J,Br)}{2J'(Br)+1}\right)\frac{\pi e^2}{mc}\int_{-\infty}^{\infty}F(\nu)g(\nu)d\nu$$

$$\times\left[\int_{\text{Scattering Volume}}\varepsilon dV\right][Tn]$$

Georgia Tech Reserch Group (See Bradshaw and Davis, 1982.)

The LIF signal, D, in counts/pulse, is expressed in terms of efficiency terms such that

$$D = E_{\lambda_1} \times E_f \times E_d \times E_e \times V \times [OH]$$

where

$$E_{\lambda_1} = \begin{pmatrix}\text{Optical pumping}\\ \text{efficiency at } \lambda_1\end{pmatrix} = \left[1 - \exp\left(-\frac{P_{\lambda_1}\sigma_{\lambda_1}}{a_{\lambda_1}}\right)\right] \times f_2 \times S_{\lambda_1}$$

with P_{λ_1} representing the number of laser photons per shot at the pumping wavelength λ_1

σ_{λ_1} effective absorption cross section for OH at λ_1

a_{λ_1} cross sectional area of laser beam

f_i fraction of total OH population in quantum states that can be pumped at 282 nm with a laser line width, $\Delta\lambda$

S_{λ_1} saturation parameter which is unity under conditions in which the period of time required to deplete the level pumped is much longer than the repopulation time

E_f $\begin{pmatrix}\text{fluorescence}\\ \text{efficiency}\end{pmatrix} = \left(\frac{k_f}{k_f + k_d + k_q[m]}\right)$

with k_f reciprocal of fluorescence lifetime

k_d first-order rate constant for dissociation

k_q bimolecular electronic quenching rate constant

[m] concentration of quenching species

E_d $\begin{pmatrix}\text{optical}\\ \text{detection}\\ \text{efficiency}\end{pmatrix} = \gamma_{\lambda_1} \times Y_{\lambda_2} \times Z_{\lambda_2} \times \phi_{\lambda_2}$

with γ_{λ_2} fraction of total fluorescence falling within the optical transmission window

Y_{λ_2} optical collection efficiency

Z_{λ_2} optical filter transmission factor

ϕ_{λ_2} quantum efficiency of photomultiplier tube

E_e $\begin{pmatrix}\text{electronic}\\ \text{detection}\\ \text{efficiency}\end{pmatrix} = \dfrac{\text{PMT signal pulses counted}}{\text{PMT signal pulses emitted}}$

V $\begin{pmatrix}\text{volume of}\\ \text{sampling}\\ \text{region}\end{pmatrix} = a_{\lambda_1} \times \ell$

with a_{λ_1} as previously defined and ℓ equal to the length of the fluorescence volume

The relationship between the above quantities and the corresponding terms in the central equation is as follows. First, note that since the units of D in the above expression are counts/pulse, we can multiply D by the laser repetition rate N_p to extract the observed count rate S, since

$$S = DN_p$$

Considering the efficiency factors in order, we consider E_{λ_1}, the optical pumping efficiency at λ_1, first. The quantity

$$\frac{P_{\lambda_1} \sigma_{\lambda_1}}{a_{\lambda_1}}$$

in the exponent is the probability that a given pulse will induce a transition from v,J to the upper state. Since this quantity is much less than 1, we can expand the exponential such that

$$1 - \exp\left(- \frac{P_{\lambda_1} \sigma_{\lambda_1}}{a_{\lambda_1}}\right) \approx \frac{P_{\lambda_1} \sigma_{\lambda_1}}{a_{\lambda_1}}$$

Thus,

$$E_{\lambda_1} = \left(\frac{P_{\lambda_1} \sigma_{\lambda_1}}{a_{\lambda_1}}\right) f_2 S_{\lambda_1}$$

With reference to the central equation, we may equate

$$N_p\left(\frac{P_{\lambda_1} \sigma_{\lambda_1}}{a_{\lambda_1}}\right) = \frac{\pi e^2}{mc}\left[\int_{-\infty}^{\infty} F(\nu)g(\nu)d\nu\right]\left(\frac{S(J,Br)}{2J'(Br) + 1}\right) f_{v \to VIB}$$

The fraction of total OH population in the quantum state pumped by the laser, f_i, is

$$f_1 = N(v_x,J_x,\theta) = \frac{(2J_x + 1)\exp[-(hc/k\theta)T(v_x,J_x)}{\sum_v \sum_J \sum_{Br} (2J + 1)\exp[-(hc/k\theta)T(v_x,J_x)]}$$

and the saturation parameter is

$$S_{\lambda_1} = (1 + S_{SAT})^{-1}$$

The fluorescence efficiency, E_f, in the Georgia Tech expression is equal to

$$E_f + \left(\frac{k_f}{k_f + k_d + k_q[m]}\right) = \left[\frac{k^I_{v_A \to v'}}{k^I_{v_A \to v'} + k^I_Q + k^I_R}\right]\left[\frac{\sum_{J''} A(v' = 0,J';v'' = 0,J'')}{\sum_{J''} A(v' = 0,J';v'' = 0,J'') + k^I_Q}\right]$$

Georgia Tech Central equation

There is an important technical point contained in the difference between these two expressions because there are two distinct processes

involved. The first is v-v transfer in the $A^2\Sigma$ state in competition with collisional deactivation and radiation from the vibrational level initially pumped by the laser. The second is fluorescence from the ground vibrational level in competition with collisional deactivation.

The third term, the optical detector efficiency, E_d, is best taken in product with the scattering volume:

$$E_d V = Y_{\lambda_2} \times Y_{\lambda_2} \times Z_{\lambda_2} \times \phi_{\lambda_2} \times V = \left[\int_{\substack{\text{Scattering} \\ \text{Volume}}} \varepsilon dV \right] [T\eta]$$

with a direct correspondence

$$Y_{\lambda_2} = \frac{\sum_{\text{Det Transition}} A(v',v'')S(J'',Br)}{\sum_{v''}\sum_{J''}\sum_{Br} A(v',v'')S(J'',Br)}$$

$$Y_{\lambda_2} = \varepsilon$$

$$Z_{\lambda_2} = T$$

$$\phi_{\lambda_2} = \eta$$

The last term, the electronic detection efficiency, depends on the gating technique employed and, for tests of the absolute quantities discussed to this point, is best set equal to 1 by opening the detection gate to include the entire period from laser pulse to approximate three folding periods of the emission.

Harvard Research Group (See Anderson et al., 1980.)

The observed fluorescence signal, S_{OH}, in units of counts per second, is expressed in terms of the product:

$$S_{OH} = \left\{ \int F(\lambda)\sigma(\lambda)d\lambda \right\} [OH][\varepsilon T\eta] V\ Q$$

The quantities on the right hand side of the above expression are related to the central equation in the following way:

$$\int F(\lambda)\sigma(\lambda)d\lambda = N(v_x, J_x, \theta) f_{v \to v_A} \left(\frac{S(J_x, J_A)}{2J_A(Br) + 1}\right) \frac{\pi e^2}{mc} \int_{-\infty}^{\infty} F(\nu) g(\nu) d\nu$$

Harvard Central equation

$$Q = \left[\frac{k^I_{v_A \to v'}}{k^I_{v_A \to v'} + k^I_Q + k^I_R}\right]\left[\frac{\sum_{J''} A(v' = 0, J'; v'' = 0, J'')}{\sum_{J''} A(v' = 0, J'; v'' = 0, J'') + k^I_Q}\right]$$

Harvard Central equation

where all quantities have been previously defined and

$$[\varepsilon T \eta] V = \left[\int_{\substack{\text{Scattering} \\ \text{Volume}}} \varepsilon dV\right] [T\eta]$$

Harvard Central equation

Goddard Research Group

An expression for the remote laser-induced fluorescence signal which is valid for a lidar system similar to those described earlier for the measurement of tropospheric hydroxyl radical or nitric oxide is the following:

$$S = I n \bar{\sigma} \eta \varepsilon A_t \frac{1}{4\pi} \int_{z1}^{z2} T_1 T_2 \, O \, \frac{dz}{z^2}$$

where S number of photons counted in a time interval (t_1, t_2) following a single laser shot and $t_j = 2zj/c$

I number of photons emitted in the laser shot

n molecular concentration

$\bar{\sigma}$ effective absorption cross section for the transition being pumped; this includes the cross correlation of the laser bandwidth with the absorption profile and the Boltzmann distribution of population for energy levels in the molecule

η fluorescence efficiency of the molecule; this includes a cross correlation between the OH emission spectrum and the detector bandpass

ε efficiency of the detection system; i.e., the number of photons counted divided by the number of photons entering the system

A_t area of receiver telescope; $(A_t/4\pi z^2)$ is the geometrical collection efficiency of the arrangement

T_1, T_2 atmospheric transmissions at the transmitted and received wavelengths, respectively; in general, T_1 is of the form $\exp(-\alpha t)$ where α is a (hopefully small) constant

O overlap between transmitted laser beam and field of view of the receiver telescope; O is usually zero at very short ranges, increases to 1 at 0.1 - 1.0 km range, and remains 1 thereafter

z range

No term to correct for saturation has been included here, but it may be necessary under some operating conditions.

The quantities on the right hand side are related to the central equation in the following way:

$$\bar{\sigma I} = \int F(\lambda)\sigma(\lambda)d\lambda$$

$$n = [OH]$$

$$\eta = \left[\frac{k^I_{v_A \to v'}}{k^I_{v_A \to v'} + k^I_Q + k^I_R}\right]\left[\frac{\sum_{J''} A(v = 0,J';v'' = 0,J'')}{\sum_{J''} A(v = 0,J';v'' = 0,J'') + k^I_Q}\right]$$

$$A_t \frac{1}{4\pi} \int_{z_1}^{z_2} T_1 T_2 \, O \frac{dz}{z^2} = \int \varepsilon dV$$

Portland State Group

The observed signal, in units of counts/second, is

$$S_{OH} = [OH]T_c(P_f/P_{amb})N_p GL\sigma_o(OH)(n_1/n)YO_\ell O_m \Omega T_a T_m \eta T_g T_d$$

where T_c chemical transmission of inlet nozzle and tube

P_f/P_{amb} ratio of pressure in fluorescence region to ambient pressure

N_p number of laser photons per second

G White cell gain

L detected length per pass

$\sigma_o(OH)$ absorption cross section for the ($^2\Pi$,v=0 to $^2\Pi$,v=1) transition

n_1/n fractional population of the detected $^2\Pi$ rotational level

Y fluorescence yield

O_ℓ overlap between absorption line and laser line

O_m overlap between monochromator bandpass and (0,0 + 1,1) emission

Ω collector solid angle

T_a transmission of absorbing filter

T_m transmission of monochromator

M quantum efficiency of photomultiplier

T_g transmission of OH fluorescence by delayed gate

T_d efficiency of charge discriminator in detection of single photons

The terms of the above working expression are related to those of the central equation as follows. The terms T_c and (P_f/P_{amb}) are unique to the FAGE sampling process and have no equivalent terms in the central equation. However, the meaning of the term P_f/P_{amb} is implicit in the integrated fluorescence yield, Y, at lower pressure:

$$N_p GLO_\ell \Omega = \int F(\nu)g(\nu)d\nu \int \epsilon dV$$

$$\sigma_o(OH) = f_{v_x \rightarrow v_A} \left(\frac{S(J_x, J_A)}{2J_A + 1}\right) \frac{\pi e^2}{mc}$$

$$(n_1/n) = N(v_x, J_x, \theta)$$

$$O_m Y = \left[\frac{k^I_{v_A \rightarrow v'}}{k^I_{v_A \rightarrow v'} + k^I_Q + k^I_R}\right]\left[\frac{\sum_{J''} A(v' = 0,J';v'' = 0,J'')}{\sum_{J''} A(v' = 0,J';v'' = 0,J'') + k^I_Q}\right]$$

$$T_a T_m = T$$

$$\eta T_g T_d = \eta$$

In order to get a feel for the magnitudes involved, one may evaluate the expected count rate for typical values of the various parameters. The excitation term

$$N(v_x,J_x,\theta) f_{v,v''}\left(\frac{S(J,Br)}{2J'(Br) + 1}\right)\frac{\pi e^2}{mc}\int F(\nu)g(\nu)d\nu$$

is essentially the product of the number of laser photons per unit area emitted in a shot with the probability that a hydroxyl radical will absorb a photon. The form ranges from 6×10^{13} cm^{-2} for the Harvard high-repetition-rate system to perhaps 5×10^{14} photons $pulse^{-1}$ cm^{-2} for the lidar systems. The effective cross section is approximately 10^{-16} cm^2. Thus, the excitation term ranges from 6×10^{-5} to 5×10^{-2}.

The next term is the fluorescence efficiency of the hydroxyl radical. This is dependent upon pressure and temperature. Calculated values based upon measured values of quenching and transfer cross sections for N_2, O_2, and H_2O are presented in figure A7. Typical values are 1 to 2×10^{-3} throughout the troposphere.

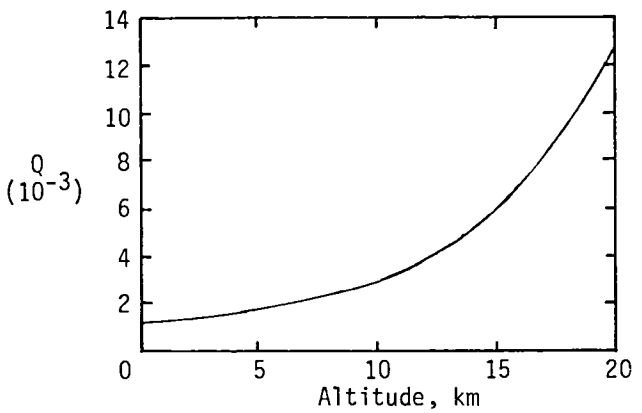

Figure A7. Variation of quenching parameter Q with altitude using constants cited in this report.

The next term is the product of the scattering volume and the geometrical collection efficiency. This ranges greatly for various systems. For lidar systems that have very large excitation volumes but low geometric collection efficiencies, this number ranges from 1 to 20 cm^3. For the contained flow systems using filter detections, values on the order of 0.1 to 0.6 cm^3 per photomultiplier tube are usual. Systems using monochromators achieve 1 to 4 $\times 10^{-3}$ cm^3.

The $[T\eta]$ term represents the efficiency with which a photon entering a collection system is detected. Typical values for this quantity are 0.01 to 0.05.

Finally, the OH concentration for midday midlatitude conditions is on the order of 5×10^6 cm^{-3}. The low pressure sampling systems experience a concentration decrease on the order of 400X, but the fluorescence efficiency term is increased by approximately 200X, so the effective OH concentration could be considered to be on the order of 2.5×10^6.

Taking the product of all these terms yields numbers on the order of 0.001 to 1. Specific estimates of counting rate for individual instruments are included in the section on direct intercomparison.

REFERENCES

Anderson, J. G., Rocket-borne ultraviolet spectrometer measurement of OH resonance fluorescence with a diffusive transport model for mesospheric photochemistry, J. Geophys. Res., 76, 4634-4652, 1971.

Anderson, J. G., H. J. Grassel, R. E. Shetter and J. J. Margitan, Stratospheric free chlorine measurement by balloon-borne in situ resonance fluorescence, J. Geophys. Res., 85, 2869, 1980.

Bradshaw, J. and D. D. Davis, Sequential two photon laser induced fluorescence: A new method for detecting atmospheric trace levels of NO, Opt. Lett., 7, 224, 1982.

Dieke, G. H. and H. M. Crosswhite, The ultraviolet bands of OH: Fundamental data, J. Quant. Spectrosc. Radiat. Transf., 2, 97-199, 1961. (Originally published as Bumblebee Series Report No. 87, 1948.)

Earls, L. T., Intensities in $^2\Sigma - {}^2\Pi$ transitions in diatomic molecules, Phys. Rev., 48, 423, 1935.

Golden, D. M., F. P. Del Greco and F. Kaufman, Experimental oscillator strength of OH, $^2\Sigma^+ \rightarrow {}^2\Pi$, by a chemical method, J. Chem. Phys., 39, 3034-3041, 1963.

Herzberg, G., Spectra of Diatomic Molecules, D. Van Nostrand Co., 1950.

Hill, E. L. and J. H. Van Vleck, The quantum mechanics of the rotational distortion of multiplets in molecular spectra, Phys. Rev., 32, 250-272, 1928.

Huber, K. P. and G. Herzberg, Molecular Spectra and Molecular Structure, 4: Constants of Diatomic Molecules, Van Nostrand Reinhold, NY, 1979.

Killinger, D. K., Absorption and fluorescence spectrum of OH studies using tunable dye lasers, Ph.D. thesis, Univ. of Michigan, 1978.

Steinfeld, J. J., Molecules and Radiation: An Introduction to Modern Spectroscopy, MIT Press, 1978.

Wang, C. C. and D. K. Killinger, Effect of rotational excitation on the band oscillator strength of OH, Phys. Rev. A, 20, 1495-1498, 1979.

Wang, C. C., L. I. Davis, P. M. Selzer and R. Munoz, Improved airborne measurements of OH in the atmosphere using the technique of laser induced fluorescence, J. Phys. Res., 86, 1181, 1981.

APPENDIX B

SATURATION PHENOMENA IN LIF MEASUREMENTS

Optical saturation is the phenomenon in which the laser-induced rates of absorption and spontaneous emission between two levels, induced by a laser, become comparable to or greater than the spontaneous emission and collision rates connecting these levels. This results in the excited state population N_u acquiring a value of similar magnitude to that of the ground state, N_e. Under these conditions the observed fluorescence signal, which is proportional to N_u, is no longer linearly dependent on laser intensity I, but increases at a slower rate, and in principle ultimately becomes independent of I.

Below is described a conceptual picture of optical saturation using a two-level picture. This is, however, inadequate for the description of a real experiment involving a molecule, such as OH, for several reasons, which will be explained briefly; these are the multilevel nature of the electronic states and energy transfer among them (Kotlar et al., 1980; Crosley, 1981) and effects due to spatial (Daily, 1978a, b), spectral (Killinger and Wang, 1979), and temporal (Van Dijk et al., 1979; Lucht et al., 1980) fluctuations in the laser pulse.

There exists insufficient knowledge concerning these processes and a lack of the needed fundamental parameters to permit one to calculate from first principles the effects of saturation at a given intensity. The same general concerns (collisional rates, collisional population redistribution among excited state levels, overlap of the laser and absorption lines) exist in somewhat different form in the linear regime. For those experiments in which an OH calibration cell is continually monitoring fluorescence from a split portion of the laser beam, operation in the saturation regime should pose no problems with the data analysis. This will be true if the spectral power density beam profile and collisional environment within the calibration cell are made the same (through focussing, filtering and choice of buffer atmosphere) as in the test section. For experiments in which continual reference to such calibration cell is not made, however, optical saturation can complicate the data analysis, and operation in a linear regime is recommended.

A TWO-LEVEL MODEL AND HOMOGENEOUS LASER

Here, to obtain a conceptual picture of optical saturation, we consider a two-level treatment (fig. B1) which ignores the multilevel

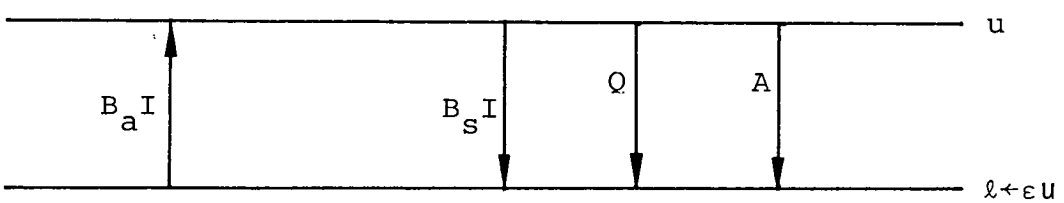

Figure B1

vibrational and rotational nature of OH, the temporal evolution of the populations, and temporal, spatial, and spectral fluctuations of the laser.

The upper state u is pumped by the laser at a rate B_aI, and returns to the lower state ℓ by stimulated emission, spontaneous emission, and collisional quenching at the respective rates B_sI, A, and Q (all in sec^{-1} units). The B's are Einstein absorption/stimulated emission coefficients related by the level degeneracies $B_s = (g_\ell/g_u)B_a$ and are calculable knowing A. Applying a steady state approximation to N_u and noting that the total population $N_o = N_u + N_\ell$ is constant yields

$$\frac{dN_u}{dt} = 0 = B_aI\ N_g - (B_sI + Q + A)\ N_u$$

$$N_u = \frac{B_aIN_o}{B_aI\ (1 + (g_\ell/g_u) + Q + A)}$$

In the linear regime, where $B_aI << Q + A$, the signal is proportional to $B_aI\ N_g/(Q + A)$, since $N_u << 1$ and $N_g \simeq N_o$; $(Q + A)^{-1}$ is the fluorescence efficiency. As I increases to the saturation regime, the signal increases less rapidly than a linear dependence; as I becomes so large that $B_aI >> Q + A$, then

$$N_u \to \frac{g_uN_o}{g_u + g_\ell}$$

Were the situation this simple for OH, it would suggest that one should operate in a saturation regime not considering other factors such as laser-produced OH, since the signal becomes independent of I and, in particular, independent of collisional effects. This was the basis for the suggestion (Daily, 1977) and initial flurry of activity (Baronavski and McDonald, 1977a, b; Allen et al., 1977; Daily and Chan, 1978; Boncyzle and Shirley, 1979; Pasternack et al., 1978; Allen et al., 1979; Van Dikj et al., 1979) applying saturated LIF as a diagnostic tool for radicals in flames; of special interest was its potential use in turbulent flames where single shot data must be used and the collisional environment thus cannot be characterized. However, a recognition of the quantitative problems described in the section below has demanded some parametric treatments and the bulk of the present effort has reduced to only one research group (Lucht et al., 1980).

The two-level model nonetheless permits an approximation of the laser intensities for the onset of optical saturation in OH at 1 atm of air. We calculate I for the case in which $B_aI = Q + A$. At 1 atm, $Q \sim 1.5 \times 10^9\ sec^{-1} >> A$. For the $Q_1(2)$ transition in the (1,0) band, $B_a \sim 8 \times 10^5\ cm^2\ erg^{-1}$ so that $B_aI = Q$ corresponds to $I = 2000\ erg/cm^2$. For a pulse energy of 1 mJ, a pulse length of 10 nsec, and a 0.01Å bandwidth in the ultraviolet, this corresponds to a beam diameter of $\sim$2 mm (i.e., a power of 4 MW/cm^2 at this bandwidth).

INADEQUACIES OF THE TWO-LEVEL MODEL

Problems with the simple picture presented above are two-fold; laser beam inhomogeneities and energy transfer among the many vibrational and/or rotational levels in a real molecule.

For a 10-nsec laser, one finds that none of the spatial, spectral, or temporal profiles are reproducible from shot to shot, and that, for example, there can be a time dependence of the mode structure (chirping) during a single pulse. Thus the degree of saturation will vary with space and time. If the laser beam characteristics were well known, these effects could be quantified. It has been shown (Daily, 1978a) that a Gaussian beam never reaches the saturation asymptote due to residual edge intensity remaining in a linear regime when the center is highly saturated; this can be accounted for if the laser beam spatial profile is known. Effects of mode structure for a variety of cases of relative mode spacing and width, and absorption line breadth, have also been treated (Killinger and Wang, 1978; Killinger, 1978) and can be calculated for defined conditions. Similar conclusions apply to a known temporal profile of the laser pulse (Van Dijk et al., 1979).

None of these remains constant enough for the corrections to be applied on a prior basis; measurements of the variation for an individual pulse are virtually impossible at the present time. Fortunately, experience in saturation experiments (Baronavski and McDonald, 1977a, b; Allen et al., 1977, 1979; Boncyzle and Shirley, 1979; Pasternack et al., 1978) indicate that the effects are well behaved on a pulse-averaged basis although empirical correction factors may be needed. This can be accounted for, with cancelling corrections, by using a continually referenced calibration cell having the same beam profile and average power density as in the test cell.

The existence of rotational and/or vibrational levels in each electronic state can potentially lead to much greater errors. The two-level model would apply if $Q >> R, V$, denoting rotational and vibrational relaxation rates (Crosley, 1981). If however, $R, V >> Q$, the effective saturation parameter becomes Q times the upper state partition function (Kotlar et al., 1980). For OH the situation is intermediate (Crosley and Smith, 1980) and is complicated by the rotational level dependence of both the ratios Q/R in $v' = 0$ and Q/V for $v' = 1 \rightarrow v' = 0$ transfer.

Parametric approaches to these effects exist (Berg and Shackleford, 1979; Lucht et al., 1980) but have yet to receive detailed experimental verification. More details are considered in a time-dependent model (Kotlar et al., 1980), although the critical collisional rate constants (vibrational transfer with $X^2\Pi_i$) and the final state dependence of quenching collisions can only be guessed. An equipartition of energy scheme was used to suggest that a quenching collision from $v' = 0$ returns the OH to $v'' = 0$ about half the time, and to higher v" otherwise. A vibrational transfer rate of $\sim 8 \times 10^{-12}$ cm^3 sec^{-1} within $X^2\Pi_i$ was assumed. Under these conditions the model indicated significant depletion of the $v'' = 0$ population, hole burning in the rotational distribution within $v'' = 0$, and a high ($\sim 10^5$) buildup of the total OH population into $v'' \geq 1$ levels during and shortly after the laser pulse.

Because of the hole burning, the effective Boltzmann factor $\Delta n/n$ at high I, averaged over the pulse, could be less than one-fifth the normal calculated value.

The need to estimate key parameters precludes attaching quantitative significance to the results of this model, but the values used should be reasonable enough to draw operative conclusions. First, the use of a reference cell having the same collisional environment and laser intensity (that is, the same ratios V/Q, R/Q, and B_aI/Q) in the test section should permit operation in a saturation regime with no greater errors than for the linear case. However, if a reference cell is not used, significant errors can result from saturation, due to the reduction in the effective Boltzmann factor, the calculation of whose actual value depends crucially on unknown rates. Although the intensity at which saturation should become noticeable can be estimated from currently known rate constants, it is best at present to ascertain empirically (measuring the signal as a function of I) that one is not appreciably saturating the transition.

REFERENCES

Allen, J. E., W. R. Anderson, and D. R. Crosley, Optoacoustic pulses in a flame, Opt. Lett., 1, 118-120, 1977.

Allen, J. E., W. R. Anderson, D. R. Crosley, and T. D. Fansler, Energy transfer and quenching rates of laser-pumped electronically excited alkalis in flames, Proc. 17th International Symp. on Combustion, Combustion Institute, 797-809, 1979.

Baronavski, A. P. and J. R. McDonald, Application of C_2 concentrations in an oxygen-acetylene flame. An application of saturation spectroscopy, J. Chem. Phys., 66, 3300-3301, 1977a.

Baronavski, A. P. and J. R. McDonald, Application of saturation spectroscopy to the measurement of C_2, $^3\Pi_\mu$ concentrations in oxy-acetylene flames, Appl. Opt., 16, 1897-1901, 1977b.

Berg, J. O. and W. L. Shackelford, Rotational redistribution effect on saturated laser-induced fluorescence, Appl. Opt., 18, 2093-2094, 1979.

Boncyzle, P. A. and J. A. Shirley, Measurement of CH and CN concentration in flames by laser-induced saturated fluorescence, Combustion and Flame, 34, 253-264, 1979.

Crosley, D. R. and G. P. Smith, Vibrational energy transfer in laser-excited A2 sigma + OH as a flame thermometer, Appl. Opt., 19, 517-520, 1980.

Crosley, D. R., Collisional effects on laser-induced fluorescence flame measurements, Opt. Engr., 20, 511-521, 1981.

Daily, J. W., Saturation effects in laser induced fluorescence spectroscopy, Appl. Opt., 16, 568-571, 1977.

Daily, J. W., Saturation of fluorescence in flames with a Gaussian laser beam, Appl. Opt., 17, 225-229, 1978a.

Daily, J. W., Detectability limit and uncertainty considerations for laser induced fluorescence spectroscopy in flames, Appl. Opt., 17, 1610-1615, 1978b.

Daily, J. W. and C. Chan, Laser-induced fluorescence measurement of sodium in flames, Combustion and Flame, 33, 47-53, 1978.

Killinger, D. K., Absorption and fluorescence spectrum of OH studied using tunable Dte lasers, Ph.D. thesis, Univ. of Michigan, 1978.

Killinger, D. K. and C. C. Wang, Direct measurements of the Gibbs free energy of OH using a CW tunable laser, J. Chem. Phys., 71, 1582, 1979.

Kotlar, A. J., A. Gleb, and D. R. Crosley, A multilevel model of response to laser-fluorescence excitation in the hydroxyl radical, Laser Probes for Combustion Chemistry, D. R. Crosley, ed., 137-144, 1980.

Lucht, R. P., O. W. Sweeney, and N. M. Lauren deau, Balanced cross rate model for saturated molecular fluorescence in flames using a nanosecond pulse length laser, Appl. Opt., 19, 3295-3300, 1980.

Pasternack, L., A. P. Boronavski, and J. R. McDonald, Application of saturation spectroscopy for measurement of atomic Na and MgO in acetylene flames, J. Chem. Phys., 69, 4830-4837, 1978.

Van Dijk, C. A., P. J. T. Zeegers, and C. T. J. Alkemade, Redistribution on population among the higher levels of Na atoms in an H_2-O_2-Ar flame, J. Quant. Spect. & Rad. Trans., 21, 115-122, 1979.

APPENDIX C

DETAILED PERFORMANCE CALCULATIONS:

WAYNE STATE UNIVERSITY/FORD MOTOR CO.

The laser-generated OH through ozone dissociation was defined in equations (5) and (6) of the main text. Repeated here, they are:

$$[OH]^{laser} = A_c' F(\chi)[OH]^{laser}_{total} = A_c [OH]^{laser}_{total} \quad (C1)$$

$$[OH]^{laser}_{total} = \sigma_o \phi E[O_3] \frac{k[H_2O]}{k[H_2O] + k_n[N_2] + k_o[O_2]} \quad (C2)$$

where $F(\chi) = 1 - \left(\frac{2}{\chi}\right)\left[1 - \frac{1 - \exp(-\chi)}{\chi}\right]$

$\chi = A\Delta t$

$A = k[H_2O] + k_n[N_2] + k_o[O_2]$

Expressing $[H_2O]$ in torr, $[O_3]$ in ppbv, and E in J cm^{-2}, and using rate constants $k = 2.3 \times 10^{-10}$ cm^3 sec^{-1} and $k_n = k_o = 3 \times 10^{-11}$ cm^3 sec^{-1} (from Streit et al., 1976), a value of 0.88 for the quantum yield of $O(^1D)$, and $\sigma_o = 3.45 \times 10^{-18}$ cm^2 (from Calvert and Pitts, 1966), equation (C1) becomes

$$[OH]^{laser}_{total} = (11 \pm 5) \times 10^8 A_c[H_2O][O_3]E \quad (C3)$$

where A_c is a correction factor introduced by Wang et al. (1981) to account for deviations from a thermalized rotational distribution for the laser-generated OH and for other possible processes not included in the rate equation analysis. Wang et al. (1981) have also determined experimentally that the overall numerical coefficient including A_c is $(1.1 \pm 0.6) \times 10^8$ under ambient conditions, so that $A_c = 0.1 \pm 0.05$. Equation (C2) with $A_c = 0.1$ is at least semiquantitatively valid in assessing the ozone interference level in any OH measurements under ambient conditions. Using these equations, the ozone interference level corresponding to various humidity and ozone concentrations can be calculated readily. For the results presented in tables 6 and 7 of the text, the laser operated at 2.5 mJ per pulse with a beam expanded to 25 cm, or approximately 0.005 cm^{-2}.

The signal equation used for the LIF-lidar system by the Ford group is

$$(\text{OH signal}) = A[\text{OH}]\frac{\sigma_o(\text{OH})}{\Delta\eta_{eff}}\,\eta(\Delta n/n) \tag{C4}$$

where [OH] is the concentration of OH, $(\Delta n/n)$ is the fraction of the OH population residing in the rotational level from which the exciting transition originates, $\sigma_o(OH)$ is the integrated absorption cross section for the particular rotational-electronic transition, $\Delta\eta_{eff}$ is the effective line width for the transition, η is the overall fluorescence efficiency under ambient conditions, and A is a constant determined by the overall excitation and collection efficiencies. This constant can be evaluated most conveniently by noting that the Raman scattered signal owing to nitrogen molecules occurs around 3025Å, for which the excitation configuration and collection efficiencies are the same for all practical purposes. This N_2 Raman scattered signal is given by

$$(N_2 \text{ signal}) = A[N_2]\sigma_R(N_2) \tag{C5}$$

where $[N_2]$ is the nitrogen concentration in air, and $\sigma_R(N_2)$ is the cross section for Raman scattering of nitrogen. Elimination of A in these two equations gives

$$[\text{OH}] = \frac{(\text{OH signal})}{(N_2 \text{ signal})} \times \frac{[N_2]\sigma_R(N_2)\ \Delta\eta_{eff}}{\sigma_o(\text{OH})\ \eta(\Delta n/n)} \tag{C6}$$

The appropriate values for the parameters that occur in the above equations are summarized in table C1.

TABLE C1. VALUES FOR THE PARAMETERS OF EQUATION (C6) (SEA LEVEL CONDITIONS)

Parameter	Value
$\sigma_R(N_2)$	7.4×10^{-29} cm^2/molecule
$\sigma_o(OH)$; $Q_1(2)$	0.82×10^{-16} cm^2 cm^{-1}
$\Delta n/n$ (computed value)	0.196
η	0.7×10^{-3}
Doppler width (computed value)	0.11 cm^{-1}
Laser line width	0.1 cm^{-1}
Collision-broadened width	0.17 cm^{-1}
$\Delta\eta_{eff}$, effective line width	0.3 cm^{-1}

In the OH measurements, the exciting radiation is tuned periodically on and off the OH resonance, and the detection electronics are gated for a fixed duration both during and after the laser excitation. For ground-based measurements at Niwot Ridge, data are recorded from four photon-counting channels: the Spex photomultiplier count for on-line and off-line intervals, called A and B respectively, and the Raman monitor count for the same corresponding intervals, called R_A and R_B. For the OH signal levels encountered, the Spex count is essentially in the linear regime and no correction due to saturation need be considered. In this case, the Spex A count is composed of three parts:

$$A = aI_A + bI_A + S \tag{C7}$$

where I_A represents the on-line laser intensity, aI_A the OH fluorescence portion of the count, bI_A the background fluorescence, and S the solar background. Similarly,

$$B = b'I_B + S' \tag{C8}$$

where I_B represents the off-line laser intensity, $b'I_B$ the background fluorescence portion of this count and S' the solar background. For the Raman monitor, the solar background is comparatively negligible, but the effects of saturation must be considered. The Raman monitor counts can be represented implicitly by

$$R_A = cI_A(1 - R_A/R_S) \qquad R_B = c'I_B(1 - R_B/R_S) \tag{C9}$$

where R_S is the saturation count and cI_A and $c'I_B$ are the Raman counts without saturation. When the spectrometer is tuned to the nitrogen Raman line, the A and B counts can be represented as

$$A_R = xI_A \qquad B_R = x'I_B \tag{C10}$$

The simplified form of these equations is chosen to illustrate the intensity dependence and presence of background counts in the data. The "constants" a, b, b', c, c', x, x' include, of course, many factors such as collection efficiencies, concentrations of species, etc. It is the ratio, a/x, of OH signal to nitrogen Raman signal which we wish to use in equation (C6) to obtain the OH concentration. To extract the constant, a, from the data, we first compute the quantity

$$DEL = A/R_A - B/R_B \tag{C11}$$

and then perform a linear least-squares regression over the measurement time period of the values of this quantity versus the quantity $R_A/R_B - 1$. DEL is the difference between on-line and off-line signals normalized to equal intensity of excitation. The expression $(R_A/R_B - 1)$ is a measure of the difference between on-line and off-line intensities.

The intercept of the regression $a/c(1 - R_A/R_S)^{-1}$ is now divided by

$$A_R/R_A = x/c\ (1 - R_A/R_S)^{-1} \tag{C12}$$

to obtain the ratio of OH signal to nitrogen Raman signal, a/x, used in equation (C6). The uncertainty in the value obtained for the intercept of the regression is given by

$$\sigma = \sigma_{RES}\left[\frac{1}{n} + \frac{\overline{(R_A/R_B - 1)^2}}{\sum_i [(R_A/R_B)_i - (R_A/R_B)]^2}\right]^{\frac{1}{2}} \tag{C13}$$

where n is the number of data points in a measurement time period, i indexes the particular data points, x represents the mean value of x, and σ_{RES} is the standard deviation of the residuals of the data from the computed linear fit.

Values for σ, when expressed in equivalent OH concentration, ranged from 0.4×10^6 to 1.4×10^6 OH/cm^3 with an average of 0.9×10^6 OH/cm^3. The lowest value closely approached the "shot noise" limit of the photon statistics for the measurement. For a typical half-hour measurement period with 12 data points, the average value corresponds to a detection limit of 0.5×10^6 OH/cm^3 for 95 percent confidence and 0.7×10^6 for 99 percent confidence.

For airborne operations, the higher levels of solar background from the wingtip preclude the use of photon-counting detection. Charge digitizing apparatus is used instead, and although it is somewhat more complicated, saturation of the detection system is less of a problem and the analysis of the data can be more straightforward. The data acquisition system records fluorescence signal, solar background, Raman monitor, UV intensity, and water vapor discharge signal for each laser shot. The acquisition program computes and displays results on the basis of a 2000 laser shot run using a straightforward analysis routine similar to that described above. However, since all the data are stored on a per-shot basis, they may be analyzed later by further refined analysis programs. In fact, the analysis described below is what we currently prefer, as it tends to give somewhat better results.

For simplicity, we have opted to analyze our data using statistical techniques appropriated for stationary processes. Recognizing that the background levels and other quantitatives measured vary with time, we have chosen time intervals for acquisition and analysis of data sufficiently short that the assumption of stationary processes is reasonable. For situations where the conditions of measurement are changing rapidly, the analysis may give misleading results.

The simplest approach uses just the on-line and off-line fluorescence signals and their respective UV intensities. Subtraction of equation (C8) from equation (C7) gives

$$DIFF = aI_A + bI_C \tag{C14}$$

where

$$DIFF = A - B$$

$$I_C = I_A - I_B$$

and we have assumed S = S' and b = b'.

Equation (C14) describes a linear equation whose two parameters, a and b, can be determined through a least-squares fit according to standard procedures. Accordingly, the parameter a is given by

$$a = \{[DIFF*I_A][I_C{}^2] - [I_AI_C][DIFF*I_C]\}/\Delta \tag{C15}$$

$$\Delta = [I_A{}^2][I_C{}^2] - [I_AI_C]^2 \tag{C16}$$

and the corresponding variance is given by

$$V(a) = s^2[I_C{}^2]/\Delta \tag{C17}$$

Here the square brackets denote the sum of the products of the quantities therein over the entire set of observations, and s^2 is the sample variance. Since the laser operates for ten shots between frequency switching and there are a total of 2000 laser shots per run, one may form from each run 100 groups, each of which contains ten pairs of on-off observations, and apply the above equations to each group. The resulting 100 OH values are then processed in the usual manner to yield a mean value and standard deviation. (There are two "usual" manners for the variance, adding up the individual variances or computing it from the 100 OH values, and they give essentially the same results.) Note that the separate solar background measurement is not used in this analysis, nor is the fluorescence explicitly normalized to UV intensity: that is accomplished in effect by the two-parameter fit.

REFERENCES

Calvert, J. G. and J. N. Pitts, Photochemistry, John Wiley, NY, 1966.

Streit, G. E., C. J. Howard, A. L. Schmeltekopf, J. A. Davidson and H. I. Schiff, Temperature dependence of $O(^1D)$ rate constants for reactions with O_2, N_2, CO_2, O_3, and H_2O, J. Chem. Phys., 65, 4761, 1976.

Wang, C. C., L. I. Davis, P. M. Selzer and R. Munoz, Improved airborne measurements of OH in the atmosphere using the technique of laser-induced fluorescence, J. Geophys. Res., 86C, 1181, 1215, 1981.

APPENDIX D

DETAILED PERFORMANCE CALCULATIONS:

GODDARD GROUP

Two systems were described. The first used polarization to reduce scattered solar flux, the principal source of noise. The second used a narrowband detector and a different excitation wavelength. The results, which consider these systems, were presented in the table emphasizing anticipated technology improvements (table 7 in text) because the analysis for each system required estimates of critical parameter even though each system would use existing technology. For the first, the information about the degree of polarization of the scattered solar flux was not measured but was estimated as 60 percent for viewing straight up with a solar zenith angle of 75 percent at sea level. The expected performance of this system therefore depends on the reliability of this estimate. For the second system, two estimates were required. First, the expected throughput of a Fabry-Perot interferometer operating at 309 nm, based on the performance exhibited by similar instruments working at other wavelengths, was estimated to be 3 percent. Second, the fluorescence efficiency of the proposed OH lines was estimated as 4×10^{-5}, since these quantities have not been measured to date. As before, the projections of system performance depend upon the accuracy of the estimates of these quantities.

The laser-generated OH was calculated from the expression

$$[OH]^{laser} = 0.92 \times 10^{8} [H_2O][O_3]E$$

where $[H_2O]$ is in torr, $[O_3]$ is in ppbv, and E is in J cm^{-2}. For the marine boundary layer case $[H_2O]$ = 25 torr and $[O_3]$ = 25 ppbv. Using 1 mJ per laser shot with a beam diameter of about 3.5 in. resulted in $[OH]^{laser} = 1 \times 10^{6}$ molec cm^{-3}. For the middle troposphere case the expression used was

$$[OH]^{laser} = 3.6 \times 10^{9} E$$

where E is in J cm^{-2}. For this case, 10 mJ per laser shot was assumed, resulting in $[OH]^{laser} \approx 6 \times 10^{5}$ molec cm^{-3}.

The expression for the remote laser-induced fluorescence signal which is valid for a lidar system similar to those described earlier for the measurement of tropospheric hydroxyl radical is the following:

$$S = In\ \bar{\sigma}\eta\varepsilon\ A_t\ \frac{1}{4\pi} \int_{z_1}^{z_2} T_1 T_2 O\ \frac{dZ}{Z^2}$$

where

S	number of photons counted in a time interval (t_1, t_2) following a single laser shot and $t_j = 2z_j/c$
I	number of photons emitted in the laser shot
n	molecular concentration
$\bar{\sigma}$	effective absorption cross section for the transition being pumped; this includes the cross correlation of the laser bandwidth with the absorption profile and the Boltzmann distribution of population for energy levels in the molecule
η	fluorescence efficiency of the molecule; this includes a cross correlation between the OH emission spectrum and the detector bandpass
ε	efficiency of the detection system; i.e., the number of photons counted divided by the number of photons entering the system
A_t	area of the receiver telescope and $(A_t/4\pi z^2)$ is the geometrical collection efficiency of the arrangement
T_1, T_2	atmospheric transmissions at the transmitted and received wavelengths respectively; in general, T_1 is of the form $\exp(-\alpha t)$ where α is a (hopefully small) constant
O	overlap between the transmitted laser beam and the field of view of the receiver telescope; O is usually zero at very short ranges, increases to 1 at 0.1 to 1.0 km range, and remains 1 thereafter
Z	range

No term to correct for saturation has been included here but may be necessary under some operating conditions.

The correspondence between the central equation and the Goddard signal expression is shown by the following:

$$I\bar{\sigma} = N(v_x, J_x, X^2\Pi, \theta) f_{v_x - v_A} \left(\frac{S(J_x, J_A)}{2J_A + 1} \right) \cdot \frac{\Pi e^2}{mc} \left[\int_0^{\Delta t} dt \int_{-\infty}^{+\infty} F(\nu, t) g(\nu) d\nu \right]$$

$$\eta = [OH(X^2\Pi)]$$

$$\eta = \left[\frac{k^I_{v_A \to v_X}}{k^I_{v_A \to v_X} + k^I_Q + k^I_R} \right] \left[\frac{\sum_{\text{allowed } J''} A(v'=0,J';v''=0,J'')}{\sum_{\text{allowed } J''} A(v'=0,J';v''=0,J'') + k^I_Q} \right]$$

$$\frac{EA}{4\pi} \int_{z_1}^{z_2} T_1 T_2 \frac{O(Z)}{Z^2} = \left[\int_{\text{scattering volume}} EdV \right] T\eta$$

In order to get a feel for the magnitudes involved, one may evaluate S given some "reasonable" values of the various parameters for an OH measurement:

I	$\sim 10^{15}$ per millijoule of laser energy
n	$\sim 10^{7}$ cm^{-3}
$\bar{\sigma}$	$\sim 10^{-16}$ cm^2
η	~ 0.01
ε	~ 0.01
A_t	~ 500 cm^2
T_1, T_2	~ 1
$\int_{z_1}^{z_2} \frac{O(Z)dZ}{Z^2}$	can vary a great deal with various choices of system parameters; 9×10^{-4} is a realizable value for a 10-mrad field of view and $z_2 = 150$ m (corresponding to a time interval of 1 μsec)

Then

$$S = 10^{15} \times 10^{7} \times 10^{-16} \times 10^{-2} \times 10^{-2} \times (5 \times 10^{2}) \times (9 \times 10^{-4}) = 45$$

This says nothing about the ability to measure OH because we know nothing about interferences, but it does say that one will not be signal limited in the absence of background.

The principal source of noise for the lidar measurements is statistical noise from the large background count arising from scattered solar flux. So-called white fluorescence has been of a much lower magnitude because of the absence of any physical objects in the scattering volume. All the other systems do have some sort of flow

tube or beam stop which provides a potential source for contaminants as well as a scattering (and possibly fluorescing) surface.

The procedure consists of four measurements made in almost simultaneous pairs (time between measurements < 1 msec). The system is tuned onto the hydroxyl line with the laser, and a signal and background are measured. Then it is tuned off the OH line and a signal and background are measured. The measured quantities are S_{ON}, B_{ON}, S_{OFF}, and B_{OFF}; S_{ON} and S_{OFF} can be broken down as shown:

$$S_{ON} = F_{ON\ FLUORESCENCE} + W_{WHITE\ FLUORESCENCE} + B_{BACKGROUND}$$

$$S_{OFF} = W_{WHITE\ FLUORESCENCE} + B_{BACKGROUND}$$

Assuming B_{ON} is the same as the $B_{BACKGROUND}$ in S_{ON} and B_{OFF} is the same for S_{OFF}, we get

$$F + W = S_{ON} - B_{ON}$$

$$W = S_{OFF} - B_{OFF}$$

Scaling F and W for laser power, we can solve for F:

$$F = (S_{ON} - B_{ON}) - \frac{I_{ON}}{I_{OFF}} (S_{OFF} - B_{OFF})$$

The uncertainty of F, σ_F, can be calculated using the statistical uncertainties of the four measured quantities (assuming I_{ON} and I_{OFF} are very well determined). Then

$$\sigma_F^2 = \sigma_{S_{ON}}{}^2 + \sigma_{B_{ON}}{}^2 + \left(\frac{I_{ON}}{I_{OFF}}\right)^2 \left(\sigma_{S_{OFF}}{}^2 + \sigma_{B_{OFF}}{}^2\right)$$

In practice, $\sigma_{S_{ON}}$ and $\sigma_{S_{OFF}}$ are by far the largest terms in the expression, and (I_{ON}/I_{OFF}) is $\sim$1. Then

$$\sigma_{S_{ON}} = \sqrt{S_{ON}}$$

and

$$\sigma_{S_{OFF}} = \sqrt{S_{OFF}}$$

These values are dominated by solar background photons and are therefore almost equal.

Solar background fluxes have been estimated by scaling results from the Goddard balloon lidar flight of October 1980. These values vary depending on parameters such as viewing direction, solar zenith angle, telescope field of view, and overall detection efficiency. These estimates are included in our calculated signal to noise ratios, tabulated in the text.

APPENDIX E

DETAILED PERFORMANCE CALCULATIONS

GEORGIA TECH GROUP

Operational Characteristics for Two Tropospheric Environments

(1) CONDITIONS FOR SYSTEM INTERCOMPARISON

Case A Marine Boundary Layer

1 atm total pressure

25 ppbv O_3

25 torr H_2O

5×10^6 ambient OH/cm^3

Total background of OH equivalents:

(i) 1×10^7 OH equivalents

(ii) 1×10^8 OH equivalents

probed OH produced via O_3/H_2O interference

given by $[OH] = 5.75 \times 10^7 E \frac{F}{F_{10}\ ns}$

where E is in mJ

Case B Mid Troposphere

0.5 atm total pressure

60 ppbv O_3

0.3 torr H_2O

probed OH produced via O_3/H_2O

Interference given by:

$[OH] = 3.6 \times 10^6 E \frac{F}{F_{10}\ ns}$

fluorescence efficiency = 2×10^{-3}

(2) SIGNAL STRENGTH EVALUATION

$S(OH) = E_{\lambda_1} \times E_f \times E_d \times E_e \times V \times [OH]$

where E_{λ_1} = optical pumping efficiency

E_f = fluorescence efficiency

E_d = optical detection efficiency

E_e = electronic efficiency

V = effective sampling volume

For <u>current field system</u> consisting of

1. 85 J/pulse at 500 ps 1 cm^2 beam
2. two lasers at 20 pps each (one on line and one off line)
3. $E_e = 1.0$
4. $V = 1.5\ cm^3$/PMT
5. 12 PMT's
6. fluorescence sampled within a 50 Å bandwidth filter = 0.75
7. 0.3 quantum yield of PMT
8. optical collection and transmission efficiency = 3×10^{-3}
9. $\frac{F}{F_{10\ ns}} = 0.1$

<u>Case A</u> Signal Strength

$S(OH) = 1.0 \times 10^7$ [OH] per laser pulse

at $[OH] = 5 \times 10^6/cm^3$

then S(OH) = 600 photons/min

<u>Case B</u> Signal Strength

$S(OH) = 2.0 \times 10^7$ [OH] per laser pulse

for 5×10^6 OH/cm^3 then

S(OH) = 1200 photons/min

(3) BACKGROUND (B) TOTAL SOURCE STRENGTH

$B = 1 \times 10^8$ OH equivalents

and $B = 1 \times 10^7$ OH equivalents

Case A Background B

B = 12000 photons/min

and B = 1200 photons/min

Case B Background B

B = 24000 photons/min

and B = 2400 photons/min

(4) SIGNAL-TO-NOISE RATIO (S/N)

$$S/N = \frac{S(OH)}{\sqrt{S(OH) + 2B}}$$

(5) PERFORMANCE OF PRESENT GA TECH SYSTEM

Equivalent Background	Integration Time	[OH] Interference	% [OH] Interference	S/N D=1	S/N D=5	S/N D=20
Case A - MARINE BOUNDARY LAYER [OH] = 5×10^6 cm^{-3}						
1×10^8	20 min	5×10^5	10%	17.	NA	NA
1×10^8	1 min	5×10^5	10%	3.8	NA	NA
1×10^7	20 min	5×10^5	10%	49.	NA	NA
1×10^7	1 min	5×10^5	10%	11.	NA	NA
Case B - MID-TROPOSPHERE [OH] = $5 \times 10^6/cm^3$						
1×10^8	20 min	3×10^4	0.6%	24.	NA	NA
1×10^8	1 min	3×10^4	0.6%	5.3	NA	NA
1×10^7	20 min	3×10^4	0.6%	69.	NA	NA
1×10^7	1 min	3×10^4	0.6%	16.	NA	NA

NA - Integration time de-rating factor is given as D=1 for GA Tech system using <100 μs time-separated lasers (of/off line) which will "freeze" the atmosphere under all conditions.

(6) SPECIAL COMMENTS ON CURRENT GA TECH SYSTEM

Case A - For the background levels given, the minimum detectable concentration (MDC) for a S/N $\geq$ 2 is seen to range from $2.6 \times 10^5/cm^3$ to $8.3 \times 10^5/cm^3$. However, based upon information from GAMETAG flights (as to the background levels) we feel a more conservative MDC for a S/N = 2 ranges from $8 \times 10^5/cm^3$ to $1.5 \times 10^6/cm^3$. These values are all given for 20 minute integrations.

Case B - For the background levels given, the minimum detectable concentration (MDC) for a S/N = 2 is seen to range from $1.8 \times 10^5/cm^3$ to $5.8 \times 10^5/cm^3$. However, based again on information from the GAMETAG flights (as to the background levels) we feel a more conservative MDC for a S/N = 2 ranges from $3 \times 10^5/cm^3$ to $6 \times 10^5/cm^3$. These values are all given for 20 minute integration times.

(7) POTENTIAL IMPROVEMENT IN ANTICIPATED GA TECH SYSTEM

1. 85 μJ/pulse 300 ps 1 cm^2
2. Two lasers at 100 pps each
3. All other factors the same as section (2)
4. F/F_{10} ns = 0.05

Case A

S(OH) = 3000 photons/min

B = 6000 photons/min and 60000 photons/min

Case B

S(OH) = 6000 photons/min

B = 12000 photons/min and 120000 photons/min

Equivalent Background	Integration Time	[OH] Interference	% [OH] Interference	S/N D=1	S/N D=5	S/N D=10
Case A - MARINE BOUNDARY LAYER [OH] 5×10^6 cm^{-3}						
1×10^8	20 min	2.5×10^5	5%	38.	NA	NA
1×10^8	1 min	2.5×10^5	5%	8.5	NA	NA
1×10^7	20 min	2.5×10^5	5%	110.	NA	NA
1×10^7	1 min	2.5×10^5	5%	25.	NA	NA

Equivalent Background	Integration Time	[OH] Interference	% [OH] Interference	S/N D=1	S/N D=5	S/N D=10
Case B - MID-TROPOSPHERE [OH] = 5×10^6 cm^{-3}						
1×10^8	20 min	1.5×10^4	0.3%	54.	NA	NA
1×10^8	1 min	1.5×10^4	0.3%	12.	NA	NA
1×10^7	20 min	1.5×10^4	0.3%	154.	NA	NA
1×10^7	1 min	1.5×10^4	0.3%	36.	NA	NA

NA - integration time de-rating factor given as D=1 for GA Tech system using <100 μs on/off line cycling time.

Case A - As noted earlier we believe that the workshop agreed-upon noise level is too optimistic for an in situ LIF system; thus we expect the MDC (S/N = 2) to be in the range of $3.5 \times 10^5/cm^3$ to $7 \times 10^5/cm^3$ for a 20 minute integration time.

Case B - See Case A comment: MDC (S/N = 2) expected to be in the range of $1.4 \times 10^5/cm^3$ to $3 \times 10^5/cm^3$ for a 20 minute integration time.

APPENDIX F

DETAILED PERFORMANCE CALCULATIONS:

PORTLAND STATE GROUP

For the Portland State University FAGE instrument, laser-induced OH is calculated from

$$[OH]_{laser} = C_1[O_3]_{amb}[H_2O]_{amb}$$

where $[OH]_{laser}$ is in units of signal-equivalent ambient number density, and $[O_3]_{amb}$ and $[H_2O]_{amb}$ are also ambient densities, all in molec cm^{-3}. The coefficient C_1 is proportional to the square of the laser flux and also to the expression

$$F = Y\,[M]\left(1 - \frac{\dfrac{k_4(1-\exp(-k_2[M]\Delta t))}{k_2[M]\Delta t} - \dfrac{k_2(1-\exp(-k_4[M]\Delta t))}{k_4[M]\Delta t}}{k_4 - k_2}\right)$$

which is strongly dependent upon pulsewidth and pressure. [M] is the total number density, k_2 is the total $O(^1D)$ removal rate constant, and k_4 is the groundstate thermalization rate constant. $C_1 = 7.5 \times 10^{-26}$ cm^3 $molec^{-1}$ has been measured experimentally with the FAGE instrument sampling ambient air enriched with ozone.

The FAGE signal function is

$$S_{OH} = C_{cal}[OH]_{amb}$$

where C_{cal} is measured in a large transparent chamber in which FAGE measures S_{OH} while $[OH]_{amb}$ is simultaneously measured by hydrocarbon decay using gas chromatography with flame-ionization detection. C_{cal} varies with excitation overlap and with alignment and cleanliness of the White-cell and detection optics; at [OH] = 5×10^6 cm^{-3} we have observed S_{OH} = 7 counts/min.

The dominant noise sources in FAGE are the photon-counting fluctuations associated with the OH signal and the fluorescence background as well as concentration fluctuations in OH and in the species causing the background. Baric filtering and temporal filtering suppress the background by factors of 10 each. After suppression, the remaining fluorescence background in urban air is in the 10^7 ambient OH cm^{-3} equivalent range.

In tables 6 and 7 of the text, the signal-to-noise ratio is calculated as SNR=S/D S + 2B. Here S is the number of counts of OH fluorescence observed at $[OH]_{amb} = 5 \times 10^6$ cm^{-3} with the calibrated response C_{cal} = 7 photons/min in the stated integration

times. B is the stated atmospheric-pressure background, reduced by a factor of 100 via baric and temporal filtering. The degradation factor D = 1 is for photon-noise-limited condition. D = 5 and D = 20 allow for possible large concentration fluctuations between the signal and background measurements.

In table 7 of the text, Portland State assumes a reduction in laser linewidth, improving the overlap with the pumped transition by a factor of 2.5.

APPENDIX G

DETAILED PERFORMANCE CALCULATIONS:

HARVARD GROUP

The technique proposed by the Harvard group for the measurement of OH density in the troposphere has many elements in common with a system that is currently used for in situ measurement of OH in the stratosphere. The proposed experiment utilized laser-induced fluorescence detection of OH in the A-X band. The sampling configuration is the enclosed flow technique, whereby the air samples flow at high velocity through a 5-in.-i.d. flow tube that houses the detection optics.

The theory of LIF detection of ambient OH is well documented elsewhere in this publication. When applied to the proposed technique, a signal equation of the following form is obtained:

$$S_{OH}\ (\text{cts/sec}) = \int F(\text{photons/cm}^2\text{sec})\,\sigma(\text{cm}^2)\,d\lambda\,[OH](\text{molec/cm}^3)\,V(\text{cm}^3)\,Q\,\varepsilon T\eta \qquad (G1)$$

where, in addition to the self-evident terms, we have:

- V sample volume element defined by overlap of projected area of laser beam and projected area of detector field of view
- Q fluorescence efficiency; that is, fraction of $A^2\Sigma^+$ state OH radicals that fluoresce rather than collisionally deactivate
- ε geometric collection efficiency of detector
- T optical transmission of detector optics
- η efficiency of converting a photon incident on PMT photocathode into an observed count

In our working expression the nonvariable terms in equation (G1) are collected into a single product given by C_{OH}:

$$S_{OH} = C_{OH}\left(\frac{\text{cts/sec}}{Q \cdot \text{molec/cm}^3 \cdot \text{mW}}\right) E(\text{mW})\,Q\,[OH] \qquad (G2)$$

where

$$C_{OH} = \int g_{laser}(\lambda)\,\sigma(\lambda)\,d\lambda\,V\,\varepsilon T\eta$$

and $g_{laser}(\lambda)$ represents the laser line width function.

Deriving values of [OH] from the observed count rate due to OH fluorescence requires knowledge of C_{OH}, E, and Q. C_{OH} is determined in the laboratory by direct measurement of S_{OH} with a known OH density in the sample volume element at a known circulating power, E, and a

known quenching environment, Q. E is measured by monitoring Rayleigh scattering at the laser pumping wavelength, and Q is derived from the local conditions from pressure and temperature measurements.

During the calibration phase, E is recorded as the ratio of S_{Ray} to [M] , the buffer gas density. The signal equation for the S_{Ray} is analogous to the S_{OH} signal equation, the only difference being the nature of the scattering events observed, and we have:

$$S_{Ray} \text{ (cts/sec)} = C_{Ray} E[M] \tag{G3}$$

The value of C_{Ray} can be determined easily by experiment; however, its value is not used explicitly in data reduction since it cancels out in the final form of the working expression:

$$S_{OH} = C_{OH} \frac{S_{Ray/[M]}}{(S_{Ray}/[M])_{calibration}} Q[OH] \tag{G4}$$

The value of C_{Ray} does, of course, provide useful diagnostic information regarding the actual number of passes achieved by the light tapping cell when it is coupled with an independent measure of the power in the input beam. The latter is provided by photodiodes which are used to monitor laser performance.

The current stratospheric instrument has the following directly measured sensitivity:

$$C_{OH} \approx 5 \times 10^{-4} \frac{\text{cts/sec}}{Q \cdot [OH]}$$

at

$$S_{Ray}/[M] \approx 5 \times 10^{-15} \frac{\text{cts/sec}}{\text{molec/cm}^3}$$

and an input beam energy of 10 mW.

The proposed tropospheric instrument with narrowed laser performance and increased power has a projected sensitivity of:

$$C_{OH} = 5 \times 10^{-4} \times \frac{0.4\text{Å}}{0.02\text{Å}} \times \frac{20 \text{ mW}}{10 \text{ mW}} = 2 \times 10^{-2} \frac{\text{cts/sec}}{Q \cdot [OH]} \tag{G5}$$

This is the sensitivity used for the predicted performance levels of our anticipated system in table 8 of the text. For the results given in table 8 an average power of 3 mW with $Q = 8.7 \times 10^{-4}$ is assumed for the marine boundary layer cases, and an average power of 20 mW with $Q = 1.5 \times 10^{-3}$ is assumed for the middle troposphere. The current detector mode with (1,0) pumping at 2820Å and wideband (0,0) observation centered around 3090Å is assumed for these estimates.

The strengths of the various background signals present on the OH and Rayleigh detectors are relatively low. The estimates for the anticipated systems in table G1 are based upon the performance of the current stratospheric system.

The ambient OH fluorescence signal is separated from the background signals by tuning the laser off the OH absorption line and directly measuring the background signal. This approach is sufficient for the majority of background sources, which are nonresonant. The notable exception is, of course, the laser-induced OH term. The magnitude of that source and its measurement are discussed below.

The projected laser-induced [OH] values in table G1 are based on the following equation (see section in text on photolytic interference):

$$[OH]_{laser} = 3.8 \times 10^{-2} \frac{[O^3][H_2O]}{[M]} \frac{E}{N_p A} f(x) \qquad (G6)$$

where we start with the nominal operating parameters:

E 20 mW

N_p 17,000

A $\pi r^2 = \pi(0.5\ cm)^2 = 0.78\ cm^2$

f(x) 0.56 at 1 atm T = 296 K
0.46 at 0.5 atm T = 256 K

Equation (G6) predicts the density of laser-induced OH that is formed and detected during a single pulse in a laser beam of peak flux equal to E/N_pA. However, the light trapping cell multiply reflects the laser beam through the sample volume element at least 40 times. The net flux through the volume element is increased since the $\sim$1 cm diameter laser beams overlap spatially. The net increase in flux is about a factor of 10, depending on the actual geometry of the light trapping pattern we choose. The values of laser-induced OH reported in table G1 take this effect into account.

The minimum flow velocity to clear the sample volume element between pulses at N_p = 17,000 is

$$V = 17{,}000 \times 1\ cm = 17{,}000\ cm/sec = 380\ mph$$

The actual contribution from laser-induced OH to the observed signal must be measured directly when it is present. If it is negligible, it must be demonstrated as such.

Fortunately, experimental susceptibility to the resonant interference can be readily mapped by performing nighttime measurements, when the ambient OH concentration is extremely low. This strategy would require simultaneous H_2O and O_3 density measurements during both day and night.

Alternatively, the enclosed flow technique allows for a chemical null experiment specifically tailored to separate the ambient OH signal from the laser-induced OH signal. A flow of C_3H_6 can be mixed into the sample flow at a concentration suitable to reduce ambient OH density by a factor of $\sim$100 on a millisecond time scale. The laser-induced OH signal is unaffected since it is operative over a nanosecond time scale. The efficiency and presence of any possible side effects can be checked in the laboratory and by a suitable strategy of complementary daytime and nighttime measurements. The comparison between the chemical addition null experiment and the conventional null experiment, tuning the laser off the absorption line, provides another diagnostic check of system performance.

TABLE G1

Background Source	Current Stratospheric System	Proposed Tropospheric System	Comments
S_{3090} nonresonant background fluorescence	<5		No prediction made. Presence of many more compounds in the troposphere makes any prediction unreliable.
S_{3090} chamber scatter	<5	<5	
S_{3090} Raman Rayleigh	<5	<5	
S_{3090} solar scatter	70	<5	Improved baffling and a narrowed PMT gas width will decrease this source.
S_{3090} dark count	<1	<1	
S_{3090} laser-induced OH	<5		See text.
S_{2820} chamber scatter	<1	<1	
S_{2820} dark count	<1	<1	
S_{2820} solar scatter	<1	<1	

APPENDIX H

REDUCTION OF DATA FOR RADIOCHEMICAL METHOD:

WASHINGTON STATE UNIVERSITY GROUP

We postulate the following very general model for the chemistry of the air before and after the addition of the carbon-14 monoxide. Beginning with the ambient, which we assume to be in steady state, we write

$$\frac{dn}{dt} = P_o - \frac{n}{\tau_o} \qquad \text{(H1)}$$

where n is the OH concentration as a function of time, t

P_o is the production rate of OH radicals, assumed independent of n

τ_o is the lifetime of the radicals against chemical loss, a process assumed to be only first-order in n

The production term includes several components, some of which will vanish promptly when the air is transferred out of the light, for example into the instrument inlet. We write

$$P_o = P_p + P \qquad \text{(H2)}$$

where P_p is the photolytic (promptly light-dependent) part, and P is the residue. Furthermore, let us write

$$P = f P_o = fn/\tau_o \qquad \text{(H3)}$$

where f is the non-photolytic fraction of the source term. The value of f can be estimated from models and can be measured, but will often not be known with any great accuracy.

After the admixing of the carbon-14 monoxide the kinetic equation (H1) will be changed by the addition of another loss term, $-k\ n_{CO}\ n = -n/\tau'$, where k is the rate coefficient for the OH + ^{14}CO reaction under the prevailing conditions, n_{CO} is the concentration of carbon-14 monoxide and τ' is the lifetime of hydroxyl against reaction specifically with carbon-14 monoxide. If the initial (injection point) concentration of hydroxyl is n°, we may solve to find n(t) after the carbon-14 monoxide is added:

$$n(t) = (n^\circ - P\tau)\ e^{-t}/\tau + P\tau \qquad \text{(H4)}$$

where τ, the overall lifetime of hydroxyl, is given by

$$1/\tau = 1/\tau_o + 1/\tau' \qquad \text{(H5)}$$

This equation can be rewritten as

$$n(t) = n^\circ[(1 - f\tau/\tau_o)\ e^{-t/\tau} + f\tau/\tau_o] \qquad (H6)$$

Given n(t) we can calculate the concentration n_{CO_2} of CO_2 arising from the reaction

$$^{14}CO + OH \rightarrow {}^{14}CO_2 + H$$

which we assume to be the dominant source. Thus

$$n_{CO_2} - n^\circ_{CO^2} = \frac{\tau n^\circ}{\tau'} [(1 - f\tau/\tau_o)\ (1 - e^{-T/\tau}) + fT/\tau_o] \qquad (H7)$$

where n_{CO_2} is the initial $^{14}CO_2$ concentration and T is the duration of the reaction from mixing to quenching. A useful parameter is the normalized sensitivity S*,

$$S^* = \frac{\tau'}{Tn^\circ} (n_{CO_2} - n^\circ_{CO_2}) \qquad (H8)$$

or

$$S^* = \frac{\tau}{T} [(1 - f\tau/\tau_o)\ (1 - e^{-T/\tau}) + fT/\tau_o] \qquad (H9)$$

Values of S* can be calculated from equation (H9), and tend to cluster just below unity. Similarly, the strength of the dependence of S* on parameters, such as the reaction time T, can be assessed by computing $\partial \ln S^*/\partial \ln T$, and so on. Typical values are shown in tables H1 and H2 for representative sea-level and 8-km-altitude conditions respectively. It should be noted that S* shows a generally weak dependence on the operating conditions, indicating that the measurement results are not critically dependent on measurement of any parameters other than the activity of the carbon-14 dioxide, the mixing ratio of carbon-14 monoxide, the reaction time and the flow rate. In particular, the dependence upon f is very weak, with typical values of $\partial \ln S^*/\partial f$ ranging downward from a maximum of 0.14, an important point insofar as f is poorly known. Total ignorance of f, combined with an assumption that f = 0.5, cannot produce an error in n° exceeding 7%.

Reduction of the data begins with the assay, the time-integrated aliquot of the carbon-14 monoxide admixed flow. From the volume of the assay container, its increase in pressure during the measurement, and the laboratory temperature, the number of moles of air in the container are calculated. The contents are then transferred to a proportional beta-counter and the total

carbon-14 content (corrected for counting efficiency) is obtained. From these data the concentration n_{CO} of carbon-14 monoxide in the reactor can be computed, using the reactor temperature and pressure.

From the net carbon-14 dioxide counts, again corrected for counter efficiency, the reactor effluent mass flow rate, the run duration and the reactor temperature and pressure we compute the net increase in carbon-14 dioxide concentration at the reactor exhaust, $(n_{CO_2} - n^{\circ}_{CO_2})$. The ratio of this quantity to n_{CO}, determined from the assay, permits calculation of the hydroxyl concentration at the injector,

$$n^{\circ} = (n_{CO_2} - n^{\circ}_{CO_2})/(S^* \; k \; n_{CO} \; T) \qquad (H10)$$

apart from a small correction for wall losses in the diffuser-reactor unit.

The external hydroxyl concentration requires additional corrections for losses of radicals to the injector nozzles (1 to 2%), to the walls of the inlet tube (believed to be about 4%) and due to chemical decay during the transit time (less than about 2%). Overall errors of less than 20% appear to be currently attainable (provided the problem of turbulence due to misalignment of the external airfoil is resolved). With some improvement in flow and temperature monitoring the overall errors could be reduced to less than 15%.

TABLE H1 FRACTIONAL ERROR COEFFICIENTS AT SEA LEVEL IN CLEAN AIR

Coeff.	Quantity	f = 0.0	0.2	0.4	0.6	0.8	1.0
$\frac{\partial \ln S^*}{\partial \ln T}$	Reaction time	-0.26	-0.23	-0.20	-0.17	-0.15	-0.13
$\frac{\partial \ln S^*}{\partial \ln \tau_O}$	OH lifetime	+0.11	+0.09	+0.06	+0.03	+0.01	-0.01
$\frac{\partial \ln S^*}{\partial \ln \tau^1}$	^{14}CO concentration	+0.14	+0.14	+0.14	+0.14	+0.04	+0.04
$\frac{\partial \ln S^*}{\partial f}$	Non-photolytic fraction	+0.14	+0.13	+0.13	+0.13	+0.12	+0.12

TABLE H2 FRACTIONAL ERROR COEFFICIENTS AT 8 km ALTITUDE IN CLEAN AIR

Coeff.	Quantity	f = 0.0	0.2	0.4	0.6	0.8	1.0
$\frac{\partial \ln S^*}{\partial \ln T}$	Reaction time	-0.14	-0.13	-0.12	-0.12	-0.11	-0.10
$\frac{\partial \ln S^*}{\partial \ln \tau_O}$	OH lifetime	-0.04	+0.03	+0.02	+0.01	+0.01	0.00
$\frac{\partial \ln S^*}{\partial \ln \tau^1}$	^{14}CO concentration	+0.10	+0.10	+0.10	+0.10	+0.10	+0.10
$\frac{\partial \ln S^*}{\partial f}$	Non-photolytic fraction	+0.05	+0.05	+0.05	+0.05	+0.05	+0.05

1. Report No.	2. Government Accession No.	3. Recipient's Catalog No.
NASA CP-2332		

4. Title and Subtitle	5. Report Date
ASSESSMENT OF TECHNIQUES FOR MEASURING TROPOSPHERIC H_xO_y	December 1984
	6. Performing Organization Code: 176-20-07-70
7. Author(s): James M. Hoell, Editor	8. Performing Organization Report No.: L-15847
9. Performing Organization Name and Address: NASA Langley Research Center, Hampton, VA 23665	10. Work Unit No.
	11. Contract or Grant No.
12. Sponsoring Agency Name and Address: National Aeronautics and Space Administration, Washington, DC 20546	13. Type of Report and Period Covered: Conference Publication
	14. Sponsoring Agency Code

15. Supplementary Notes

16. Abstract

In its continuing efforts to direct its applications programs towards relevant national needs, NASA is conducting the Tropospheric Chemistry Program, the long-range objective of which is to apply NASA's space technology to assess and predict human impact on the troposphere, particularly on the regional to global scale. One area of required research is instrumentation development, which is aimed at improving the capability to measure important trace gases and aerosols which are key species in the major atmospheric biogeochemical cycles. To focus on specific needs, the Instrumentation Workshop for H_xO_y Tropospheric Species was conducted in August 1982. The workshop discussed current measurement needs and instrument capabilities for H_xO_y species, including OH, HO_2, and H_2O_2. This report documents the workshop activities and conclusions.

17. Key Words (Suggested by Author(s))	18. Distribution Statement
Tropospheric H_xO_y species Instrumentation: H_xO_y Instrumentation: OH, HO_2, H_2O_2	Unclassified - Unlimited Subject Category 46

19. Security Classif. (of this report)	20. Security Classif. (of this page)	21. No. of Pages	22. Price
Unclassified	Unclassified	138	A07

For sale by the National Technical Information Service, Springfield, Virginia 22161 NASA-Langley, 1984

National Aeronautics and
Space Administration

Washington, D.C.
20546

Official Business
Penalty for Private Use, $300

THIRD-CLASS BULK RATE

Postage and Fees Paid
National Aeronautics and
Space Administration
NASA-451

NASA

POSTMASTER: If Undeliverable (Section 158 Postal Manual) Do Not Return